Tarnished: The Toxic Potential of Silver Nanoparticles

Brittany A. Weldon

A dissertation
submitted in partial fulfillment of the
requirements for the degree of

Doctor of Philosophy

University of Washington
2016

Reading Committee:

Elaine M. Faustman, Chair
Terrance J. Kavanagh
William Griffith

Program Authorized to Offer Degree:
Public Health- Environmental and Occupational Health Sciences

University of Washington

Abstract

Tarnished: The Toxic Potential of Silver Nanoparticles

Brittany A. Weldon

Chair of Supervisory Committee:
Professor Elaine M. Faustman
Department of Environmental and Occupational Health Sciences

Recent technological developments have employed the use of a wide array of nano-scaled materials referred to generally as engineered nanomaterials (ENMs). Silver nanoparticles (AgNPs) are ENMs that are nano-sized particles of silver. Silver has also long been noted for its antimicrobial properties, however recent advances in the ability to synthesize AgNPs have led to a surge of use in consumer and commercial products. Applications of AgNPs range from use in clothing, food storage, pacifiers, toys, washing machines, cooking tools, personal care products, cleaning products, and paints. While AgNPs are integrated into these products, usage and time, or even their own functional design may cause the release of silver nanoparticles from the products and may result in human and environmental exposure to silver and silver nanoparticles. The goal of my dissertation work was to add to the growing body of literature to assess potential risks to human health from exposure to AgNPs. In this work, we assessed potential health risks to workers exposed to AgNPs using literature on AgNP toxicity and exposure in the workplace. We use these data to model and analyze dose response and critical effects and characterize the potential risk to workers and suggest an occupational exposure limit (OEL) to protect workers from

adverse health effects. We found that the liver is the most sensitive target organ to AgNPs, and that exposures in the workplace may exceed the level determined to prevent adverse liver effects. Next, we investigated the potential for AgNPs to affect potentially sensitive populations by disrupting neurodevelopment using a three dimensional organotypic mouse midbrain in vitro model. We found that developing neural cultures are adversely affected by AgNP exposure and that developmental stage at the time of exposure significantly affects the extent of toxicity. We found developing neural cultures were more sensitive to smaller AgNPs and we observed no significant difference between AgNPs with different coatings. We also found evidence that the toxicity observed may have resulted from uptake and association of AgNPs with cell cultures, rather than through dissolution of particles in culture medium. Finally, we show how in vitro studies of inorganic ENMs can be applied to risk assessment to inform potential susceptibility such as age or genetic susceptibility using a case study of cadmium-containing quantum dot ENMs with applications for AgNP risk assessment.

Table of Contents

List of Figures

List of Tables

Acknowledgements

I'd like to thank my advisor Elaine Faustman for her dedication and commitment to being an amazing academic advisor, mentor, and role model for myself and the many other students who have trained with her. Throughout the four years I've spent in her lab, Elaine has given me so many unique opportunities to be involved in work beyond what would be typical for a grad student, and has pushed me to do work I didn't think I was capable of. Throughout this, Elaine has been endlessly patient and encouraging along the way. I'd like to thank Terry Kavanagh for sharing a small chunk of his endless bank of knowledge with me, for his sagely advice, patience, and endless stories. I've learned so much from Terry and he is a true inspiration to never stop learning—or I'll never catch up with him! I'd like to thank Bill Griffith for his statistical and technical help, patience and calming support that really helped keep me sane. In the hardest and most frustrating times, that made all of the difference. I'd like to thank Alison Cullen for her guidance and encouragement to apply my work beyond the lab, and understand how the work we do really can have big impacts in the world. And thanks to my committee member and GSR Bill Altemeier for his willingness to provide insights and application of my work. I'd also like to thank Steve Whittaker for taking me on as an intern with King County and getting me excited and invigorated to apply my training to have a positive impact on public health.

I have had so much support from the Faustman lab- especially from Tomomi Workman who has tirelessly worked to help me with statistics and modeling, and has been a great friend and coworker. I will miss spending days talking over the cubicle walls with you and stuffing my face with the delicious baked goods you bring in. I'd like to thank Sungwoo Hong for all of his help in planning and running experiments in the lab. Julie Park taught me the ropes in the lab and has been an amazing colleague and friend. I'd like to thank Keh Duong and Marissa Smith for years of laughs and endless support. There are so many past students and post docs from the Faustman lab that I have learned so much from, and continue to learn so much from, especially Susanna Wegner and Sean Harris. I could not have made it this far without you guys.

I'd like to dedicate this work to my parents, Ellen and Brian, who sacrificed so much to make sure their three crazy daughters had all of the opportunities in the world. Their tireless work and striving for a better life has been inspiring and motivating for all of us. Even as an adult, albeit a whiny grad student, mom was always just a phone call away for a pep talk or a 'quit complaining and just do it' talk. And dad has always been there with a new joke and story of a new adventure. I'm so grateful to have such amazing parents and people to learn from. I'd like to thank my sisters Jen and Steph for their constant support and laughs.

Though I told him I'd list Jon Nagata in my acknowledgements before him (hah!), I'd like to thank my partner, Trevor. Trev, you've been endlessly supportive, encouraging, and willing to talk through even the most obscure aspects of my research. You've kept a smile on my face, food in my mouth, adventure in my heart, and love in my life. I'm so lucky to have you.

Finally I'd like to thank several collaborators for the opportunity to work with them on the OEL project- Il Je Yu, Gunter Oberdorster, and Carsten Kneur. Russell Dills was incredibly supportive and helpful in running metals analysis in our micromass work. Thanks to the DEOHS staff and faculty who keep the wheels of this place running and opportunities for students aplenty. And finally, I'd like to thank the funding support for my work from the Institute of Translational Health Sciences, NIH/NIEHS grants U19ES019545, P30ES07033, RD83573801, USEPA grant 83573801, and Public Health- Seattle & King County.

Chapter 1

Introduction

Brittany A. Weldon

Engineered Nanomaterials

Recent technological developments have employed a wide array of nano-scale materials (<100nm), referred to generally as Engineered Nanomaterials (ENMs), for their attractive qualities including small size, large surface area, charge, and lightness of weight. These unique properties of ENMs also create the potential for ENMs to interact with biological systems in ways that are dependent on their nanoscale dimensions. The utilization of ENMs in medicine, manufacturing, and industry continues to accelerate, however much is still unknown about their potential for toxicity in humans.

Silver Nanoparticles- antimicrobial effect

Silver is known to have antibacterial properties, which has led to the development of silver nanoparticles (AgNPs) for antimicrobial functionalization of consumer and commercial products (Sondi and Salopek-Sondi, 2004; Cho, 2005; Morones et al., 2005; Li et al., 2008). At least three major mechanisms of antibacterial effect of AgNPs have been identified including interaction between the AgNP and disruption of bacterial cell membranes, AgNP penetration of cell membranes, and the dissolution, or dissolving, of AgNPs into silver ions. Ag has been shown to disrupt Na/K, Ca2+, and Mg2+ ATPase activity, leading to ion imbalance and potentially cellular death (Hussain et al., 1994; Atli and Canli, 2013). Ag+ may also compete for Na+ channels, disrupting ion flow and bypassing biological barriers (Bury and Wood, 1999). Once inside the cell body, silver particles and silver ions have the potential to disrupt structural proteins, enzymes, RNA and DNA in bacterial cells, largely due to silver's affinity for phosphorus or sulfur-containing compounds (Zhao and Stevens, 1998; Morones et al., 2005;

Li et al., 2008; Reidy et al., 2013). Disruption of these processes can then lead to bacterial cell death. Accordingly, it has been proposed that it is biologically plausible for silver and AgNPs to interact with eukaryotic cells by similar mechanisms.

AgNPs primary physicochemical properties

AgNPs are manufactured in various shapes and sizes, and can be coated with a variety of different compounds to optimize desired attributes of particles (Sun and Xia, 2002). These physicochemical properties of AgNPs can affect the solubility, dissolution capacity, and physical behaviors of AgNPs and result in differing levels of antibacterial functionalization and potential toxicity (Ma et al., 2012; Utembe et al., 2015).

Local Environmental effects on toxicity

The local environment where AgNPs interact with biological materials can affect the antibacterial capacity and toxicity. Environmental conditions such as pH, temperature, humidity, environmental medium (air or liquid), local chemistry, or presence of organic material can affect the physical and chemical behavior and efficacy of AgNPs (Reidy et al., 2013; Utembe et al., 2015).

Dissolution of AgNPs, the process by which nanoparticles dissolve into solution, has been shown to depend on particle size, pH and temperature of the solution, ions present in the solution, aggregation state, and incubation time (Stebounova et al., 2011; Ma et al., 2012; Leo et al., 2013). When compared with larger micro-sized particles, smaller nanoparticles have been observed to dissolve faster due to their high surface to volume ratio. Ma et al. (2012) found the dissolution of AgNPs to range from 1% for 80 nm particles to 60% for 5 nm particles at pH 8 during three and two months of incubation, respectively. The smaller size of nanoparticles suggest higher dissolution rate and lower biodurability, or

the ability to resist biochemical alteration, and thus greater potential to cause pathogenicity (Utembe et al., 2015). While antibacterial effects of AgNPs may be due partially to interaction of the silver particle with surfaces of bacterial cells, Ag ions have been suggested to be the factor most responsible for AgNP toxicity (Zhao and Stevens, 1998; Morones et al., 2005).

The presence of protein in a particle's local environment has been shown to result in the formation of a protein coating, or protein corona, around AgNPs. The protein corona can act as a stabilizer of AgNPs, and reduce the dissolution rate in media, and thus antimicrobial efficacy and toxicity (Shannahan et al., 2013; Duran et al., 2015). Local environmental conditions such as environmental media (air or liquid) and humidity have been shown to affect particle interactions. The presence of liquid or humidity can result in particle aggregation (the process by which particles bond covalently to each other), has been observed to occur in *in vitro* cultures. Particle aggregation results in less total surface area of particles relative to the sum total of the individual particles, and thus reduces that reactive potential. Particles and aggregates may also agglomerate, or weakly bond together, in liquid or humid environments resulting in similar surface area relative to the sum total of the particles and aggregates of particles. Larger surface area creates a greater number of surface reactive atoms within the particle which increases the potential for reactivity with biological systems. The surface area of particles and aggregates is a factor of critical consideration in AgNP exposures as surface area has been observed to be the most reliable dose metric for AgNP toxicity when measuring exposure concentration, however measuring the total delivered dose, or dosimetry, may be the best dose metric (Oberdorster et al., 2005). AgNP coatings including citrate and polyvinylpyrrolidone (PVP) act to stabilize AgNPs by reducing aggregation and agglomeration and controlling ion release from particles and me be used to optimize efficacy of AgNPs in various products.

Use in consumer products

Silver's high antimicrobial capacity has led to the utilization of AgNPs in many consumer and commercial products. AgNPs are the most frequently applied nanomaterial to consumer products and have been associated with 441 products, representing nearly half of the total number of products that contain nanomaterials (957) in the consumer product inventory of the emerging nanotechnologies project managed by the Woodrow Wilson Center (Woodrow Wilson International Center for Scholars, 2015). These products include clothing, washing machines, toothpaste, pacifiers, toys, humidifiers, cutlery, water filters, and cutting boards. Because silver is so highly conductive, AgNPs have also been applied into conductive inks in printed electronics in semiconductors, radio frequency identification (RFID), flexible printed circuit boards (FPCBs), and solar cells.

AgNP exposure- through products

While AgNPs are integrated into a variety of products, usage and time, as well as some products' functional design may result in the release of AgNPs from those products, creating the potential for human and environmental exposures. AgNPs have been shown to readily disassociate from functionalized materials (Levard et al., 2012) including textiles (Benn, T. M. and Westerhoff, 2008; Geranio et al., 2009), paints (Kaegi et al., 2010), toothbrushes (Mackevica et al., 2017), food containers (Echegoyen and Nerin, 2013), as well as from children's products such as blankets and toys (Benn, T. et al., 2010; Quadros et al., 2013). In addition, AgNPs and Ag ions may be designed to be released from products such as AgNP injection into washing machines, AgNP aerosol sprays, and humidifiers. Human exposure may also occur through direct contact with AgNP-containing products such as oral exposure through AgNP-containing toothpaste or dermal exposure through wearing AgNP-containing textiles.

The release of AgNPs from products results in environmental distributions of Ag and AgNPs through a variety of waste streams. Ultimately, AgNPs can be transported to soil, water systems, landfills, and in air where they can go on to disrupt biota, ecosystems, or lead to further human exposure (Keller et al., 2013).

While integrating AgNPs into consumer, commercial, and medical products may reduce (to varying levels of efficacy) a user's exposure to potentially harmful bacteria, the risk of the adverse health effects from exposure to AgNPs in humans from these exposures has yet to be thoroughly characterized.

Dissertation Outline

The overall goal of my dissertation is to better characterize and assess the potential risks of health effects in humans associated with exposure to AgNPs. As such, it was my goal to assess the risk of health effects from exposure to silver nanoparticles through high exposure scenarios in occupational settings. It was also my goal to investigate the potential for AgNPs to interact with and disrupt the developing central nervous system. Additionally, I propose a framework for comparing *in vitro* and *in vivo* toxicity assessments of engineered nanomaterials, and translating their results to risk assessment and human health.

Chapter 2: The increased application of AgNPs and integration into various consumer products can be expected to impact the exposure of workers to AgNPs during manufacturing, handling, and disposal of AgNP-containing products. While silver dusts, consisting of micro-sized particles and soluble silver compounds have established occupational exposure limits (OELs), silver nanoparticles exhibit different physicochemical properties from bulk materials. Currently, no OEL has yet been suggested specifically for AgNPs. *Chapter 2* will discuss work we have done to assess potential risks to workers that may be

exposed to AgNPs in occupational settings. We determined inhalation of airborne AgNPs to be the exposure route of highest exposure and potential risk and we suggest an OEL for aerosolized AgNPs in the workplace.

Chapter 3: The use of AgNPs in consumer products and medical equipment geared toward children and maternal usage creates the potential for AgNP exposure to the developing brain. Like other heavy metals, silver has been shown to interact with the developing nervous system. Silver has been found in fetal brain and other tissue following maternal exposure to AgNPs during pregnancy and lactation. Thus, there is a potential for exposure during this critical period of development. In *Chapter 3* I will discuss the development and use of a 3 dimensional *in vitro* neurodevelopment model to characterize toxicity of AgNPs of differing sizes and shapes on developing neural cell cultures.

Chapter 4

Because of the rapid rate of development and use of engineered nanomaterials including AgNPs, there is a need to accelerate the pace of risk assessment of these materials. While *in vitro* studies have long been used to suggest mechanisms and possible endpoints of toxicity for risk assessments, there is a potential to better use *in vitro* studies to inform *in vivo* studies and risk assessments for ENMs. Because of the unique physicochemical characteristics of nanoparticles, there has been some question as to the utility of *in vitro* studies of ENMs. The goal of the study discussed in *Chapter 4* was to utilize benchmark dose analysis to determine whether *in vitro* findings of ENM toxicity could have predicted *in vivo* findings in the literature, and thus could be used to better inform ENM risk assessments.

Chapter 5

In *Chapter 5* I will summarize key findings and future directions of this research.

Hypotheses and Specific Aims

To address my research goals, I have developed three related hypotheses and specific aims to test these hypotheses.

Chapter 2

Hypothesis: AgNPs present different health effects from silver dust and soluble silver and require an additional OEL to protect workers from adverse health effects.

Specific Aim. Determine the risk of health effects from silver nanoparticle exposure by inhalation in workers and develop a health-based occupational exposure limit.

Chapter 3

Hypothesis: AgNPs have the potential to disrupt developing neural cell cultures and AgNP size and coating will affect the extent of toxicity.

Specific Aim. Characterize the effects of AgNPs on developing 3- dimensional organotypic mouse midbrain cultures and the extent to which developmental stage at time of exposure, particle size, and particle coating contribute to uptake of particles and cell death.

Chapter 4

Hypothesis: Toxicity of AgNPs observed in vivo can be predicted through in vitro experiments.

Specific Aim: Utilize benchmark dose analysis to compare *in vitro* experimental results to *in vivo* observations of ENMs and determine how observations *in vitro* can inform *in vivo* effects in ENM risk assessments.

Chapter 5 Conclusions and future directions.

Chapter 1 References

Atli, G. and M. Canli (2013). "Metals (Ag(+) , Cd(2+) , Cr(6+)) affect ATPase activity in the gill, kidney, and muscle of freshwater fish Oreochromis niloticus following acute and chronic exposures." Environ Toxicol **28**(12): 707-717.

Benn, T., B. Cavanagh, et al. (2010). "The release of nanosilver from consumer products used in the home." J Environ Qual **39**(6): 1875-1882.

Benn, T. M. and P. Westerhoff (2008). "Nanoparticle silver released into water from commercially available sock fabrics." Environ Sci Technol **42**(11): 4133-4139.

Bury, N. R. and C. M. Wood (1999). "Mechanism of branchial apical silver uptake by rainbow trout is via the proton-coupled Na(+) channel." Am J Physiol **277**(5 Pt 2): R1385-1391.

Cho, K. H., J. E. Park, et al. (2005). "The study of antimicrobial activity and preservative effects of nanosilver ingredient." Electrochimica Acta **51**(5): 956-960.

Duran, N., C. P. Silveira, et al. (2015). "Silver nanoparticle protein corona and toxicity: a mini-review." J Nanobiotechnology **13**: 55.

Echegoyen, Y. and C. Nerin (2013). "Nanoparticle release from nano-silver antimicrobial food containers." Food Chem Toxicol **62**: 16-22.

Geranio, L., M. Heuberger, et al. (2009). "The behavior of silver nanotextiles during washing." Environ Sci Technol **43**(21): 8113-8118.

Hussain, S., E. Meneghini, et al. (1994). "Potent and reversible interaction of silver with pure Na,K-ATPase and Na,K-ATPase-liposomes." Biochim Biophys Acta **1190**(2): 402-408.

Kaegi, R., B. Sinnet, et al. (2010). "Release of silver nanoparticles from outdoor facades." Environ Pollut **158**(9): 2900-2905.

Keller, A. A., S. McFerran, et al. (2013). "Global life cycle releases of engineered nanomaterials." Journal of Nanoparticle Research **15**(1692).

Leo, B. F., S. Chen, et al. (2013). "The stability of silver nanoparticles in a model of pulmonary surfactant." Environ Sci Technol **47**(19): 11232-11240.

Levard, C., E. M. Hotze, et al. (2012). "Environmental transformations of silver nanoparticles: impact on stability and toxicity." Environ Sci Technol **46**(13): 6900-6914.

Li, Q., S. Mahendra, et al. (2008). "Antimicrobial nanomaterials for water disinfection and microbial control: potential applications and implications." Water Res **42**(18): 4591-4602.

Ma, R., C. Levard, et al. (2012). "Size-controlled dissolution of organic-coated silver nanoparticles." Environ Sci Technol **46**(2): 752-759.

Mackevica, A., M. E. Olsson, et al. (2017). "The release of silver nanoparticles from commercial toothbrushes." J Hazard Mater **322**(Pt A): 270-275.

Morones, J. R., J. L. Elechiguerra, et al. (2005). "The bactericidal effect of silver nanoparticles." Nanotechnology **16**(10): 2346-2353.

Oberdorster, G., E. Oberdorster, et al. (2005). "Nanotoxicology: an emerging discipline evolving from studies of ultrafine particles." Environ Health Perspect **113**(7): 823-839.

Quadros, M. E., R. t. Pierson, et al. (2013). "Release of silver from nanotechnology-based consumer products for children." Environ Sci Technol **47**(15): 8894-8901.

Reidy, B., A. Haase, et al. (2013). "Mechanisms of Silver Nanoparticle Release, Transformation and Toxicity: A Critical Review of Current Knowledge and Recommendations for Future Studies and Applications; Review." Materials **6**(6): 2295-2350.

Shannahan, J. H., X. Lai, et al. (2013). "Silver nanoparticle protein corona composition in cell culture media." PLoS One **8**(9): e74001.

Sondi, I. and B. Salopek-Sondi (2004). "Silver nanoparticles as antimicrobial agent: a case study on E. coli as a model for Gram-negative bacteria." J Colloid Interface Sci **275**(1): 177-182.

Stebounova, L. V., A. Adamcakova-Dodd, et al. (2011). "Nanosilver induces minimal lung toxicity or inflammation in a subacute murine inhalation model." Part Fibre Toxicol **8**(1): 5.
Sun, Y. and Y. Xia (2002). "Shape-controlled synthesis of gold and silver nanoparticles." Science **298**(5601): 2176-2179.
Utembe, W., K. Potgieter, et al. (2015). "Dissolution and biodurability: Important parameters needed for risk assessment of nanomaterials." Part Fibre Toxicol **12**: 11.
Woodrow Wilson International Center for Scholars, W. (2015). "The project on emerging nanotechnologies." from http://www.nanotechproject.org/inventories/.
Zhao, G. and S. E. Stevens, Jr. (1998). "Multiple parameters for the comprehensive evaluation of the susceptibility of Escherichia coli to the silver ion." Biometals **11**(1): 27-32.

Chapter 2

Occupational exposure limit for silver nanoparticles: Considerations on the derivation of a general health-based value

Brittany A. Weldon[1,2], Elaine M. Faustman[1,2], Günter Oberdörster[3], Tomomi Workman[1,2], William C. Griffith[1,2], Carsten Kneuer[4], Il Je Yu[5*]

[1]Institute for Risk Analysis and Risk Communication, University of Washington, Seattle, WA
[2]Department of Environmental and Occupational Health Sciences, University of Washington, Seattle, WA, USA
[3] University of Rochester, Department of Environmental Medicine, Rochester, NY, USA
[4]Federal Institute for Risk Assessment, Berlin, Germany
[5]Institute of Nanoproduct Safety Research, Hoseo University, Asan, Korea

Nanotoxicology. 2016 Sep;10(7):945-56. (Epub 2016 Mar 16.)

Keywords: Silver nanoparticles; Occupational exposure; subchronic inhalation; Dosimetry; Clearance

*Corresponding author: Il Je Yu, Institute of Nanoproduct Safety Research, Hoseo University, 165, Sechul-ri, Baebang-myun, Asan, Chungnam, 336-795, Korea, Email: u16701916@chollian.net, Tel: 82-41-540-9630, Fax: 82-41-540-9630

Abstract

With the increased production and widespread commercial use of silver nanoparticles (AgNPs), human and environmental exposure to silver nanoparticles are inevitably increasing. In particular, persons manufacturing and handling silver nanoparticles and silver nanoparticle containing products are at risk of exposure, potentially resulting in health hazards. While silver dusts, consisting of micro-sized particles and soluble compounds have established occupational exposure limits (OELs), silver nanoparticles exhibit different physicochemical properties from bulk materials. Therefore, we assessed silver nanoparticle exposure and related health hazards in order to determine whether an additional OEL may be needed. Dosimetric evaluations in our study identified the liver as the most sensitive target organ following inhalation exposure, and as such serves as the critical target organ for setting an occupational exposure standard for airborne silver nanoparticles. This study proposes an OEL of 0.19 μg/m^3 for silver nanoparticles derived from benchmark concentrations (BMCs) from subchronic rat inhalation toxicity assessments and the human equivalent concentration (HEC) with kinetic considerations and additional uncertainty factors. It is anticipated that this level will protect workers from potential health hazards, including lung, liver, and skin damage.

Introduction

Silver is known to have antibacterial properties (Cho et al., 2005, Li et al., 2005, Morones et al., 2005, Sondi and Salopek-Sondi, 2004), which has led to the recent use of silver nanoparticles (AgNPs) in home appliances and consumer products such as clothing, washing machines, toothpaste, rubber nipples, toys, filters, and humidifiers. AgNPs are the most frequently applied nanomaterial to consumer products and has been associated with 441 products, representing nearly half of the total number of products that include nanomaterials (957) in the consumer product inventory of the emerging nanotechnologies project managed by the Woodrow Wilson Center (Woodrow Wilson International Center for Scholars, 2015). The application of AgNPs to consumer products continues to increase as the recent development of printed electronics also uses AgNPs as conductive ink to produce semiconductors, radio frequency identification (RFID), flexible printed circuit boards (FPCBs), and solar cells. In turn, this increased application of AgNPs and integration into these products can be expected to impact the exposure of workers to AgNPs during manufacturing, handling, and disposal. Currently, no occupational exposure limit has yet been suggested specifically for AgNPs. Data on soluble silver compounds have shown silver salts have a greater ability to cause argyria than the dust or fumes of metallic silver. The *American Conference of Governmental Industrial Hygienists* (ACGIH) determined that exposure limits of 0.01 mg/m^3 for soluble silver and 0.1 mg/m^3 for metallic silver were adequate to prevent argyria and other skin damage in workers exposed to airborne silver. Accordingly, in 2013 the ACGIH recommended a TLV-TWA of 0.1 mg/m^3 for silver metal dust and fumes and 0.01 mg/m^3 for soluble silver to protect for argyria. Identical MAK (Maximum Workplace Concentration) values of 0.1 mg/m^3 and 0.01 mg/m^3 were set in Germany and Switzerland (DFG, 2006, SUVA, 2007).

A provisional acceptable external medium-term AgNP exposure limit of 0.005 mg/m^3, a level far lower than existing silver metal dust OELs, was discussed at a Workshop jointly organized by the OECD Working Party for Manufactured Nanomaterials (WPMN), the Business and Industry Advisory Committee

(BIAC) and the Society for Risk Analysis (SRA) in 2009 (OECD, 2010). However, several uncertainties were identified at this workshop, hampering the derivation of a general exposure limit value for AgNPs. These included potential differences in toxicity between the tested AgNPs and other nanoforms and an incomplete database. Since then, new data on AgNP toxicity and exposure has emerged, allowing for the establishment of an OEL for AgNPs. This database has recently been summarized in a number of reviews (Hadrup and Lam, 2014, Schafer et al., 2013, SCENIHR, 2014). Here, we analyze the current database with regard to the question whether the existing OELs for silver and silver compounds can be expected to be sufficiently protective and, if not, how an OEL for nanoscaled silver particles may be derived to protect the health of workers.

Exposure Assessment

Workplace exposure

In manufacturing and integration of AgNPs into various products, large amounts of AgNPs can be released into air from production equipment. Workers in these facilities have the potential to become highly exposed to AgNPs. The highest occupational exposure to AgNPs may be occur during the production of the AgNPs. Two different synthesis processes are currently in place: liquid and gas phase synthesis. Liquid phase synthesis usually yields dispersions of stabilized, surface-coated AgNPs while gas phase synthesis results in uncoated metallic silver particles. AgNP exposure in the workplace was assessed to determine the most likely routes and the range of AgNP exposures occurring. Several workplace exposure studies in these settings are summarized in Table 1.

Lee et al. (2011) reported on the release of AgNPs during the liquid phase synthesis process, where the AgNPs were manufactured by mixing sodium citrate with silver nitrate in an attrition milling operation. In this case, the silver metal concentrations of AgNPs ranged from 0.03 to 0.43 $\mu g/m^3$. Park et

al. (2009) investigated the production of 10-250nm AgNPs during a liquid phase synthesis production process. The emitted AgNPs were observed to be released during the opening of a reactor hatch, and most particles were identified as agglomerated forms. No mass concentration was reported in this study.

Gas-phase synthesis inductive coupled plasma methods are often applied for mass production of AgNPs. Lee et al. (2011) reported personal exposure to AgNPs to be 0.12 -1.02 μg/m^3 in a gas phase production facility. Particles released into workplace air were observed to be aggregated and agglomerated, resulting in a wide range of measured particle concentrations. They suggested that while AgNPs initially synthesized as primary nanoparticles may have agglomerated or aggregated in the workplace air, gas phase synthesis may pose a higher exposure scenario compared to liquid phase synthesis.

The exposure of workers to AgNPs in printed electronics workplace where AgNP inks are used as conductive ink showed personal exposure measures of AgNPs ranged from non-detectable to 0.24 μg/m^3, indicating lower exposure in the printed electronic workplace when compared to AgNP production (Lee et al., 2013b).

Additionally, workplace exposure may result from the handling of AgNPs for the production of intermediates or treated goods, as well as during manipulation of those during production of more complex articles and through disposal facility work through incineration of AgNP-containing products (Quadros and Marr, 2010). Unfortunately, no further relevant exposure studies were identified.

Worker exposure assessment and health surveillance

Currently, few human health studies are available on AgNP exposure. A surveillance case study of two workers involved in the manufacture of silver nanomaterials reported by Lee et al (2012a) found two male workers who had worked for 7 years manufacturing silver nanomaterials exposed to silver concentrations of 0.35 and 1.35μg/m^3 based on personal air sampling showed silver blood levels of 0.034

and 0.0135μg/dl and urinary silver levels of 0.043μg/dl and not detected, respectively. No health effects were observed. A 3-day continuous exposure study by Lee et al (2012b) at an AgNP production facility was also performed and found the AgNP precursor injection room showed the highest concentrations of AgNPs, ranging from 5.01-288 μg/m^3. Other locations in the facility showed concentrations of 1.3 μg/m^3. Meanwhile, personal sampling concentrations ranged from 0.04-2.43 μg/m^3 over the 3 days of sampling. Agglomerated AgNPs were also reported in the workplace, however agglomerated particles are suspected to have occurred due to changes in environmental conditions. Lee et al. (2012b) suggest that their AgNP monitoring study strongly supported mass-based exposure assessments (μg/m^3) for simple industrial hygienic purposes, consistent with other assessments of nanomaterials in the workplace (Pauluhn, 2010).

One case report identified a 27-year-old man involved in plating mobile telephone subunits with aerosolized silver for 4 years that presented with general argyria and hallmark blue-gray skin and mucosa pigmentation with elevated serum silver levels of 15.44 μg/dL (normal range, 1.1–2.5 μg/dL) and a urinary silver concentration of 243.2μg/L (normal range, 0.4–1.4 μg/L). No other adverse physical or organ effects were observed (Cho et al., 2008). Although the exact use of AgNPs in the workplace was uncertain, exposure to silver particles, whether nanoscale or non-nanoscale, appeared to induce the general argyria within 4 years. When compared to the argyria patient, the levels of silver in the workers' blood and urine indicated a much lower exposure than reported in Lee's AgNP production facility studies (Lee et al., 2011, Lee et al., 2012b, Lee et al., 2013b).

Hazard Assessment

Animal studies were evaluated for potential health effects from AgNPs. Our review identified acute, subacute, and subchronic whole body inhalation studies in male and female rats, subacute and subchronic oral administration studies in male and female rats, acute and subacute dermal and eye

irritation studies in rabbits and guinea pigs, as well as genotoxicity studies after oral and inhalation exposures to AgNPs. A subacute oral toxicity study in male and female mice was identified but excluded from the analysis as it examined tetrahydrofolate coated material and showed major deviations from international test guidelines (Park et al., 2010). Emphasis was placed on inhalation toxicity as this was determined to be the major route of exposure for workers described in workplace exposure assessments. All studies in our review followed Organization for Economic Cooperation and Development (OECD) testing guidelines and good laboratory practice (GLP) regulations. No chronic, carcinogenicity, or reproductive toxicity studies, including those for developmental toxicity, were found for AgNPs.

Inhalation toxicity

Sung et al. (2011) investigated the acute inhalation (4 hour) toxicity of uncoated AgNPs with a count median diameter (CMD) of 18-20 nm generated by the evaporation-condensation method in gas-phase in Sprague-Dawley rats of both sexes. Tested aerosol concentrations ranged from 76 $\mu g/m^3$ to the highest achievable concentration of 750 $\mu g/m^3$. No significant body weight or lung function changes were observed at any dose and the LC_{50} of AgNPs could not be established in the experiments (Sung et al., 2011).

Subacute (28 day) inhalation toxicity of uncoated AgNPs (CMD 13-15nm) was studied in male and female rats at concentrations of 0.65 $\mu g/m^3$, 3.48 $\mu g/m^3$, and 61.2 $\mu g/m^3$. Rats did not show any significant changes in body weight relative to AgNP exposure. No significant changes in the hematology and blood biochemical values in either the male or female rats were reported (Ji et al., 2007).

Subchronic (90 day) inhalation toxicity of AgNPs (CMD 18-19nm) was studied in male and female rats using concentrations of 0, 49, 133, and 515 $\mu g/m^3$ (Sung et al., 2009). Histopathological examinations of the liver found a concentration-dependent increase in bile-duct hyperplasia and abnormalities found in livers from both the male and female rats. Examinations of the lung found concentration-dependent

increases in lesions related to AgNP exposure. This included mixed inflammatory cell infiltrate in lung, chronic alveolar inflammation, and small granulomatous lesions at the highest concentration (Sung et al., 2009). Evaluation of lung function showed tidal volume significantly decreased during the 90 days of AgNP exposure in males and significant changes in bronchoalveolar lavage assessments in male and female rats. The authors identified 133 $\mu g/m^3$ as the no observed adverse effect level (NOAEL) for AgNPs in this study (Sung et al., 2008).

Recovery

A subchronic inhalation toxicity study of uncoated AgNPs (CMD 14-15 nm) that included a 12-week post exposure recovery period investigated with male and female Sprague Dawley rats exposed to concentrations of 49 $\mu g/m^3$, 117 $\mu g/m^3$, and 381 $\mu g/m^3$ (Song et al., 2013). Histopathological examination of lung samples from rats was performed immediately following the 12 week exposure, 4 weeks and 12 weeks after the exposure for each of the 4 exposure groups (control, 49, 133, and 381 $\mu g/m^3$). Histopathological examination included incidence of mixed cell infiltrate, perivascular and chronic alveolar inflammation, and alveolar macrophage accumulation. Significant responses observed include alveolar inflammation in males ($p<0.05$) and females ($p<0.05$) and macrophage accumulation in males ($p<0.05$) and females ($p<0.05$). There was a partial recovery from effects over the 12 weeks after exposure for the alveolar inflammation (males and females $p<0.05$) and macrophage accumulation (males and females $p<0.05$). Histopathology from this study found lung inflammation to be persistent after the 12 week recovery period in males exposed to the highest dose of AgNPs. An exposure-related lung function decrease in tidal volume was observed in the male rats after the 12-week exposure period. This decreased function was sustained 12 weeks after the exposure cessation. Female rats did not show consistent lung function changes either during the exposure period or following the exposure cessation. This suggested a

persistence of lung function changes and inflammation induced by AgNP inhalation exposure above 117 μg/m^3 and after recovery.

A study comparing particle size effects from inhalation exposure of 15 nm and 200 nm AgNPs (the latter being agglomerated into 410 nm entities) found a size-dependent effect in a 4-day study in male rats. At similar exposures of 179 and 167 μg/m^3, the 15 nm AgNPs elicited stronger toxicity than the agglomerated 410 nm AgNPs presumably due to differences in the internal alveolar dose and the release rate of the silver ions (Braakhuis et al., 2014).

Although inhalation exposure studies are most relevant for occupational settings, studies with oral and dermal administration were also examined for similar toxicity targets. It can be expected that part of the deposited dose from inhalation becomes available via the GI-tract following mucociliary clearance and swallowing/ingestion.

Oral administration

A 28 day subacute oral toxicity study of 60 nm AgNPs in male and female rats performed by Kim et al. administered doses of 30, 300, and 1,000 mg/kg of body weight. No significant changes in body weight occurred, however significant dose-dependent changes were found in the alkaline phosphatase and cholesterol values in both the male and female rats, indicating that exposure to more than 300 mg/kg of AgNPs may result in liver damage with an increased incidence of bile-duct hyperplasia (Kim et al., 2008). The NOAEL reported by the authors for this subacute study was 30 mg/kg of body weight (lowest tested dose).

A subchronic oral toxicity (90 day) study of AgNPs (average 56 nm) was conducted at doses of 30, 125, and 500 mg/kg of body weight and investigated effects in male and female rats (Kim et al., 2010). A significant decrease in the body weight of the male rats ($p<0.05$) was recorded after 4 weeks of exposure.

Consistent with the 28-day oral toxicity study, significant dose-dependent changes of alkaline phosphatase and cholesterol were found and histopathology assessments indicated a higher incidence of bile-duct hyperplasia in exposed male and female rats compared to controls. The NOAEL reported by the authors from this study was 30 mg/kg body weight (lowest tested dose).

Dermal and eye toxicity

It has been established that percutaneous exposure to powdered silver, silver solutions, and dental amalgams can induce allergic contact dermatitis (Catsakis and Sulica, 1978, Heyl, 1979, Marks, 1966). Acute eye and dermal irritation/corrosion tests using rabbits were conducted with using AgNPs (average 10 nm) and revealed no significant clinical signs or mortality and no acute irritation or corrosion reaction for the eyes and skin (Kim et al., 2013). A skin sensitization test using guinea pigs reported AgNPs as a weak skin sensitizer, showing discrete or patchy erythema (Kim et al., 2013). A subacute (28 day) dermal toxicity study with rabbits using a AgNP containing product (6% silver w/w) at doses of 250, 500, and 1000 mg/kg/day resulted in no dose-dependent clinical signs, mortality or body weight changes. Furthermore, no increased silver concentrations were found in the blood and urine.

Genotoxicity of AgNPs

A bacterial mutation test (Ames test) and *in vitro* chromosome aberration test in the presence and absence of a metabolic activation system were negative for genotoxicity of AgNPs (Kim et al., 2013). However, because of limited bacterial cell uptake, bacterial mutagenicity tests are usually considered to be of limited relevance for testing nanoparticles (OECD, 2014).

In vitro studies with various forms of AgNPs in human and mammalian cells showed an induction of DNA damage at cytotoxic doses (AshaRani et al., 2009). An *in vivo* genotoxic effect study in rats was examined using a micronucleus test after 28 days of oral administration of AgNPs (average 60 nm) at 0,

30, 300, and 1000 mg/kg/day. The results were negative for AgNPs at all exposures (Kim et al., 2008). *In vivo* genotoxicity testing was also conducted after exposing male and female rats to 18 nm AgNPs via inhalation for 90 days at concentrations of 0, 49, 133, and 515 μg/m^3 (Kim et al., 2011). Results showed no statistically significant differences in the micronucleated polychromatic erythrocytes, indicating that exposure to AgNPs by inhalation for 90 days did not induce genetic toxicity in the male and female rat bone marrow *in vivo*. The ratio of polychromatic to normochromatic erythrocytes remained unchanged. In contrast, rats exposed to AgNPs (14–15 nm) at aerosol concentrations of 49, 117, and 381 μg/m^3 for six hours/day over 12 weeks showed a positive response for DNA damage in lung cells in the highest exposure group using a Comet assay. These *in vivo* genotoxicity results from the rat bone marrow micronucleus test and lung cells after subchronic inhalation exposure suggest that a threshold value may be established for AgNPs for DNA damage and that genotoxicity may be limited to the primary sites of contact and organs experiencing high exposures. Additionally, a recent review of the available database provided by the Scientific Committee on Emerging and Newly Identified Health Risks (SCENIHR, 2014) reported indirect effects on genotoxicity observed at high doses.

Methods

Overview

In order to derive a health-based OEL for AgNPs, we developed a framework (Figure 1) to approach the relevant literature and assess the observed endpoints of toxicity with respect to occupational exposures and hazards. Briefly, we identified the most relevant studies to best represent occupational scenarios. From these studies, we identified significant toxicity endpoints. We used individual animal tissue silver concentration data to determine delivered dose at the individual animal and

tissue level. We then modeled the dose response for each endpoint and calculated a benchmark dose (BMD) for each endpoint. We used tissue silver concentration data and aerosol exposure concentration from the study to determine the aerosol concentration level at each BMD. We used these benchmarks as a basis for comparison of endpoint sensitivity and determined the critical effect as the effect(s) occurring at the lowest levels of response. The aerosol concentration at the BMD of the critical effect was then used to derive an OEL with toxicokinetic considerations and other uncertainty factors.

Selection of Point of Departure

The point of departure (POD) used in the OEL derivation can be selected using the NOAEL or the Benchmark Dose (BMD). The NOAEL, which represents a single tested dose, can be used to identify a level at which no statistically or biologically significant responses are seen in a dose-response assessment. Alternatively, the BMD is the dose corresponding to a specified biologically significant level of response (e.g., percentage change or change in standard deviation from controls) and can be interpolated between test doses based on modeling of the standard response measures in the range of biological observation (Allen et al., 1994, Faustman et al., 1994, Kimmel et al., 1995, Wignall et al., 2014). The BMD approach allows for the incorporation of variability in the estimation as the 95% confidence limit of the BMD is calculated from the variability in the dose-response data and presented as the BMDL. The BMDL, the 95% lower confidence bound at the critical effect, was used as point of departure to reflect the variability in the experimental data.

Dose-Response and BMD Modeling

Following the framework presented, Sung et al.'s 2008 and 2009 investigations of occupationally relevant subchronic AgNP inhalation studies in rats was selected for our study. The exposures used in these studies were designed to represent a 5 day work week and provided the most relevant animal model

for our investigation of health risk in the workplace in the absence of chronic exposure data. We discuss an approach to extrapolate this subchronic exposure to chronic workplace exposures.

Dose-response data from all observed effects in the Sung et al. studies were evaluated for suitability for BMD modeling utilizing a modified version of EPA's technical guidance framework for benchmark dose modeling (US EPA, 2012). Datasets that did not pass fitness criteria (e.g. lack of statistically significant dose response in a given experiment) were excluded from further analysis. Endpoints showing significant responses were modeled based upon maximum likelihood utilizing EPA's Benchmark Dose Software version 2.6 (USEPA, 2015) and results were plotted using the R statistical package. Dose-response curves were modeled as total silver in target organ as delivered dose and response. BMDs and BMDLs were calculated with the biologically significant benchmark response factor of a 10% difference in response relative to the control for dichotomous endpoints and a 1 standard deviation difference in response relative to the control for continuous endpoints (Slob, 2002, US EPA, 2012, Davis et al., 2011, Kavlock et al., 1995). Dose-response models generated by the software were evaluated both for statistical fit using maximum log likelihood values and for biological plausibility through visual inspection of the curve. BMDs and BMDLs were reported as target organ dose (ng Ag/organ). To determine the exposure concentration ($\mu g/m^3$) at the BMDs, target organ dose was regressed relative to exposure concentration in the study (Supplemental Figure 1). The regression equation was used to calculate the exposure concentration at the BMD and BMDLs, and are referred to as "Dosimetrically Adjusted BMCs and BMCLs." Dosimetrically adjusted BMCs and BMCLs were reported in exposure concentration $\mu g/m^3$ and are represented as "BMCs" and "BMCLs."

Critical Effect

To select an endpoint of response for derivation of the OEL, the critical effect was determined by comparison of BMDs and BMDLs as well as BMCs and BMCLs for all significant endpoints. The critical effect

is defined as the endpoint at which the lowest statistically significant indication of adverse health effects in any organ occurs with increasing biologically relevant dose.

Dosimetric extrapolation

Dosimetric extrapolation of animal findings to human relevance is the first step in estimating human delivered dose from animal data (Oller and Oberdorster, 2010). To address this, NIOSH's human equivalent concentration equation for engineered nanomaterials (NIOSH, 2013) was modified using relevant allometric and biological scaling ratio corrections. Ventilation rate, clearance rate, alveolar surface area, and deposition rate differences between humans and rats were incorporated to determine the human equivalent concentration at the dosimetrically adjusted POD (HEC_BMCL) for the identified critical effect as described in Equation [1]. The Multiple-Path Particle Dosimetry Model program (MPPD, version 2.11, Asgharian et al., 2009) was utilized to model the deposition rate of 18-19 nm AgNPs (average particle count median diameter, Sung et al., 2009) in humans under light exercise conditions and rats at rest from occupational inhalation exposure in the workplace (de Winter-Sorkina and Cassee, 2003).

Derivation of the OEL

The calculated HEC_BMCL was divided by uncertainty factors to determine a health-based OEL. The derived OEL for AgNPs represents an 8 hour work day, 5 day work week, working 50 weeks per year over a 45 years working lifetime. This derivation provides an estimate that is designed to be protective of lung and liver endpoints of toxicity from a lifetime of occupational exposure to AgNPs. An alternative approach to setting workplace exposure limits by estimating a DNEL is included in the supplemental information. Equation [1] describes the Human Equivalent Concentration derived OEL equation.

$$HEC\_BMCL = \frac{Rat\ BMCL}{\left(\frac{Ventilation\ rate\ human}{Ventilation\ rate\ rat}\right) x \left(\frac{Depostion\ rate\ human}{Depostion\ rate\ rat}\right) x \left(\frac{Clearance\ rate\ human}{Clearance\ rate\ rat}\right) x \left(\frac{Alveolar\ Surface\ Area\ rat}{Alveolar\ Survace\ Area\ human}\right)}$$

$$OEL = \frac{HEC\_BMCL}{Uncertainty\ Factors}$$

[1]

Results

Dose-Response and BMD Modeling Results

The 90 day (13 week) *in vivo* subchronic inhalation studies investigating the effects of 18-19 nm sized AgNPs by Sung et al. showed significant liver and lung toxicity endpoints including liver abnormalities and bile duct hyperplasia in both male and female rats ($p<0.05$), lung inflammation in both male and female rats ($p<0.01$), as well as significant increases in lung infiltrate in female rats ($p<0.01$) (Sung et al., 2009). In female rats, significant changes in albumin, LDH ($p<0.01$) and total protein ($p<0.05$) were seen in bronchoalveolar lavage (BAL) assessments, and male rats showed significant changes in albumin in BAL ($p<0.05$) and in tidal volume functional endpoint ($p<0.01$) when comparing exposed groups to controls (Sung et al., 2008). Polymorphonuclear neutrophil (PMN) cell count was also assessed, however was not used in estimations due to lack of statistical significance.

The dichotomous *in vivo* data were best fit with a multistage polynomial degree 2 model consistently for all histopathology endpoints (Figure 1). This model has been shown to be biologically plausible when modeling dose responses in *in vivo* systems and is commonly used to model dichotomous dose-response data (Davis et al., 2011, NIOSH, 2013). The multistage polynomial degree 2 model function has the form:

$$f(x) = \gamma + (1-\gamma)[1 - \exp\{-(\beta_1 \mathrm{X} + \beta_2 \mathrm{X}^2)$$

[2]

Significant BAL and functional changes from Sung et al., 2008 were modeled as continuous endpoints using a best-fit linear model and are shown in Figure 2. BMDs and BMDLs were calculated for all endpoints as tissue burden (ng Ag/organ). Dosimetrically adjusted BMCs and BMCLs, the aerosol AgNP concentration ($\mu g/m^3$) at each BMD and BMDL, were calculated using tissue silver burden and exposure regression (Supplemental Figure 1). All benchmark doses and concentrations calculated are summarized in Table 2.

Selection of Critical Effect

Comparison of BMDs (ng Ag/organ) shown in Figure 3 indicates BMDs for liver endpoints are lower than in lung endpoints, suggesting higher liver sensitivity to silver than lung. Female liver abnormalities showed the lowest BMD and BMDL. The next lowest BMD and BMDL were seen again in females with bile duct hyperplasia. These same endpoints of toxicity were also observed in male rats however at higher doses. All other endpoints assessed were observed to have very similar BMD and BMDL values, respectively.

Figure 4 shows the comparison of derived dosimetrically adjusted BMCs and BMCLs among observed male and female endpoints of toxicity. The 95% confidence limits for dosimetrically corrected BMCs across endpoints are observed to overlap for both gender specific responses indicating similarity in response in both male and female liver and lung responses. The female bile-duct hyperplasia BMC and BMCL are observed to be within range of the BMC and BMCLs for other liver histopathology-based endpoints. Similarly, female liver endpoints are observed to show the lowest BMCs when compared to other BMCs. The double blinded pathology assessments in the Sung, 2009 study indicated “minimal” bile duct hyperplasia in control and “mild to moderate” at higher doses. The National Toxicology Program Atlas (Maronpot, 2014) suggests that these endpoints are significant and that dose-response effects of

abnormality and hyperplasia supports evidence of toxic insult. They note that bile duct hyperplasia is rarely seen in subchronic studies, yet this was reported by Sung et al., 2009. The 95% lower confidence limit of the BMC for female bile duct hyperplasia covers most of the variability in POD for other female liver effects and represents a specific, quantitative endpoint. Thus, the BMCL for female bile duct hyperplasia (25.55 μg/m^3) will serve as the POD in our derivation of an OEL to protect at the most sensitive level of biological effect. The benchmark concentrations for this endpoint were lower than Sung et al.'s (2009) suggested NOAEL of 133 ug/m^3.

OEL Derivation

To derive an OEL, a human equivalent concentration (HEC) at the rat derived BMC and BMCL was calculated by adjusting for toxicokinetic differences affecting dosimetry. To adjust for ventilation rate, factors of 10 m^3/day and 0.1015 m^3/day were used for humans and rats, respectively (NIOSH, 2013). An interspecies dose normalizing factor of alveolar surface area (2422 cm^2 rat, 634,620 cm^2 human) was used (Miller et al., 2011, NIOSH, 2013) as well as a conservative clearance adjustment of 10 to 1 for rat to human (Snipes, 1989). Deposition rate differences between rats and humans were adjusted using the MPPD model generated values specific for 18.5 nm particles. The MPPD model found the pulmonary deposition fraction (shown as P, Supplemental Figure 2) of 18.5 nm particles to be 0.348 in humans and 0.29 in rats. MPPD input parameters are summarized in Supplemental Tables 1 and 2 and include consideration of ventilation during light exercise relevant for occupational settings. The rat BMCL and described dosimetric adjustment factors are used to calculate the HEC_BMCL as shown in Equations [3] and [4].

Uncertainty Factors

The HEC_BMCL is divided by uncertainty factors, as consistent with NIOSH's approach in deriving an OEL for engineered nanomaterials and largely equivalent to ECHA REACH guidance (NIOSH 2013, ECHA 2012). An uncertainty factor of 3 is used to account for uncertainties in toxicodynamic differences between species (Brown et al., 2005, Jarabek et al., 2005, US EPA, 1994). An uncertainty factor of 2 is included for extrapolation of subchronic effects to chronic effects and an intra species factor of 5 is applied to account for variability within workers (Aschberger et al., 2010, ECHA, 2012). A modifying factor for severity of endpoint was considered as some evidence of DNA damage in the Comet assay was observed with high exposure concentration in a 12 week inhalation exposure study (Cho et al., 2013), however Kim et al. (2011) found no statistically significant evidence of chromosomal breakage in these same test animals. Additional summaries of the genotoxicity data suggests indirect effects at only high doses, therefore a modifying factor of 1 is used (SCENIHR, 2014) (Foldbjerg et al., 2011). Uncertainty factors for sensitivity of children were not considered in the derived OEL as our estimates are aimed to protect worker populations that do not include children.

$$HEC\_BMCL = \frac{25.55\mu g/m^3}{\left(\frac{10m^3/day}{0.1015m^3/day}\right)x\left(\frac{0.348}{0.290}\right)x\left(\frac{10}{1}\right)x\left(\frac{2422cm^2}{634{,}620cm^2}\right)} = 5.66\mu g/m^3 \quad [3]$$

$$OEL = \frac{5.66\mu g/m^3}{3\ x\ 2\ x\ 5\ x\ 1} = 0.19\mu g/m^3 \quad [4]$$

OEL Recommendation

The rat derived Dosimetrically Adjusted BMC of 25.55 μg/m^3 at the critical effect of bile duct hyperplasia in female rats would provide a derived HEC_BMCL of 5.66 μg/m^3 and an OEL of 0.19 μg/m^3 to protect against liver and lung damage from inhalation of AgNPs in the workplace shown in equation [4].

Discussion

There is a need to develop an OEL to protect workers from potential adverse health effects from workplace exposure to AgNPs. While various methods have been proposed to derive OELs, an OEL that integrates dosimetry and adjusts for interspecies differences and intraspecies variability provides insight on the level of control needed to provide safe working environments without possibility of long-term or persistent health effects. The OEL derivation presented considers dosimetric tissue distribution of silver to target organs while adjusting for toxicokinetics, toxicodynamics, and variability of effects from chronic exposure to AgNPs in workers. The recommended OEL of 0.19 μg/m^3 falls within range of measurable levels in workplace air by area and personal sampling shown in Table 1.

The OEL presented is calculated using a dosimetrically adjusted BMCL derived from the BMDL calculated by delivered dose. Calculating BMDs by delivered dose to the target organ, as opposed to an exposure concentration, represents the dosimetry of silver as it is distributed throughout the body. Consideration of tissue dosimetry allows for the comparison of sensitivity of tissues to nanomaterials due to differing tissue conditions (Brown et al., in press). Comparisons of BMDs by total silver in target organs showed BMDs for liver endpoints to be two orders of magnitude lower than BMDs for lung endpoints in females. This is of particular interest as while lesser amounts of silver are observed to be deposited in liver, significant adverse liver effects occurred at lower doses compared to lung. Our method allowed for the detection of liver sensitivity to AgNPs that was able to be translated to units measurable in the

workplace. Our findings point to the significance of consideration of dosimetry in OEL estimations for engineered nanomaterials.

A linear increase of silver with increasing exposure concentration is observed in female and male liver and lung in Sung et al. (2009) (Supplemental Figure 1). Soluble and semi-soluble nanoparticles (including silver) have been observed to be absorbed systemically (Landsiedel et al., 2012) and evidence of translocation of silver from the air-blood barrier (Geiser and Kreyling, 2010) support the potential for effects in liver and other organs resulting from inhalation exposure. This linear relationship suggests there is limited need for consideration of particle overload and saturation in this exposure range and suggests a relatively consistent rate of deposition and retention throughout the exposure range evaluated. Correcting for dosimetry when deriving an OEL may be even more critical in cases where a non-linear tissue dose to exposure concentration relationship exists.

Dissolution and clearance of AgNPs following exposure were critical factors considered in deriving an OEL for AgNPs. AgNPs have been observed to be partially soluble *in vitro* and *in vivo*. Dissolution of AgNPs has been shown to depend on particle size, pH of the solution, ions present in the solution, aggregation state, and incubation time (Leo et al., 2013, Ma et al., 2012, Stebounova et al., 2011). When compared with larger micro-sized particles, smaller nanoparticles have been observed to dissolve faster due to their high surface to volume ratio. Ma et al. (2012) found the dissolution of AgNPs to range from 1% for 80 nm particles to 60% for 5 nm particles at pH 8 during three and two months of incubation, respectively. The smaller size of nanoparticles suggest higher dissolution rate and lower biodurability and thus greater potential to cause pathogenicity (Utembe et al., 2015). This generally supports the potential of silver from AgNPs in tissues other than lung having occurring from absorption of silver through the lung by dissolution. Some differences in lung clearance rates in rats exposed to different AgNP concentrations could be raised from differential dissolution rates of AgNP and involvement of macrophages in the clearance process depending on concentration. Secondary AgNP generation after dissolution further

complicates the clearance process (van der Zande et al. 2012; Walczak et al. 2013; Loeschner et al. 2011). Currently no technological tools are available to differentiate primary AgNPs from secondary AgNPs, thus the differential clearance among different concentrations of AgNP could not be explained completely.

Our calculations assume that silver in AgNPs is at least partially soluble and that the silver observed in tissues is due to the exposure. This assumption is supported by the observed linear increase in silver tissue content with exposure concentration shown in Supplemental Figure 1. While many non-soluble nanoparticles have not been observed to distribute systemically, soluble nanomaterials such as silver have been suggested to behave similarly to biologically available chemicals (Landsiedel et al., 2012).

When determining human health risk from rat derived dosimetry data in our study, toxicokinetic factors were important considerations. When AgNPs are inhaled by rats or humans, they may deposit within the airway or deep lung. In the airway, particles may be removed by mechanical clearance while AgNPs deposited in the deep lung may be absorbed by dissolution or mechanically cleared into the airway. Mechanical clearance may lead to ingestion of AgNPs and potential further absorption through the GI tract. Additionally, AgNPs may be absorbed from the deep lung into the interstitium where Gregorratto et al. suggest slower clearance and recovery than other routes (Gregoratto et al., 2010).

The deposition and subsequent dissolution of AgNP can occur throughout the respiratory tract. Therefore, calculation of the HEC should consider deposition, retention, and dissolution of AgNP in all regions. However, the AgNP deposited in the tracheobronchial and the upper (head) respiratory tract will be cleared by mucociliary action rapidly within 24 hr into the GI tract, with a very small fraction of Ag becoming "dissolved" during tracheobronchial transit, and some dissolution and uptake occurring in the GI tract with a short transit time as well. Since our estimation of the BMCL is based on liver silver content, the dissolution in these areas is already included. Our approach to derive the HEC BMCL is based on the amount in the alveolar region because this is the area with a very long retention and, therefore, represents

by far the main AgNP dose in the body, in contrast to the transient levels in the other regions with no accumulation. Therefore, the short-lived tracheobronchial deposition does not significantly contribute to the high retained lung burden so that correlating the observed effects in the liver with the retained alveolar dose is well justified.

The basis of the Sung et al. (2009) subchronic inhalation study utilized in our estimation assumes there to be minimal airborne silver GI tract uptake by the study animals. This assertion is supported in the literature finding that in inhalation studies "oral and dermal uptake of different micro- and nano-sized test materials has been proven to be negligible" (Keller et al., 2014). In reviewing relevant information on AgNPs SCENIHR (2014) concluded that although systemic uptake through the GI-tract following inhalation cannot be fully excluded, the quantitative information available would suggest oral absorption rates of <0.1 to 4%. We estimate this from the data as Park et al. (2011) found 1-4% oral bioavailability of AgNPs from oral administered doses. Loeschner et al. (2011) observed a urinary excretion fraction of <0.1% of AgNPs from ingestion. When considering less than 100% of the AgNPs deposited in the lung is transferred to the GI tract, we estimate <0.1-4% of inhaled AgNPs are absorbed through the GI tract. Additionally, because the BMD or BMDL are calculated by delivered dose and related external exposure, this issue remains of little additional relevance for setting the OEL. Our methods assumed that the dissolution, absorption, and retention rates of AgNPs in the lung are similar in rats and humans and that equal tissue dose in humans and rats will elicit similar responses across species.

Subchronic inhalation studies by Song et al. (2013) investigating clearance and recovery from effects of AgNP exposure in rats observed significantly different lung clearance half-times of silver ($p<0.001$) of 16, 62, and 42 days in low, middle, and high exposed males respectively, and 21, 81, and 38 days in low, middle, and high exposed females (Supplemental Figure 4). No significant differences were observed between genders ($p>0.2$). Organ silver concentrations and recovery from effects were measured for 84 days in the lung. However, *in vivo* dissolution rates were not available from the lung. In order to

determine the potential impact of clearance and retention for our calculations, a sensitivity analysis was performed where all silver measured in the lung was assumed to have resulted from particle clearance, dissolution was null, and dissolved silver from the earlier exposure period was not retained in the lung. Lung clearance rates over the 84 day recovery period were observed to have a range of half-times of 18 to 69 days (Supplemental Figure 4). Lung clearance rates in humans over the same period would be approximately 690 days (Gregoratto et al, 2010; Borm et al., 2015). Thus, the rates in the rat were 10 to 38 times faster than humans. The OEL presented is calculated using the slower rate observed of 10 to 1 (690 days and 69 days, respectively). Using the fastest clearance rate observed (18 days) in the rat would impact the OEL by making it a factor of 3.8 higher and would be reflective of "clearance" by dissolution and not by mechanical clearance. Recovery data from Song et al., 2013 in liver and kidney (Supplemental Figures 5 and 6) show a linear decrease in silver tissue burden. These half-times suggest dissolution and absorption of silver is occurring in the lung.

A variety of toxicokinetic data indicate that silver, in ionic form or as AgNPs, whether ingested orally or via injection or inhalation, can be distributed to most organs including the liver, kidneys, lungs, spleen, brain, blood, ovaries, and testes (Ji et al., 2007, Kim et al., 2008, Lankveld et al., 2010, Lee et al., 2013a, Park et al., 2010, Song et al., 2013, Sung et al., 2009, van der Zande et al., 2012). The tissue distribution data indicated that the inhalation of AgNPs with an average diameter of 18-19 nm (Sung et al., 2009) and 12-15 nm (Ji et al., 2007) and the oral administration of 56-60 nm AgNPs showed similar tissue distributions. Interestingly, silver biopersistence was observed in the brain and testes after the oral administration of silver nitrate, uncoated AgNPs, and PVP-coated AgNPs for 28 days, followed by 8 weeks of recovery (Lankveld et al., 2010). Such biopersistence in the brain and testes was also observed after the oral administration of citrate-coated AgNPs for 28 days, followed by 4 months of recovery (Lee et al., 2013a). This suggests that biological barriers, such as the blood-brain barrier and blood-testis barrier, may play a role in silver clearance from these tissues (Lee et al., 2013a).

The observation of bile duct hyperplasia in rats after subchronic inhalation to AgNPs was found to be consistent with a subchronic oral dosing study by Kim et al (2010) that also found increased incidence of bile duct hyperplasia in F344 rats after 90 day oral dosing. Additionally, a recent study by US NCTR by Boudreau et al (2016) indicated that gender differences in silver accumulations were noted for a number of tissues and organs, with accumulations significantly higher in female SD rats, especially in the kidney, liver, jejunum, and colon. In this way, hepatotoxicty in females may be due to more accumulation of silver in the liver. A gender-related distribution of silver in the kidneys was also consistent with results from oral and inhalation studies and suggest higher silver levels in females compared to males at the same exposures (Kim et al., 2008, Kim et al., 2010, Lee et al., 2013a, Song et al., 2013, Sung et al., 2009). Thus, the calculated OEL based on female liver endpoints may be more protective for males than females.

Our OEL estimation is based on studies investigating 18-19 nm uncoated AgNPs. Studies by (Ji et al., 2007, Song et al., 2013, Sung et al., 2009) suggest that coatings on AgNPs do not appear to have effects on *in vivo* ADME when compared with the use of uncoated AgNPs. Such studies include AgNPs generated by evaporation/condensation, as used in some inhalation toxicity studies, dry powder, as used in some oral toxicity studies (Kim et al., 2008, 2010), and PVP-coated AgNPs (Loeschner et al., 2011, van der Zande et al., 2012). When evaluating the toxicity of the citrate-coated AgNPs used in the Lee et al. study (2013a), the extent of the toxicity was quite similar to that of the uncoated dry powder used in the previous studies by Kim et al. (2008, 2010). With respect to silver release, uncoated and citrate-coated AgNPs utilized in our selected study may be expected to represent a worst-case scenario over AgNPs with other stabilizers such as SDS and Tween 80 (Li et al., 2012).

When comparing the size of AgNPs in inhalation toxicity testing (18-19 nm) with agglomerated AgNPs in the workplaces, the agglomerated particles, defined as collection of weakly or medium strongly bound *particles* where the resulting external surface area is similar to the sum of the surface area of the individual

components (ISO TS 80004-2, 2015), have similar surface area as sum of individual nanoparticles. Thus surface Ag ion generation would be similar as the sum of individual AgNPs. Although the agglomerated Ag may exhibit different lung deposition when compared with individual AgNPs, 18-19 nm particle sizes are estimated have greatest potential for alveolar deposition according to ICRP (1994) and the MPPD model (2009). Furthermore, primary particle sizes of AgNPs measured in the workplace were nearly 20 nm (Lee et al., 2011). Therefore, our estimation would be worst-case scenario in the workplace.

While our estimation of a health protective OEL for AgNPs includes a robust analysis of factors contributing to health effects from AgNP exposures in the workplace, several limitations have been identified. The proposed OEL is based largely on animal data that assumes AgNPs will have similar biological effects in humans as observed with rats in the studies utilized. This factor is accounted for by inclusion of an uncertainty factor and considerations for toxicokinetic and toxicodynamic differences in humans and tested animals, however the difference in effect remains uncertain. The lack of available AgNP dissolution data for humans and rats *in vivo* limits the ability to determine differences in absorption and delivered dose between species as well as in determining the amount absorbed through lung or by mechanical clearance and absorption through the GI system. Data gaps on carcinogenicity and reproductive toxicity of AgNPs currently exist, which may potentially identify sensitive effects from exposure. In addition, the health effects from the biopersistence of silver in the brain and testes and gender difference in kidney biodistribution need to be considered and evaluated in future studies. This publication has provided an HEC-based OEL for silver nanoparticles. The scientific basis for calculating the HEC is provided and may be used to form the basis of OELs for country- or workplace-specific situations.

Conclusions

Although there is a lack of long-term toxicity data, exposure data, and human health effects information, an OEL for AgNPs is needed to protect workers' health from exposure due to differences in

physicochemical properties of nano and micro-sized silver particles. The current OELs for silver dust and soluble silvers are 100 and 10 μg/m^3, respectively (ACGIH, 2013), while the OSHA PEL and NIOSH REL for silver dust and soluble silvers are 10 μg/m^3 to protect against argyria from exposure. In contrast, AgNPs present other health effects including liver and lung toxicity in animal studies. The proposed OEL of 0.19 μg/m^3, derived from dosimetric measurements of silver in lung and liver, as well as recovery studies, is expected to prevent liver and lung damage and argyria from AgNPs exposure in workers. Exposure mitigation technologies, including isolation and encapsulation, industrial ventilation, and administrative control to limit access to the high exposure area should be implemented to lower workplace exposure levels below the proposed OEL.

Declaration of Interest

The authors declare no competing financial interests. This work was done in collaboration with the NCNHIR Consortium and supported by NIH/NIEHS grants U19ES019545, P30ES07033 and RD83573801, and supported by the "Development of Technologies on Safety Evaluation and Standardization of Nanomaterials and Nanoproducts (10059135)" through the Korea Evaluation Institute of Industrial Technology by the Korean Ministry of Trade, Industry & Energy.

Chapter 2 References

Acgih 2013. TLVs and BEIs. Cincinnati: American Conference of Governmental Industrial Hygienists.

Allen BC, Kavlock RJ, Kimmel CA,Faustman EM 1994. Dose-response assessment for developmental toxicity. II. Comparison of generic benchmark dose estimates with no observed adverse effect levels. *Fundamental and applied toxicology : official journal of the Society of Toxicology,* 23**,** 487-95.

Aschberger K, Johnston HJ, Stone V, Aitken RJ, Hankin SM, Peters SA, Tran CL,Christensen FM 2010. Review of carbon nanotubes toxicity and exposure--appraisal of human health risk assessment based on open literature. *Crit Rev Toxicol,* 40**,** 759-90.

Asharani PV, Low Kah Mun G, Hande MP,Valiyaveettil S 2009. Cytotoxicity and genotoxicity of silver nanoparticles in human cells. *ACS Nano,* 3**,** 279-90.

Borm P, Cassee FR,Oberdorster G 2015. Lung particle overload: old school -new insights? *Part Fibre Toxicol,* 12**,** 10.

Boudreau MD, Imam MS, Paredes AM, Bryant MS, Cunningham CK, Felton RP, Jones MY, Davis KJ,Olson GR 2016. Differential Effects of Silver Nanoparticles and Silver Ions on Tissue Accumulation, Distribution, and Toxicity in the Sprague Dawley Rat Following Daily Oral Gavage Administration for 13 Weeks. *Toxicol Sci*.

Braakhuis HM, Gosens I, Krystek P, Boere JA, Cassee FR, Fokkens PH, Post JA, Van Loveren H,Park MV 2014. Particle size dependent deposition and pulmonary inflammation after short-term inhalation of silver nanoparticles. *Part Fibre Toxicol,* 11**,** 49.

Brown JM, Bai W, Shannahan JH, Altemeier WA, Mcmahan R, Tetley TD, Ryan MP, Porter AE, Liu R, Xia T, Smith J,Thrall BD in press. Consortium Perspective on Silver Nanoparticle *In vitro* Toxicity: Role of Cell Specificity and Variability in Biological Response.

Brown JS, Wilson WE,Grant LD 2005. Dosimetric comparisons of particle deposition and retention in rats and humans. *Inhalation toxicology,* 17**,** 355-85.

Catsakis LH,Sulica VI 1978. Allergy to silver amalgams. *Oral Surg Oral Med Oral Pathol,* 46**,** 371-5.

Cho EA, Lee WS, Kim KM,Kim SY 2008. Occupational generalized argyria after exposure to aerosolized silver. *J Dermatol,* 35**,** 759-60.

Cho HS, Sung JH, Song KS, Kim JS, Ji JH, Lee JH, Ryu HR, Ahn K,Yu IJ 2013. Genotoxicity of silver nanoparticles in lung cells of Sprague Dawley rats after 12 weeks of inhalation exposure. *Toxics,* 1.

Cho KH, Park JE, Osaka T,Park SG 2005. The study of antimicrobial activity and preservative effects of nanosilver ingredient. *Electrochimica Acta,* 51**,** 956-960.

Davis JA, Gift JS,Zhao QJ 2011. Introduction to benchmark dose methods and U.S. EPA's benchmark dose software (BMDS) version 2.1.1. *Toxicology and applied pharmacology,* 254**,** 181-91.

De Winter-Sorkina R,Cassee FR 2003. From concentration to dose: factors influencing airborne particulate matter deposition in humans and rats. Netherlands National Institute for Public Health and the Environment (RIVM).

Dfg 2006. MAK- und BAT-Werte-Liste. Deutsche Forschungsgemeinschaft.

Echa 2012. Guidance on information requirements and chemical safety assessment Chapter R.14: Occupational exposure estimation. European Chemicals Agency

Faustman EM, Allen BC, Kavlock RJ,Kimmel CA 1994. Dose-response assessment for developmental toxicity. I. Characterization of database and determination of no observed adverse effect levels. *Fundamental and applied toxicology : official journal of the Society of Toxicology,* 23**,** 478-86.

Foldbjerg R, Dang DA,Autrup H 2011. Cytotoxicity and genotoxicity of silver nanoparticles in the human lung cancer cell line, A549. *Arch Toxicol,* 85**,** 743-50.

Geiser M,Kreyling WG 2010. Deposition and biokinetics of inhaled nanoparticles. *Particle and fibre toxicology,* 7**,** 2.

Gregoratto D, Bailey MR,Marsh JW 2010. Modelling particle retention in the alveolar-interstitial region of the human lungs. *J Radiol Prot,* 30**,** 491-512.

Hadrup N,Lam HR 2014. Oral toxicity of silver ions, silver nanoparticles and colloidal silver--a review. *Regul Toxicol Pharmacol,* 68**,** 1-7.

Heyl T 1979. Contact dermatitis from silver coat. *Contact Dermatitis,* 5**,** 197.

Jarabek AM, Asgharian B,Miller FJ 2005. Dosimetric Adjustments for Interspecies Extrapolation of Inhaled Poorly Soluble Particles (PSP). *Inhalation Toxicology,* 17**,** 317-334.

Ji JH, Jung JH, Kim SS, Yoon JU, Park JD, Choi BS, Chung YH, Kwon IH, Jeong J, Han BS, Shin JH, Sung JH, Song KS,Yu IJ 2007. Twenty-eight-day inhalation toxicity study of silver nanoparticles in Sprague-Dawley rats. *Inhal Toxicol,* 19**,** 857-71.

Kavlock RJ, Allen BC, Faustman EM,Kimmel CA 1995. Dose-response assessments for developmental toxicity. IV. Benchmark doses for fetal weight changes. *Fundamental and applied toxicology : official journal of the Society of Toxicology,* 26**,** 211-22.

Keller J, Wohlleben W, Ma-Hock L, Strauss V, Groters S, Kuttler K, Wiench K, Herden C, Oberdorster G, Van Ravenzwaay B,Landsiedel R 2014. Time course of lung retention and toxicity of inhaled particles: short-term exposure to nano-Ceria. *Archives of toxicology,* 88**,** 2033-59.

Kim JS, Song KS, Sung JH, Ryu HR, Choi BG, Cho HS, Lee JK,Yu IJ 2013. Genotoxicity, acute oral and dermal toxicity, eye and dermal irritation and corrosion and skin sensitisation evaluation of silver nanoparticles. *Nanotoxicology,* 7**,** 953-60.

Kim JS, Sung JH, Ji JH, Song KS, Lee JH, Kang CS,Yu IJ 2011. *In vivo* Genotoxicity of Silver Nanoparticles after 90-day Silver Nanoparticle Inhalation Exposure. *Saf Health Work,* 2**,** 34-8.

Kim YS, Kim JS, Cho HS, Rha DS, Kim JM, Park JD, Choi BS, Lim R, Chang HK, Chung YH, Kwon IH, Jeong J, Han BS,Yu IJ 2008. Twenty-eight-day oral toxicity, genotoxicity, and gender-related tissue distribution of silver nanoparticles in Sprague-Dawley rats. *Inhalation toxicology,* 20**,** 575-83.

Kim YS, Song MY, Park JD, Song KS, Ryu HR, Chung YH, Chang HK, Lee JH, Oh KH, Kelman BJ, Hwang IK,Yu IJ 2010. Subchronic oral toxicity of silver nanoparticles. *Particle and fibre toxicology,* 7**,** 20.

Kimmel CA, Kavlock RJ, Allen BC,Faustman EM 1995. The application of benchmark dose methodology to data from prenatal developmental toxicity studies. *Toxicology letters,* 82-83**,** 549-54.

Landsiedel R, Fabian E, Ma-Hock L, Van Ravenzwaay B, Wohlleben W, Wiench K,Oesch F 2012. Toxico-/biokinetics of nanomaterials. *Archives of toxicology,* 86**,** 1021-60.

Lankveld DP, Oomen AG, Krystek P, Neigh A, Troost-De Jong A, Noorlander CW, Van Eijkeren JC, Geertsma RE,De Jong WH 2010. The kinetics of the tissue distribution of silver nanoparticles of different sizes. *Biomaterials,* 31**,** 8350-61.

Lee JH, Ahn K, Kim SM, Jeon KS, Lee JS,Yu IJ 2012a. Continuous 3-day exposure assessment of workplace manufacturing silver nanoparticles. *Journal of Nanoparticle Research,* 14.

Lee JH, Kim YS, Song KS, Ryu HR, Sung JH, Park JD, Park HM, Song NW, Shin BS, Marshak D, Ahn K, Lee JE,Yu IJ 2013a. Biopersistence of silver nanoparticles in tissues from Sprague-Dawley rats. *Particle and fibre toxicology,* 10**,** 36.

Lee JH, Kwon M, Ji JH, Kang CS, Ahn KH, Han JH,Yu IJ 2011. Exposure assessment of workplaces manufacturing nanosized TiO2 and silver. *Inhalation toxicology,* 23**,** 226-36.

Lee JH, Mun J, Park JD,Yu IJ 2012b. A health surveillance case study on workers who manufacture silver nanomaterials. *Nanotoxicology,* 6**,** 667-9.

Lee JH, Sohn EK, Ahn JS, Ahn K, Kim KS, Lee TM,Yu IJ 2013b. Exposure assessment of workers in printed electronics workplace. *Inhalation toxicology,* 25**,** 426-34.

Leo BF, Chen S, Kyo Y, Herpoldt KL, Terrill NJ, Dunlop IE, Mcphail DS, Shaffer MS, Schwander S, Gow A, Zhang J, Chung KF, Tetley TD, Porter AE,Ryan MP 2013. The stability of silver nanoparticles in a model of pulmonary surfactant. *Environ Sci Technol,* 47**,** 11232-40.

Li P, Li J, Wu CZ, Wu QS,Li J 2005. Synergistic antibacterial effects of beta-lactam antibiotic combined with silver nanoparticles. *Nanotechnology,* 16**,** 1912-1917.

Li X, Lenhart JJ,Walker HW 2012. Aggregation kinetics and dissolution of coated silver nanoparticles. *Langmuir,* 28**,** 1095-104.

Loeschner K, Hadrup N, Qvortrup K, Larsen A, Gao X, Vogel U, Mortensen A, Lam HR,Larsen EH 2011. Distribution of silver in rats following 28 days of repeated oral exposure to silver nanoparticles or silver acetate. *Part Fibre Toxicol,* 8**,** 18.

Ma R, Levard C, Marinakos SM, Cheng Y, Liu J, Michel FM, Brown GE,Lowry GV 2012. Size-controlled dissolution of organic-coated silver nanoparticles. *Environ Sci Technol,* 46**,** 752-9.

Marks R 1966. Contact dermatitis due to silver. *Br J Dermatol,* 78**,** 606-7.

Maronpot RR 2014. Liver, Bile Duct—Hyperplasia. *In:* CESTA, M. F., HERBERT, R. A., BRIX, A., MALARKEY, D. E.,SILLS, R. C. (eds.) *National Toxicology Program Nonneoplastic Lesion Atlas.*

Miller FJ, Kimbell JS, Preston RJ, Overton JH, Gross EA,Conolly RB 2011. The fractions of respiratory tract cells at risk in formaldehyde carcinogenesis. *Inhalation toxicology,* 23**,** 689-706.

Morones JR, Elechiguerra JL, Camacho A, Holt K, Kouri JB, Ramirez JT,Yacaman MJ 2005. The bactericidal effect of silver nanoparticles. *Nanotechnology,* 16**,** 2346-53.

Niosh 2013. Occupational Exposure to Carbon Nanotubes and Nanofibers. *In:* NIOSH (ed.) *Current Intelligence Bulletin.* National Institute for Occupational Safety and Health.

Oecd 2010. Report of the Workshop on Risk Assessment of Manufactured Nanomaterials in a regulatory context. *No. 21 - ENV/JM/MONO(2010)10.* Paris: Organisation for Economic Co-operation and Development.

Oecd 2014. Genotoxicity of Manufactured Nanomaterials: Report of the OECD Expert Meeting. *ENV/JM/MONO(2014)34.* Organisation for Economic Co-operation and Development.

Oller AR,Oberdorster G 2010. Incorporation of particle size differences between animal studies and human workplace aerosols for deriving exposure limit values. *Regulatory toxicology and pharmacology : RTP,* 57**,** 181-94.

Park EJ, Bae E, Yi J, Kim Y, Choi K, Lee SH, Yoon J, Lee BC,Park K 2010. Repeated-dose toxicity and inflammatory responses in mice by oral administration of silver nanoparticles. *Environ Toxicol Pharmacol,* 30**,** 162-8.

Park J, Kwak BK, Bae E, Lee J, Kim Y, Choi K,Yi J 2009. Characterization of exposure to silver nanoparticles in a manufacturing facility. *Journal of Nanoparticle Research,* 11**,** 1705-1712.

Park K, Park EJ, Chun IK, Choi K, Lee SH, Yoon J,Lee BC 2011. Bioavailability and toxicokinetics of citrate-coated silver nanoparticles in rats. *Arch Pharm Res,* 34**,** 153-8.

Pauluhn J 2010. Multi-walled carbon nanotubes (Baytubes): approach for derivation of occupational exposure limit. *Regul Toxicol Pharmacol,* 57**,** 78-89.

Quadros ME,Marr LC 2010. Environmental and human health risks of aerosolized silver nanoparticles. *Journal of the Air & Waste Management Association,* 60**,** 770-81.

Scenihr 2014. Nanosilver: safety, health and environmental effects and role in antimicrobial resistance. Scientific Committee on Emerging and Newly Identified Health Risks.

Schafer B, Brocke JV, Epp A, Gotz M, Herzberg F, Kneuer C, Sommer Y, Tentschert J, Noll M, Gunther I, Banasiak U, Bol GF, Lampen A, Luch A,Hensel A 2013. State of the art in human risk assessment of silver compounds in consumer products: a conference report on silver and nanosilver held at the BfR in 2012. *Arch Toxicol,* 87**,** 2249-62.

Slob W 2002. Dose-response modeling of continuous endpoints. *Toxicological sciences : an official journal of the Society of Toxicology,* 66**,** 298-312.

Snipes MB 1989. Long-Term Retention and Clearance of Particles Inhaled by Mammalian Species. *Critical Reviews in Toxicology,* 20**,** 175-211.

Sondi I,Salopek-Sondi B 2004. Silver nanoparticles as antimicrobial agent: a case study on E. coli as a model for Gram-negative bacteria. *J Colloid Interface Sci,* 275**,** 177-82.

Song KS, Sung JH, Ji JH, Lee JH, Lee JS, Ryu HR, Lee JK, Chung YH, Park HM, Shin BS, Chang HK, Kelman B,Yu IJ 2013. Recovery from silver-nanoparticle-exposure-induced lung inflammation and lung function changes in Sprague Dawley rats. *Nanotoxicology,* 7**,** 169-80.

Stebounova LV, Adamcakova-Dodd A, Kim JS, Park H, O'shaughnessy PT, Grassian VH,Thorne PS 2011. Nanosilver induces minimal lung toxicity or inflammation in a subacute murine inhalation model. *Part Fibre Toxicol,* 8**,** 5.

Sung JH, Ji JH, Park JD, Yoon JU, Kim DS, Jeon KS, Song MY, Jeong J, Han BS, Han JH, Chung YH, Chang HK, Lee JH, Cho MH, Kelman BJ,Yu IJ 2009. Subchronic inhalation toxicity of silver nanoparticles. *Toxicological sciences : an official journal of the Society of Toxicology,* 108**,** 452-61.

Sung JH, Ji JH, Song KS, Lee JH, Choi KH, Lee SH,Yu IJ 2011. Acute inhalation toxicity of silver nanoparticles. *Toxicology and industrial health,* 27**,** 149-54.

Sung JH, Ji JH, Yoon JU, Kim DS, Song MY, Jeong J, Han BS, Han JH, Chung YH, Kim J, Kim TS, Chang HK, Lee EJ, Lee JH,Yu IJ 2008. Lung function changes in Sprague-Dawley rats after prolonged inhalation exposure to silver nanoparticles. *Inhalation toxicology,* 20**,** 567-74.

Suva 2007. Grenzwerte am Arbeitsplatz. Schweizerische Unfallversicherungsanstalt.

Us Epa 1994. Methods for Derivation of Inhalation Reference Concentrations and Application of Inhalation Dosimetry Research Triangle Park, NC 27711: United States Environmental Protection Agency.

Us Epa 2012. Benchmark Dose Technical Guidance. Washington, DC: United States Environmental Protection Agency.

Usepa. 2015. *Benchmark Dose Software Version 2.6.0* [Online]. Available: http://www2.epa.gov/bmds.

Utembe W, Potgieter K, Stefaniak AB,Gulumian M 2015. Dissolution and biodurability: Important parameters needed for risk assessment of nanomaterials. *Part Fibre Toxicol,* 12**,** 11.

Van Der Zande M, Vandebriel RJ, Van Doren E, Kramer E, Herrera Rivera Z, Serrano-Rojero CS, Gremmer ER, Mast J, Peters RJ, Hollman PC, Hendriksen PJ, Marvin HJ, Peijnenburg AA,Bouwmeester H 2012. Distribution, elimination, and toxicity of silver nanoparticles and silver ions in rats after 28-day oral exposure. *ACS Nano,* 6**,** 7427-42.

Wignall JA, Shapiro AJ, Wright FA, Woodruff TJ, Chiu WA, Guyton KZ,Rusyn I 2014. Standardizing benchmark dose calculations to improve science-based decisions in human health assessments. *Environmental health perspectives,* 122**,** 499-505.

Woodrow Wilson International Center for Scholars W. 2015. *The project on emerging nanotechnologies* [Online]. Available: http://www.nanotechproject.org/inventories/.

Table 1. Workplace AgNP exposure in gas and liquid phase synthesis, and printed electronic production facilities.

Study	AgNP size and coating	Route of exposure	Occupational activity	Sampling type	Exposure conc. Area	Exposure conc. Personal	Health effect
Workplace exposure							
Lee et al., 2011 Workplace C	<100 nm Coating not specified	Aerosol	Gas phase synthesis	Area & personal	0.02–1.02 μg/m^3	0.12–1.02 μg/m^3	Not reported
Lee et al., 2011 Workplace D	15–710.5 nm Citrate coating	Aerosol	Liquid synthesis & application	Area	0.03–0.43 μg/m^3	Not reported	Not reported
Lee et al., 2013b	14.3–697.8 nm Coating not specified	Aerosol	Printed electronic Production	Personal	Not reported	ND–0.24 μg/m^3	Not reported
Park et al., 2009	10–250 nm Coating not specified	Aerosol	Liquid phase synthesis	Area	Not reported	Not reported	Not reported
Health surveillance							
Cho et al., 2008	Unknown Coating not specified	Aerosol	Mobile telephone subunit production	Personal	Not reported	Not reported	Argyria ↑ Serum Ag
Lee et al., 2012b	<100 nm	Aerosol	Gas phase synthesis	Personal	Reported in	0.35 μg/m^3	None observed
	<100 nm Coating not specified	Aerosol	Gas phase synthesis	Personal	Lee et al., 2011 Reported in Lee et al., 2011	1.35 μg/m^3	None observed

Table 2. Summary of rat inhalation exposure studies utilized in assessments. BMDs and BMDLs (ng Ag/tissue) and derived dosimetrically adjusted BMCs and BMCLs (μg/m^3) for significant histopathology, BAL, and functional endpoints after subchronic inhalation of AgNPs in rats are reported.

Rodent study	AgNP size (nm)	Species, strain, sex, age	Route of exposure	Animal no/dose group	Exposure conc. ($\mu g/m^{3}$) duration	Endpoint response	BMD (BMDL) (ng Ag/ organ	Derived dosimetrically adjusted BMC (BMCL) (μg/m^3)
Sung et al., 2009	18–19	SD rat, male, 8 weeks	Inhalation	10	0, 49, 133, 515; 6 h/d; 5 d/week; 13 weeks	Liver abnormalities	540 (200)	177 (65.7)
						Bile duct hyperplasia	540 (200)	177 (65.7)
						Lung inflammation	6060 (1388)	124 (28.4)
Sung et al., 2009	18–19	SD rat, female, 8 weeks	Inhalation	10	0, 49, 133, 515; 6 h/d; 5 d/week; 13 weeks	Liver abnormalities	33.7 (13.6)	39.2 (15.8)
						Bile duct hyperplasia	94.9 (22.0)	110 (25.5)
						Lung inflammation	6904 (3110)	152 (68.5)
						Lung infiltrate	6859 (2522)	151 (55.6)
Sung et al., 2009	18–19	SD rat, male, 8 weeks	Inhalation	4	0, 49, 133, 515; 6 h/d; 5 d/week; 13 weeks	Albumin BAL	13316 (8174)	273 (168)
Sung et al., 2008	18–19	SD rat, female, 8 weeks	Inhalation	4	0, 49, 133, 515; 6 h/d; 5 d/week; 13 weeks	Albumin BAL	14447 (8441)	318 (186)
						LDH in BAL	7557 (5205)	166 (115)
						Total protein in BAL	11079 (7019)	244 (156)
Sung et al., 2008	18–10	SD rat, male, 8 weeks	Inhalation	4	0, 49, 133, 515; 6 h/d; 5 d/week; 13 weeks	Tidal volume	1448 (8646)	296 (177)

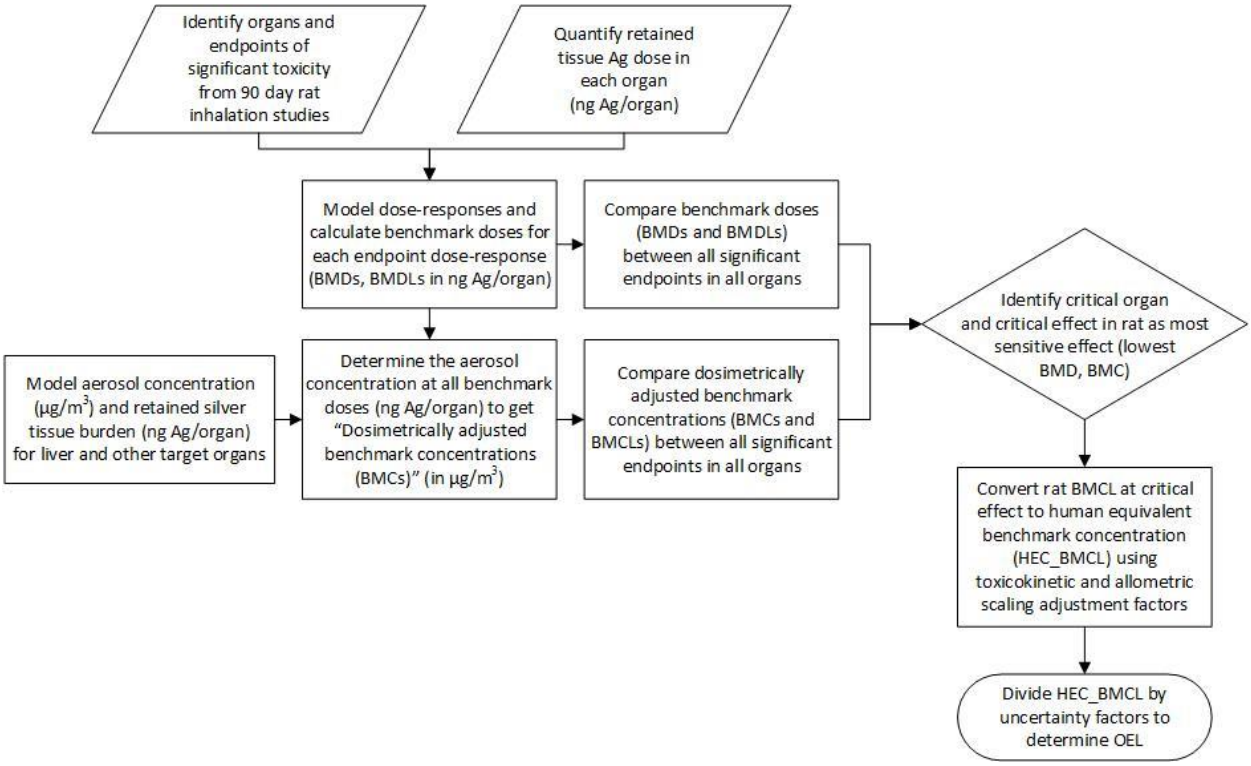

Figure 1. Mathematical framework for deriving a health-based occupational exposure limit (OEL) for silver nanoparticles (AgNPs) from *in vivo* rat inhalation studies. The OEL reflects tissue dosimetry, toxicokinetic adjustments and additional uncertainty factors.

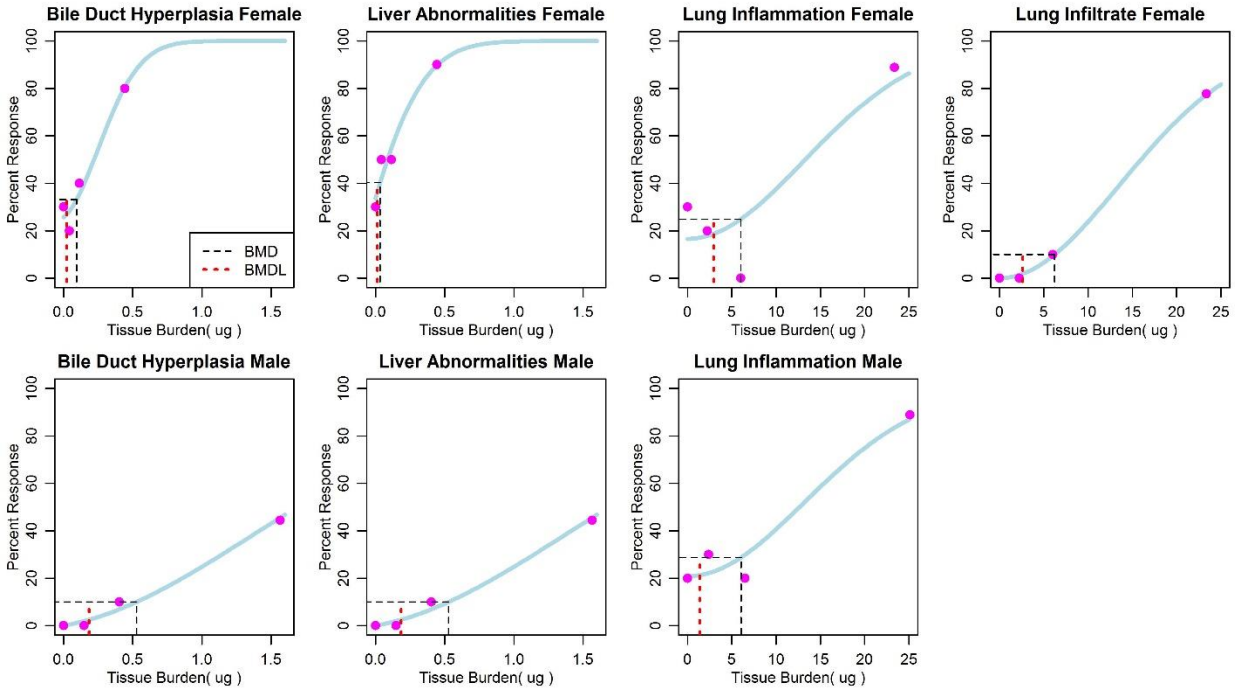

Figure 2. Benchmark dose (BMD) analysis of significant histopathology endpoints of toxicity in male and female rats after subchronic inhalation of AgNPs (Sung et al, 2009). Dose response curves are modeled as multistage polynomial degree 2 model for dichotomous data. BMDs (upper dashed lines) and BMDLs (lower dashed lines) are calculated as a 10% change in response relative to control and are indicated as tissue burden (µg silver/organ). BMDs and BMDLs are summarized in Table 2.

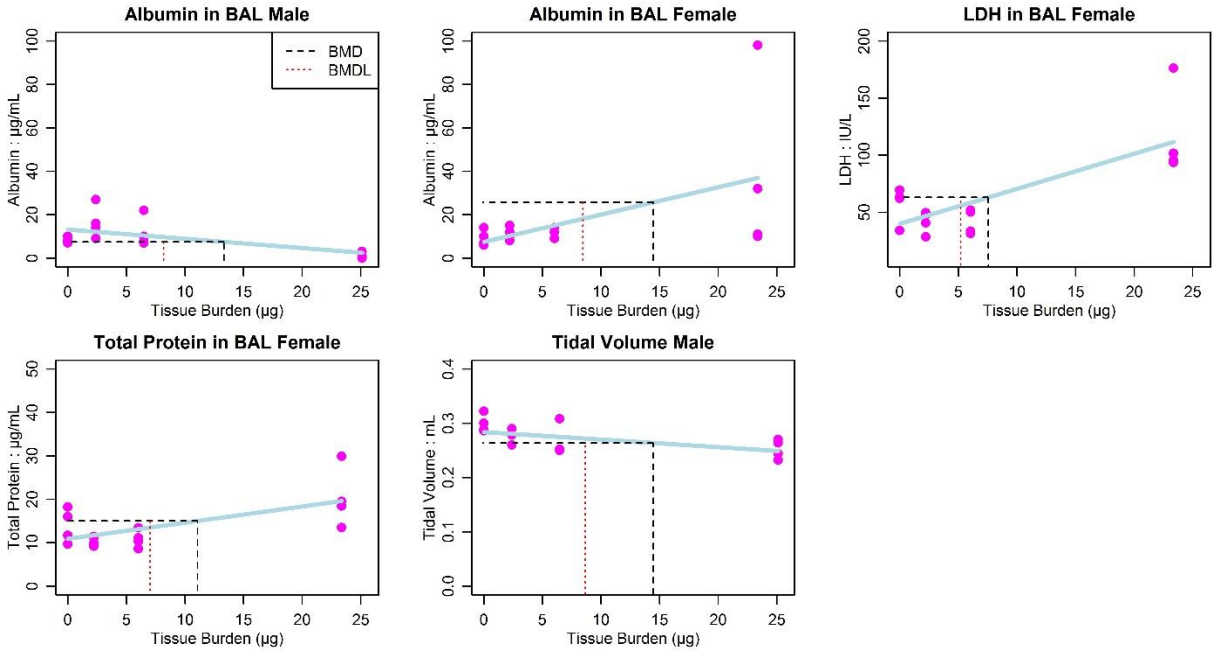

Figure 3. Benchmark dose analysis of significant endpoints of lung inflammation in male and female rats and lung function in male rats from subchronic inhalation of AgNPs (Sung et al., 2008). BMDs (upper dashed lines) and BMDLs (lower dashed lines) are calculated as a 1 standard deviation change in response relative to control and are indicated as tissue burden (µg silver/organ). BMDs and BMDLs are summarized in Table 2.

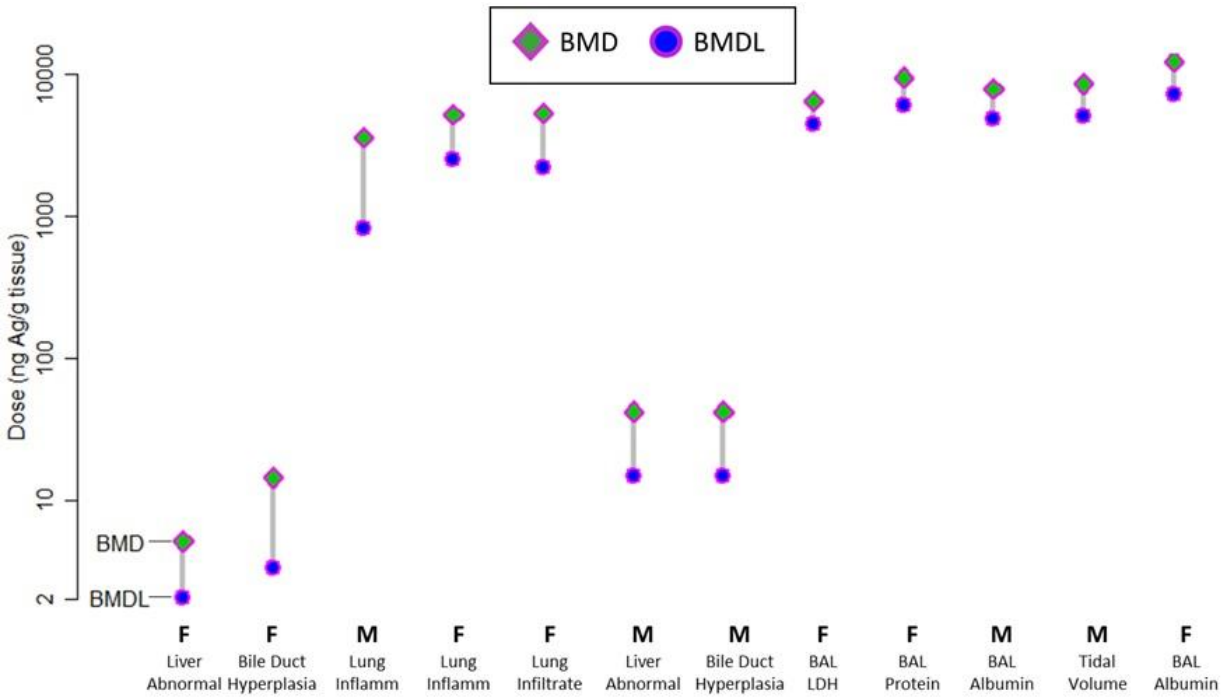

Figure 4. Benchmark dose (BMD) and 95% confidence limit of BMD (BMDL) comparison across endpoints. Histopathological, functional, and BAL endpoints are indicated across the bottom. BMDs (diamonds) and BMDLs (circles) are indicated as tissue burden (total ng silver/organ). BMDs and BMDLs are summarized in Table 2.

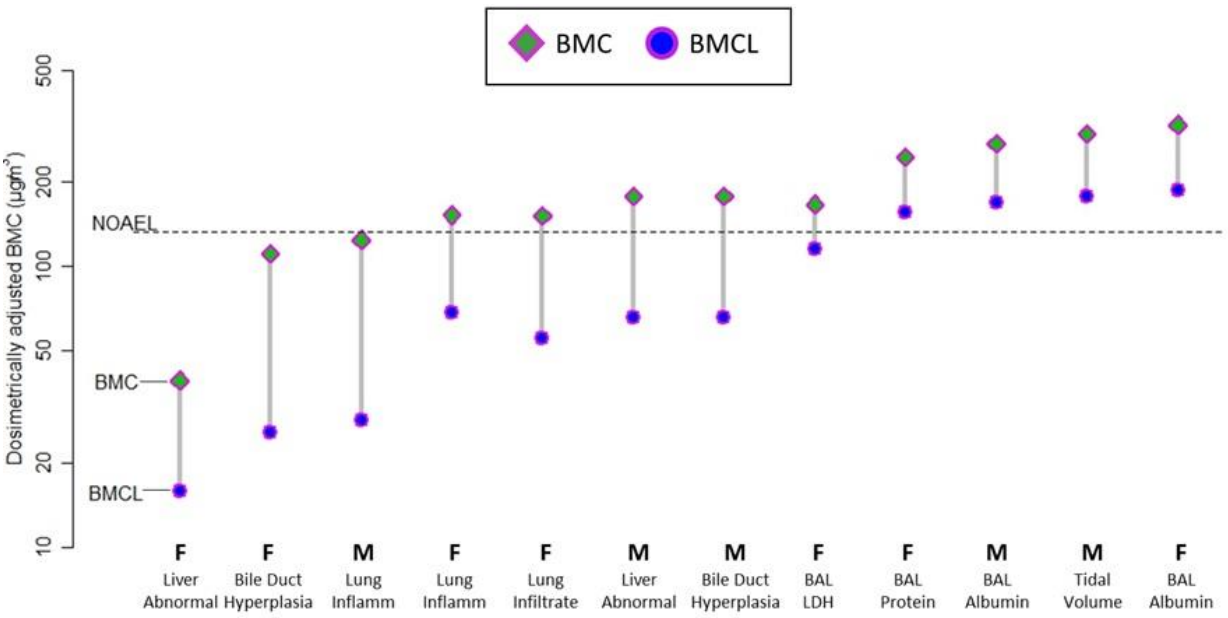

Figure 5. Dosimetrically adjusted BMC and BMCL comparison across histopathological, functional, and BAL endpoints. Endpoints are indicated across the bottom of the figure and BMCs (diamonds) and BMCLs (circles) are calculated as aerosol concentration (µg/m^3) at the BMDs and BMDLs. BMCs and BMCLs are summarized in Table 2. Sung et al., 2009 reported a NOAEL of 133 (µg/m^3) is indicated.

Chapter 3

Effects of developmental stage, particle size and coating on dosimetry and toxicity of silver nanoparticles in developing primary organotypic mouse midbrain cultures

Brittany A. Weldon[1,2] , Julie Juyoung Park[1,2] , Sungwoo Hong[1,2], Tomomi Workman[1,2], Ji Hyun Lee, Russell Dills[2], William C. Griffith[1,2], Terrance J. Kavanagh[1], and Elaine M. Faustman[1,2*]

[1]Institute for Risk Analysis and Risk Communication, University of Washington, Seattle, WA
[2]Department of Environmental and Occupational Health Sciences, University of Washington, Seattle, WA, USA

*Corresponding author: Elaine M. Faustman, Institute for Risk Analysis and Risk Communication, Department of Environmental and Occupational Health Sciences, University of Washington, Seattle, WA, USA. Email: faustman@u.washington.edu, Tel: 1-206-685-2269

Abstract

Silver nanoparticles (AgNPs) are increasingly used in consumer, commercial, and medical products for their antimicrobial properties. Human exposures to AgNPs and potential adverse effects from exposure are likely increasing with these developments. Observations of Ag in adult and fetal brain following exposures to AgNPs has led to concerns about the potential for AgNPs to elicit adverse effects on neurodevelopment and neurological function. In this study we investigated the effects of gold-cored AgNPs of differing sizes and coatings on developing murine embryonic midbrain cells grown in three-dimensional organotypic cultures. Effects were assessed at three time points of *in vitro* development corresponding to proliferation and differentiation stages of development by both nominal dose and dosimetric dose. Dosimetry was assessed in cultures using inductively coupled plasma-mass spectrometry (ICP-MS) and utilized the gold core component of the AgNPs for determination of uptake of AgNPs and silver dissolution from particles. Results by both nominal and dosimetric dose show cell death increased significantly in a dose-dependent manner at later time points that coincide with differentiation stages of development. When assessed by dosimetric dose, cultures were more sensitive to smaller particles, despite less uptake of Ag in smaller particles. We found equivalent proportions of Ag and Au in pre-exposure media and post- exposure cells, suggesting that dissolution of gold-cored AgNPs in media may not significantly contribute to the cytotoxic effects observed.

Introduction

Proper function of the central nervous system (CNS) is essential for the survival and prosperity of humans and many other species. The CNS can be damaged by many environmental and pharmacological toxicants and has been identified as a sensitive target of toxicity in a variety of exposures. The developing nervous system has been shown to be even more susceptible to perturbations than a mature nervous system (Rice and Barone, 2000). Disruption of the development of the CNS can result in lifelong neuropathologies including autism, attention deficit disorder, cerebral palsy, and mental retardation (Grandjean and Landrigan, 2006). These disorders can put immense strain on individuals, families, the healthcare system, and society. With such broad reaching and powerful implications, it is critical to address the potential for new and novel developments in drugs, chemicals, and other technologies to act as developmental neurotoxicants.

Recent technological developments have employed the use of a wide array of nano-scale materials (<100nm in at least one dimension), referred to generally as Engineered Nanomaterials (ENMs), for their attractive qualities including small size, large surface area, charge, and lightness of weight. These unique properties of ENMs also create the potential for ENMs to interact with biological systems. The utilization of ENMs in medicine, manufacturing, and industry continues to accelerate; however, much is still unknown about their potential for toxicity in many organ systems, including the developing CNS.

Silver nanoparticles (AgNPs) are ENMs that are used in many consumer products and medical devices and procedures (Woodrow Wilson International Center for Scholars, 2016). AgNPs act as antimicrobials by disrupting structural proteins, enzymes, and DNA (Reidy 2013). AgNPs have been shown to escape from nanoparticle-functionalized materials and can enter water systems, air, dust and soil (Levard et al.,

2012). Continued use of AgNPs in these and future applications increases the potential for human and environmental exposures.

Following *in vivo* oral and inhalation exposures to AgNPs, silver has been shown to translocate to the brain (although it was not specified in what form), and activate local inflammatory responses in rats (Yang et al., 2010; Loeschner et al., 2011; Patchin et al., 2016). Tang et al. observed that silver nanoparticles can cross the blood brain barrier both *in vivo* and *in vitro* (Tang et al., 2009; Tang et al., 2010). Silver has been detected in developing fetuses following oral and intravenous exposure to pregnant dams (Fennell et al., 2016). In addition, silver has been observed in the brains of fetuses following oral administration of AgNPs to lactating dams (Morishita et al., 2016), indicating a potential for exposure to silver during critical periods of CNS development.

As their applications have continued to increase over time, AgNPs have been applied to products including children's toys and clothing, as well as in products used by and marketed toward pregnant women (Woodrow Wilson International Center for Scholars, 2016). Use of AgNP-containing products during these sensitive periods of neurodevelopment creates a need for a more thorough understanding of whether exposure to AgNPs can disrupt the developing nervous system. It is our goal to characterize the potential of AgNPs to interact with and disrupt the development of the CNS using a 3-dimensional organotypic *in vitro* model. We aim to determine whether developmental stage at the time of exposure has an impact on the extent of toxicity. In addition, we examine the role of AgNP size and coating on the relative toxicity of particles at these developmental stages.

Recent innovations in *in vitro* systems have led to the development of the micromass model. The high density, 3-dimensional micromass models (developed by Flint, 1983) enable investigators to study the

formation of neural cell cultures through developmental stages of proliferation, adhesion, migration, and differentiation similar to *in vivo* development (Brown, 1995). Because of the 3-dimensional growth of micromass culture systems, stimulation with growth factors and differentiation-promoting factors is not required as development is driven primarily by cell density. Micromass techniques have enhanced our understanding of neurodevelopmental systems by serving as a model for progression of *in vivo* neurodevelopment without the use of time intensive, costly *in vivo* studies (Whittaker and Faustman, 1991; Whittaker et al., 1993; Sidhu et al., 2006; Park JY, 2017).

Because of the unique characteristics of particles in liquid media, assessments in terms of concentration (by mass, surface area, or particle number) does not allow for direct comparison of different particles. Assessing effects in terms of dosimetry, or the amount of silver in or tightly associated with cells, creates a common denominator for comparing across particles, across culture systems, and to *in vivo* studies. As such, there is a need to assess silver dosimetry *in vitro* to appropriately estimate cytotoxic potential of AgNPs of different physicochemical properties on differing cell types (Wildt et al., 2016). To address this, we assessed cytotoxicity on our cultures *in vitro* by both nominal dose (μg AgNP/mL medium) and by dosimetric dose (ng Ag/mg protein) using inductively coupled plasma-mass spectrometry (ICP-MS). We investigated differences in cytotoxic effect by both dose metrics between two particle sizes (20 nm and 110 nm) and two commonly used particle coatings (citrate and polyvinylpyrrolidone). In addition, we utilized gold (Au)-cored AgNPs, with Au serving as a tracer to determine if Ag detected in cells resulted from nanoparticle uptake, silver dissolution, externally bound particles, or combinations of contributing factors.

Materials and Methods

Silver nanoparticles

Citrate 20 or 110 nm AgNPs (AgCitrate 20 and AgCitate 110) and Polyvinylpyrrolidone (PVP)- stabilized 110 nm AgNPs (AgPVP 110) were purchased from NanoComposix (San Diego, CA). All AgNPs contained a gold core (7 nm diameter). These particles were selected by the NIEHS Centers for Nanotechnology and Health Implications Research (NCNHIR) Consortium laboratories as common particles for investigation among Centers. Physicochemical properties of the AgNPs were provided by the manufacturer and are shown in Fennell et al. (2016). AgNPs were diluted in phosphate buffered saline (PBS) using water bath sonication and stored in 1 mg/mL stock solutions in the dark.

Culture system and conditions

We utilized previously optimized micromass culture methods described in Park et al. (2017). Briefly, we time mated C57BL/6 mice and harvested primary midbrain cells from embryos of both sexes at gestation day 11. We brought midbrain cells into a single-cell suspension in medium (DMEM/F-12, 10% FBS, 1% Penicillin/Streptomycin. 1% L-Glutamate) and plated them in 10 µL drops containing 5 x 10^6 cells on matrigel-coated (1:100 matrigel: PBS) 24-well (2cm^2 well) Corning™ Primaria™ cell culture plates (Falcon, Corning, NY). After plating, cultures were incubated at 37°C for 1.5 hours to allow cells to settle and attach to plates, after which 500 uL complete medium was added to each well. Cultures received a full medium change at 24 hours after plating and subsequent half-medium changes every other day until the time of AgNP exposure. The University of Washington Institutional Animal Care and Use Committee approved all experimental procedures used in this study.

Park et al (2017) thoroughly characterized this 3D organotypic micromass culture system and showed neurodevelopmental growth patterns analogous to *in vivo* development. Briefly, cultures showed morphological changes (e.g., proliferation and migration) when observed with 400X magnification phase microscopy. Haematoxylin staining showed continued cell proliferation steadily increased over 22 days *in vitro*. Neurodevelopmental markers of proliferation (PCNA, Nestin, Sox-2) showed proliferation peaked at day in vitro (DIV) 4 and DIV 8. Markers of late differentiation (GluR1, NMDAε1, α-synuclein, EN1) peaked between DIV 8 and DIV 15, with markers of late differentiation (α-synuclein, EN1) peaking at DIV 15.

Exposure medium preparation

Stock solutions of AgNPs in PBS (1mg/mL) were dissolved in complete culture medium at concentrations of 6.25, 12.5, 25, and 50 μg/mL. ZnO served as a positive control at 50 μg/mL, and TiO_2 served as a negative control at 50 μg/mL. Stabilizer coating controls PVP40 (for PVP coated particles) and NaCitrate (for citrate- coated particles) were prepared in concentrations of 50 μg/mL and 100 uM, respectively.

Silver nanoparticle exposure

Cell culture medium was removed and 500 μL of AgNP exposure medium at varying concentrations was pipetted in each well on 24-well plates and incubated at 37°C for 24 hours. We exposed micromass cultures to AgNPs of varying sizes and coatings (AgCitrate 20, AgCitrate 110, AgPVP 110) at three separate time points, at DIV 7, 14, and 21. We assessed toxicity endpoints and dosimetry 24 hours after the exposures, at DIV 8, 15, and 22, respectively, as shown in Figure 1. For a given experiment, each treatment occurred once (not replenished), at one time point. All experimental conditions were performed in triplicate (in each biological replicate) over three biological replicates.

Lactate dehydrogenase (LDH) cytotoxicity assay

Immediately following the 24-hour exposures, we assessed LDH leakage into the medium as an indicator of cytotoxicity using Promega's Non-Radioactive Cytotoxicity Assay following the manufacturer's protocol. 50 µL of media was gently removed from each well and transferred to a 96 well plate. Assay reagent was added and allowed to react for 30 minutes before the stop solution was added and measured by spectrophotometry at 490 nm on a plate reader.

Data were normalized to a medium blank and cytotoxicity was assessed as percent maximum LDH release (as measured in cultures treated with 10% TritonX cell lysis solution provided in the assay kit, incubated at 37°C for 30 minutes for total lysis of all cells) using the equation:

$$\% \text{ LDH Max} = \frac{Absorance\ of\ treated\ or\ control\ cells - Absorbance\ of\ blank\ media}{Absorbance\ of\ Maximum\ LDH - Absorbance\ of\ blank\ media} x\ 100\%$$

Dosimetry

Following the exposure and LDH assay, we removed the exposure medium and washed the cells thoroughly to remove loosely associated and free AgNPs. We rinsed the cells 3x with 450 µL complete medium, so as to not cause any changes in pH or other culture conditions and immediately removed the media following each rinse. Fresh medium was used for each of the three rinses. After the rinses, we added a fresh 450 µL of medium to each well and scraped cells from the plate. Complete removal of cells was confirmed through visual inspection of the well plate. We retained the scraped cell fractions for ICP-MS analysis of metals (Ag and Au) taken up or tightly associated with cells in culture. Triplicate samples of exposure medium, rinses, and cells were combined for each treatment group within each biological replicate. Samples were stored in 15 mL polystyrene tubes (Corning Life Science, Corning, NY)

and stored at 4˚C until time of ICP-MS analyses. Two biological replicates of cultures (cell fractions) exposed to 25 and 50 µg/mL of the three AgNP types as well as controls were retained for determination of silver dosimetry.

Mass of Ag and Au in cell fractions were reported relative to total protein in each well. Total protein was determined in cell fractions of all dose groups following exposure by Bradford Protein Assay (Bio-Rad Laboratories, California USA).

Determination of uptake

In order to determine whether toxicity observed following AgNP exposure resulted from uptake of dissolved Ag ions (dissolution in media) or from uptake and association of whole AgNPs, we utilized AgNPs that contained a small gold (Au) core (7 nm diameter core in all particles). We used ICP-MS to detect both Ag and Au in the exposure medium (prior to exposure) and the cell fraction of cultures after 24-hour exposure, with the Au core serving as a tracer for whole or partially intact nanoparticles. We compared the relative ratios of Ag to Au to determine if Ag in the cell fraction resulted from dissolution of Ag ions in medium, from uptake or attachment of AgNPs, or from a combination of mechanisms.

ICP-MS methods

Samples were prepared for inductively-coupled mass spectrometric (ICP-MS) analysis using open-vessel microwave-assisted digestion with mixed nitric and hydrochloric acids (trace-metal grade, Fisher) with Tb added as recovery standard (EPA, 2007). The microwave (MARS Xpress, CEM Inc.) program was temperature controlled: 800 W power (100%), 10 min ramp to 90° C with a 20 min hold at final temperature. The digestate was brought to a final volume with deionized water (≥ 18 Mohm) with final

concentrations of 7% nitric acid, 2% hydrochloric acid, and 10 ng/mL Tb. The final HCl concentration was sufficient to stabilize Ag^+ as polychlorides at Ag^+ concentration ≤ 500 ng/mL.

Instrumental analysis was performed on an Agilent 7900 ICP-MS with SPS-4 autosampler and ISIS sample valve. Acquisition (RF power, 1550 W; carrier gas flow, 1.03 L/min, spray chamber temperature 2°C; helium (He) flow, 4.3 mL/min; nebulizer, Micromist) was done with He gas in the collision cell, which removes isobaric polyatomic interferences. Isotopes quantified were ^{197}Au, ^{111}Cd, and ^{107}Ag with ^{193}Ir and ^{89}Y and Tb used as internal standards. Calibrants were made from commercial stock solutions (Aristar BDH) with independent check standard from second vendor (Ultra Scientific). Stock solutions were certified reference materials (ISO Guide 34). Continuing calibration verification was performed approximately every 30 samples. Data was corrected for process blanks.

Statistical Analysis

We used R statistical software to create mixed effects dose-response model linear curves of cytotoxicity of each of the three species of AgNPs (AgCitrate 20nm, AgCitrate 110nm, and AgPVP 110nm) at three time points (DIV 8, 15, and 22) by nominal dose. Within the mixed effects model, the random effect was defined as each biological replicate to account for any variability between different preps. Analysis of variance (ANOVA) was used to determine significance of dose-response curves and determine the effect of developmental stage at time of exposure and particle type on cytotoxicity. Following ANOVA, post-hoc tests were used to make comparisons between individual time points and particle aspects for multi parameter conditions.

We modeled Ag dosimetry in cultures after 24 hours of exposure to each particle type at doses of 25 µg/mL and 50 µg/mL using a mixed effects model with biological replicate as the random effect. We

used the dosimetry mixed effects model to determine Ag mass at each exposure concentration. We then modeled the cytotoxicity dose response as a function of dosimetry using a mixed effects model, again with the biological replicate serving as the random effect.

Finally, to assess the relative ratios of Ag to Au in exposure media and cell fractions, we performed a regression analysis of Ag and Au for each particle type. Differences in slope between exposure media (prior to exposure) and cell fraction (24hr after exposure) for each particle were compared for each particle by ANOVA.

Results

AgNP cytotoxicity by nominal dose

To assess the effects of dose, timing of exposure, size, and coating of particles on our developing culture systems, we created a mixed effect dose-response model of the three species of AgNPs at three time points. Effects of dose and timing of exposure were made through comparison of these models within each particle (Figure 2), and effects of particle size and coating were made through comparison of these models within each time point (Figure 3).

Dose response effect by nominal dose

Analysis of variance (ANOVA) of these models showed a significant positive dose-response effect from exposure to Ag Citrate 20 nm at DIV 15 ($p<0.001$) and DIV 22 ($p<0.001$), but did not show a significant dose response at DIV 8 (Figure 2A, left panel). Ag Citrate 110 nm (Figure 2A, middle panel) showed a

significant dose response effect at all time points ($p<0.001$). Ag PVP 110 nm (Figure 2A, right panel) showed a significant dose response at all time points ($p<0.001$).

Developmental stage at time of exposure by nominal dose

We found that developmental time of exposure has a significant effect on the extent of cytotoxicity among all time points (Figure 2A). Post-hoc tests following ANOVA showed that overall exposures at DIV 15 showed the greatest cytotoxic effect in all particles ($p<0.001$). Cultures were more sensitive to AgCitrate 20 nm particles (Figure 2A, left panel) at DIV 15 and DIV 22 compared to DIV 8 ($p<0.001$ and $p<0.01$, respectively). AgCitrate 110 nm particles (Figure 2A, middle panel) showed the greatest cytotoxic effect at DIV 15 compared to DIV 8 and DIV 22 ($p<0.001$ and $p<0.001$). When exposed to AgPVP 110 nm particles (Figure 2A, left panel), cultures showed significantly greater cytotoxicity at DIV 15 compared to DIV 8 and DIV 22 ($p<0.001$ and $p<0.001$). In addition, cultures were slightly more sensitive to AgPVP 110 nm particles at DIV 22 compared to DIV 8 ($p<0.05$).

Particle effect by nominal dose

To assess the overall differences in effect between particles, we compared mixed effects dose-response models using ANOVA within each time point (Figure 2B). We found a significant effect of overall particle type at DIV 8 ($p<0.001$), at DIV 15 ($p<0.001$), and at DIV 22 ($p<0.05$).

Size effect by nominal dose

To investigate the effect of particle size on cytotoxicity, we compared AgCitrate 110 nm particles and AgCitrate 20 nm particles using a post hoc test following ANOVA at each time point. At DIV 8 (Figure 2B, left panel) we observed a slightly greater effect on cytotoxicity from the 110 nm particle compared to

the 20 nm particle ($p<0.05$). At DIV 22 (right panel) we observed modestly greater effect after exposure to the 20 nm particle compared to the 110 nm particle ($p<0.05$). No effect of size on toxicity was observed at DIV 15 (middle panel).

Coating effect by nominal dose

We investigated the effect of coating on cytotoxicity by comparing AgCitrate 110 nm particles and AgPVP 110 nm particles using a post hoc test following ANOVA (Figure 2B). We observed no significant effect of coating on cytotoxicity at all time points ($p>0.05$).

Dosimetry Results

To determine Ag dosimetry (uptake and tightly associated Ag) following 24 hour AgNP exposure, we harvested cell cultures and performed ICP-MS analysis for metals. The mass of Ag was reported relative to total protein in cell cultures after exposure. We found Ag in cell fractions increased linearly with exposure concentration for all particles at all time points (Figure 3). Similar amounts of Ag were observed to be associated with cells at all time points for 20 nm AgCitrate particles (Figure 3A, left panel). The 110 nm particles (both citrate and PVP coated) showed similar amounts of silver at DIV 15 and DIV 22, but showed significantly less silver uptake at DIV 8 (Figure 3A, middle and right panels). The larger (110 nm) AgNPs resulted in greater amounts of Ag in cultures compared to smaller particles at all time points (Figure 4B). No difference in uptake was observed between different coatings.

Dose-response assessment by dosimetry

We assessed the effects of dose, developmental stage, size, and coating of particles on cytotoxicity in developing cultures using a mixed effects model by dosimetric dose (μg Ag/mg protein). Developmental

stage at time of exposure was compared within each particle (Figure 4A) and effects of particle size and coating was compared within each time point (Figure 4B).

Dose response effect by dosimetry

We performed ANOVA on mixed effects models to determine the significance of dose-responses after exposure to AgNPs by Ag dosimetry. We observed a significant dose response in all particles at all time points ($p<0.001$), with the exception of 20 nm AgCitrate at DIV 8.

Effect of developmental stage at time of exposure by dosimetry

We found a significant effect of developmental stage at time of exposure for the 110 nm AgCitrate particle, where DIV 15 was significantly more sensitive than exposures at DIV 8 ($p<0.05$) and DIV 22 when corrected for dosimetry ($p<0.01$) (Figure 4A, middle panel). Cultures were more sensitive to exposure to the 110 nm AgPVP particle at DIV 15 compared to DIV 22 ($p<0.001$) (right panel). Differences in timing of exposure were not significant for the 20 nm AgCitrate particle (left panel).

Particle size effect by dosimetry

When comparing differences in effect of particles by dosimetry (Figure 4B), we found 20nm AgCitrate particles were significantly more toxic compared to 110 nm AgCitrate particles at DIV 15 ($p<0.001$) and at DIV 22 ($p<0.001$). No effect of particle size was seen at DIV 8 ($p>0.05$).

Particle coating effect by dosimetry

No differences in the effect of coating were observed between citrate and PVP-coated particles at any time points ($p>0.05$) (Figure 4B).

Determination of dissolution activity and particle uptake

We performed a regression analysis of Ag and Au in both exposure medium (prior to exposure) and in cell fractions (after 24hr exposure) to determine the difference in proportions of Ag and Au for each particle at all time points (Figure 5). Differences in slope between exposure media and cell fraction for each particle were compared for each particle by ANOVA. We did not observe a significant difference in relative amounts of Ag and Au between exposure medium and cell fractions for any particle types ($p>0.05$). This suggests that dissolution of particles in medium may not be a large contributing factor and that particle uptake may be a large component of the observed cytotoxicity. In addition, we observed a greater amount of Au relative to Ag in the 20 nm particles.

Discussion

There is a need to assess the potential for AgNPs to act as neruodevelopmental toxicants. In this study, we utilized a 3-dimensional organotypic mouse midbrain model to assess the sensitivity of developing primary mouse neural cultures to AgNPs. We investigated the effect of developmental stage at time of exposure as well as the contribution of AgNP size and coating to toxicity. In addition, we measured the contributions of dissolved Ag and intact AgNPs to observed toxicity.

In vitro models provide several advantages over the use of *in vivo* toxicity assessments as they utilize significantly fewer animals, can assess multiple endpoints simultaneously, allow for rapid, high throughput assessments, and often cost far less than animal toxicity studies. These attractive qualities of

assessing toxicity using *in vitro* models become even more powerful and necessary to keep pace with the accelerating rate of scientific and technological advancements in chemical and manufactured materials. We utilized an innovative method for assessing neurodevelopmental effects through our 3-dimensional micromass model that has been shown to grow and develop without the addition of growth factors or differentiation promoting factors (Park et al., 2017). The ability to study neurodevelopment *in vitro* without use of these factors is critical for neurodevelopmental toxicity studies as these growth factors may mask sensitivity of effects. In addition, many of these factors may be retinoic acid-based (Maden, 2007), and may sensitize neural cultures to developmental disruption as retinoic acid is a well characterized teratogen (Lammer et al., 1985). The European Centre for the Evaluation of Alternative Methods (ECVAM) has supported the use of micromass cultures as a standard alternative developmental toxicity method in an effort to reduce the number of animals used in toxicity studies (ECVAM, 2001).

Park et al. (2017) developed and thoroughly characterized a micromass culture system from primary embryonic mouse midbrains. A mouse culture system allows for higher throughput with development occurring in a shortened period of time compared to the rat and other mammalian models. In addition, the availability of many inbred genetic strains of mouse allows for the comparison of results across strains for insights on genetic influences of variability in response. This is especially useful in future comparisons across the Collaborative Cross mouse strains (Churchill et al., 2004). Neurodevelopmental processes are largely conserved across mammalian species and as such, a mouse embryonic midbrain cell model may serve as an effective tool to assess the potential for AgNPs to cause neurodevelopmental toxicity in humans.

Because AgNPs utilized in these experiments contained a small (7 nm) Au core, we used Au as a tracer of whole nanoparticles to determine the extent to which dissolution of AgNPs in medium contributed to the cytotoxicity observed. We compared the relative ratios of Ag to Au in exposure medium (before exposure) and in cell fractions (after 24 hr AgNP exposure) and hypothesized that a larger relative ratio of Ag to Au in cell cultures after exposure would suggest that AgNPs were undergoing dissolution in medium. However, we did not observe a significant difference between the relative ratios of Ag and Au in exposure medium compared to cells after exposure to any of the three particles investigated. This suggests that dissolution of particles in medium is not a major contributing factor to the cytotoxicity observed, and that particles eliciting cytotoxic effects in these cultures are either taken up by cells or are eliciting effects while tightly bound to the outside of cells. However, these data are not conclusive of this mechanism.

There has been a great deal of discussion as to whether toxic effects from AgNPs observed *in vitro* and *in vivo* are due to cellular uptake of particles or from dissolution of AgNPs into free Ag ions in media. Dissolution of AgNPs has been observed to occur both *in vitro* and *in vivo*. The rate of dissolution has been shown to depend on particle size, pH and temperature of the environment, other ions present in medium, aggregation state, and incubation time (Loeschner et al., 2011; Stebounova et al., 2011; Leo et al., 2013). Smaller nanoparticles have been observed to dissolve faster due to their high surface to volume ratio. Ma et al. (2012) found the dissolution of AgNPs to range from 1% for 80 nm particles to 60% for 5 nm particles at pH 8 during three and two months of incubation, respectively. Because smaller AgNPs have greater surface area per mass compared to larger particles, a higher degree of dissolution may occur, leading to a greater number of free Ag ions and greater toxic potential. Surface area of particles has been suggested to be the greatest predictor of AgNP toxicity compared to other physicochemical characteristics such as mass (Oberdorster et al., 2005; Braakhuis et al., 2016). The

smaller sized nanoparticles have been shown to have a higher dissolution rate and lower biodurability and thus greater potential to cause pathogenicity (Utembe et al., 2015). In addition, serum and protein in culture medium can form a protein corona around silver particles, stabilizing them and reducing the dissolution rate (Shannahan et al., 2013; Duran et al., 2015).

We observed significantly greater effects on cytotoxicity when exposures occurred at DIV 15 compared to DIV 8 and 22. This effect was consistent in both nominal dose and dosimetric dose response assessments, despite an equivalent amount of Ag associated with cells at DIV 15 and DIV 22. Park et al., 2017 observed these same micromass cultures show peaks of late phase differentiation markers α-synuclein and EN-1 at DIV 15 compared to other time points. Our findings of neural culture sensitivity during differentiation have also been observed in other *in vitro* neurodevelopment models. Greater sensitivity to metals has been shown during neural differentiation stages of development after exposure to manganese (Hernandez et al., 2011), lead (Bull et al., 1983; Silbergeld, 1992; Deng et al., 2001), and methylmercury (Barone et al., 1998).

Differentiation into specialized cell types may contribute to the increased sensitivity of cultures at later time points. The midbrain contains the greatest amount of dopaminergic neurons in the brain and they first begin to appear at embryonic day 10.5 in mice (Maxwell and Li, 2005)- roughly the time when our cultures are harvested and plated. Early dopaminergic neurons proceed through several stages of development and become functionally mature several days later which may coincide with DIV 15 in these cultures (Abeliovich and Hammond, 2007). Metals have been shown to accumulate in dopaminergic neurons (Robison et al., 2015). Increased uptake and cytotoxicity of AgNPs at DIV 15 may be due to differentiation into less specialized neurons. However, the potential for Ag+ to utilize Na+ channels may lead to increased uptake of Ag and a disruption of ion flow (Bury and Wood, 1999).

Alternatively, microglia and other phagocytic glial cell types may develop just prior to DIV 15, leading to the increased uptake of particles observed in Figure 3.

When compared by dosimetry, we found that the smaller particle (AgCitrate 20nm) had greater cytotoxic effects than larger particles at DIV 15 and DIV 22. This effect was observed despite significantly less Ag (and total Ag+Au) in cell cultures after exposure to 20 nm particles. The apparent absence of dissolution in media from either size particle (no difference in Ag:Au between media and cells), despite significant differences in particle size on toxicity may be explained by dissolution occurring primarily in lysosomes. As nanoparticles are taken up into cells, autophagosomes form around particles and other damaged cellular components. Lysosomes then fuse with autophagosomes and hydrolytic enzymes degrade its contents. Because lysosomes are more acidic (pH 4.5-6) than cytosol and other cellular components, the acidic environment may result in enhanced AgNP dissolution. Because smaller particles have greater surface area compared to larger particles, this may result in a heightened level of dissolution. As such, more dissolution may occur with smaller particles, leading to greater lysosomal dysfunction and cell death. Stern et al. (2012) and Ma et al. (2011) found lysosomes play a large role in cytotoxicity and has been proposed to be a major mechanism in nanoparticle toxicity.

Alternatively, it is possible that the 20 nm AgNPs are undergoing so much dissolution in media that the Au core becomes exposed and also undergoes dissolution and uptake into cells. This would also result in the observed lack of change in proportion of Ag to Au for 20 nm particles. Munusamy et al. (2015) found 20 nm AgNPs containing a Au core had much more rapid dissolution rate in medium (approximately 50% particle mass dissolved after 24 hours) compared to 110 nm AgNPs with an Au core (approx. 20% particle mass dissolved after 24 hours). This would not, however explain the lack of change in relative amounts of Ag to Au in 110 nm particles before and after exposure. It is possible that cytotoxicity may

be occurring through differing mechanisms of delivery of metals to cells between particle sizes, where 110 nm particles elicit effects by associating with outer layers of cell membranes or are taken up into cells as mostly undissolved particles. This may explain why much greater amounts of Ag is found in cell fractions following exposure to 110 nm particles.

Coatings such as citrate and polyvinylpyrrolidone (PVP) act to stabilize silver nanoparticles by reducing aggregation and agglomeration and controlling ion release from particles. In our study, we found no significant differences between PVP- and citrate-coated particles of the same size. Interestingly, PVP has been shown to complex with releasing Ag+ ions and has been shown to reduce cytotoxic effects of AgNPs compared to the same sized citrate-coated particles (Wang et al., 2014). However, we did not observe this effect in our study.

The present study provides valuable insights on the potential for AgNPs to interact with and disrupt developing neural cultures, however several limitations of this work have been identified. While our methods were designed to prevent large amounts of aggregation and agglomeration of particles in medium, we did not measure AgNP aggregation or agglomeration in exposure solution prior to exposures. This could potentially result in reduced delivery of AgNPs to cultures and may affect uptake and cytotoxicity. As such, the differences in behavior of different sized particles in liquid media may also affect delivery to cultures, and may lead to differences in toxic effects. We addressed some of these potential differences in delivery by assessing dosimetry after exposures to compare between particles however, the translation of particle delivery to tissue *in vivo* may be quite different. We investigated differences in relative ratios of Ag to Au before and after exposures to determine the extent by which dissolution of AgNPs in culture medium might contribute to cytotoxicity. This analysis showed that there was no significant change in ratios in any of the three particles investigated. However, our methods did

not allow for the determination of whether complete dissolution of particles occurred in medium, which could also result in the lack of change in ratio of metals. Visualization of cells after exposure by electron microscopy and measurement of particles associated with cells may better inform whether uptake of whole particles is occurring.

In summary, we have shown our 3-dimensional developing primary midbrain cultures are sensitive to AgNPs. Cultures were more sensitive to AgNP exposures at differentiation stages of development, with greater uptake of particles occurring at later time points. Cultures were more sensitive to smaller sized AgNPs, despite less overall uptake of Ag compared to larger particles. We found dissolution of AgNPs in medium may not contribute to the cytotoxic effects observed. Future work may investigate markers for dopaminergic neurons or microglia in these cultures to better inform the role of cell type differentiation and mechanisms of uptake and sensitivity observed in cultures at later time points.

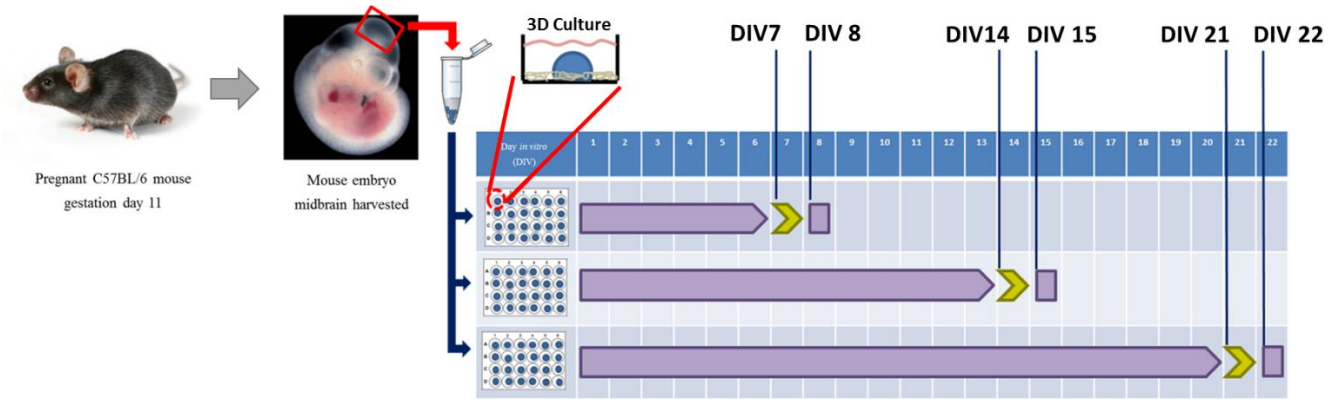

Figure 1. Primary embryonic midbrains are harvested at gestation day 11, brought into single cell suspension, and plated on 24-well plates. At day *in vitro* (DIV) 7, 14, and 21 cultures are exposed to various concentrations (µg/mL) of AgNPs. After 24-hour incubation (at DIV 8, 15, and 22), cultures were harvested and assessed for silver and gold uptake and toxicological endpoints.

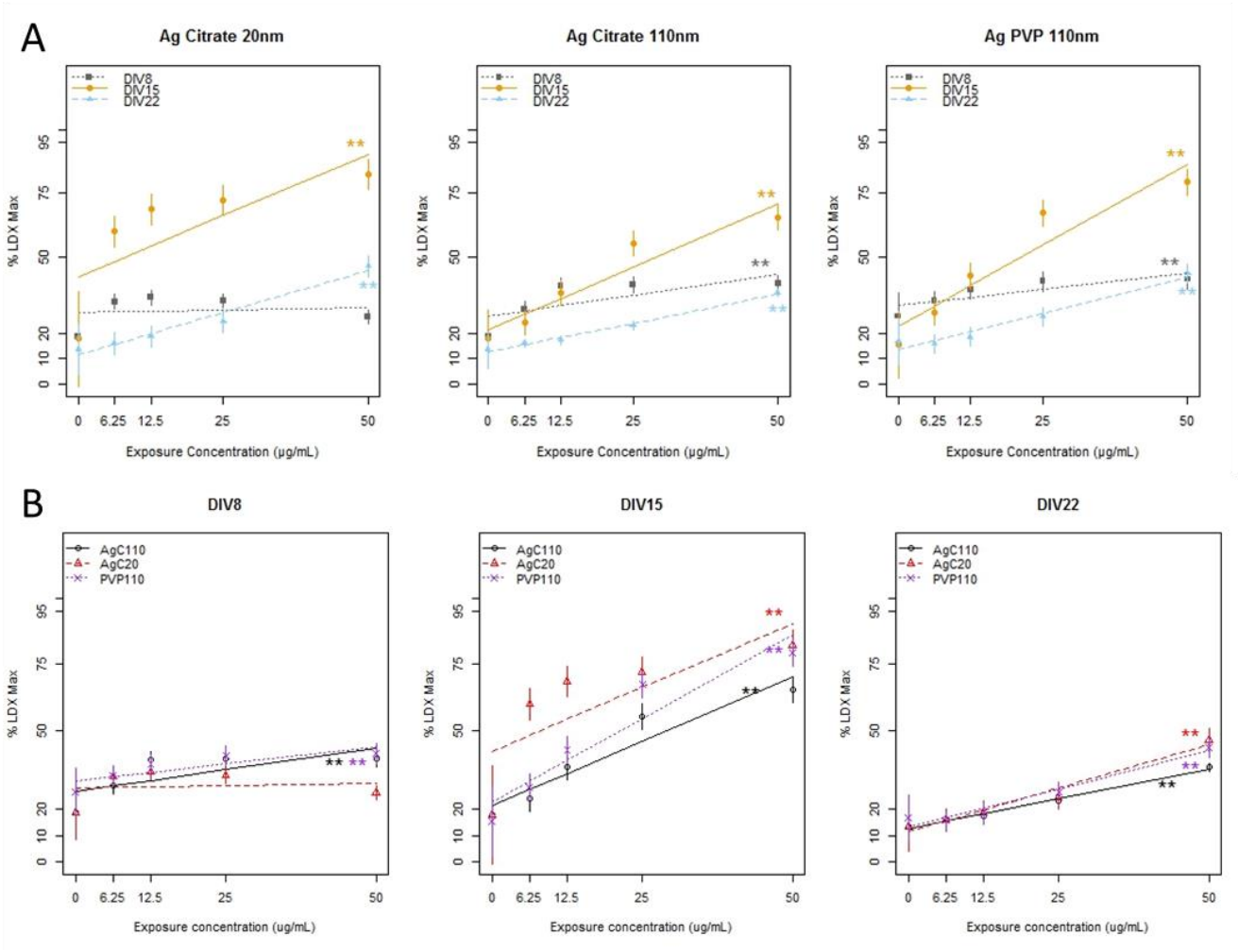

Figure 2. (A) Cytotoxicity of three AgNPs by nominal dose (exposure concentration) after 24hr exposure at three individual time points (DIV8, DIV15, DIV22). Cytotoxicity is expressed as % maximum LDH release relative to coating control assessed 24 hr post-AgNP exposure. Significant dose response is observed for all particles at DIV 15 and DIV 22. A significant dose response effect is observed at DIV 8 for 110 nm particles (middle and left panels). Greatest cytotoxicity is seen at DIV 15 for all particles. (B) Cytotoxicity of AgNPs after 24 hr exposure at three separate time points. Cytotoxicity is expressed as % maximum LDH release relative to coating control 24 hr post-AgNP exposure.

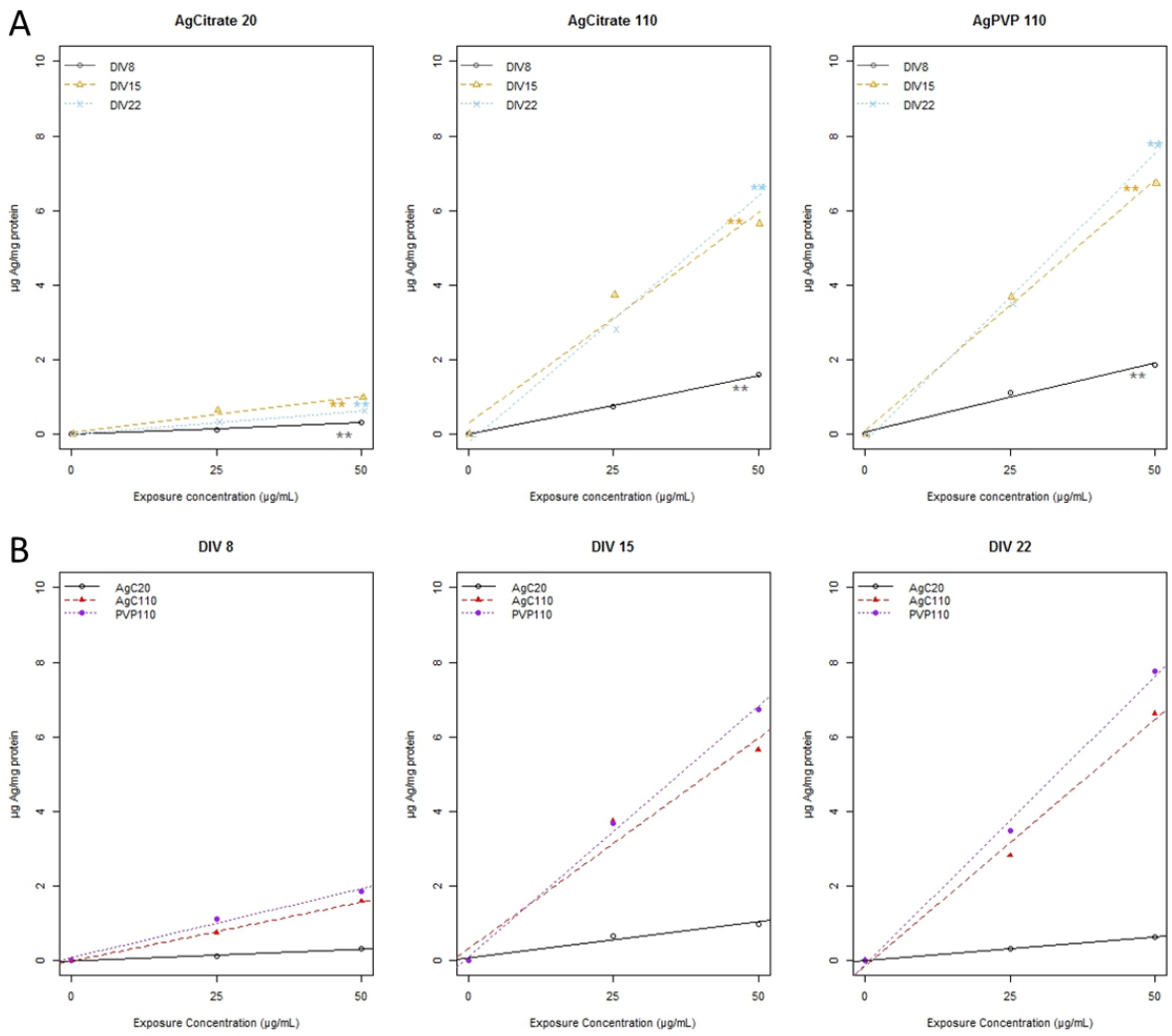

Figure 3. Dosimetry of Ag (µg Ag/mg protein) in cells after 24hr exposure to three particles by particle (A) and by DIV (B). Ag dosimetry increased linearly in all particles at all days. Greater silver dosimetry is observed at DIV 15 and DIV 22 compared to DIV 8 for all particles ($p<0.05$). Greater dosimetry is also observed in 110 nm particles at all time points ($p<0.05$).

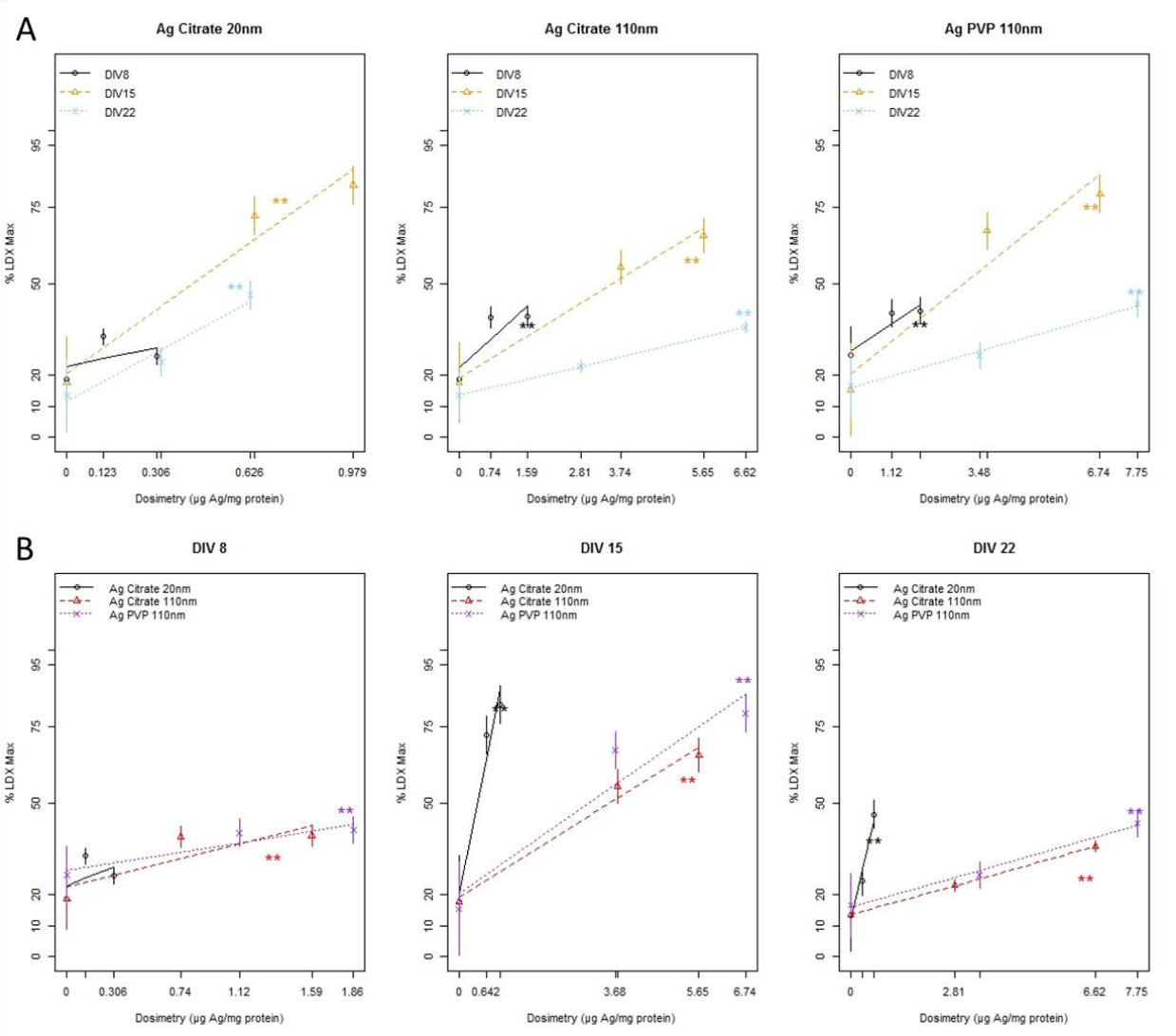

Figure 4. (A) Cytotoxicity of AgNPs after 24hr exposure at three time points by dosimetric dose. Cytotoxicity is expressed as % maximum LDH release relative to coating control assessed 24 hr post-AgNP exposure. A significant dose response effect is observed for all particles at DIV 15 and DIV 22 ($p<0.001$). A significant dose response effect is observed at DIV 8 for both 110 nm particles ($p<0.001$). (B) Comparison of cytotoxic effect of particles at three time points shows significantly greater cytotoxic effect of 20 nm particles at DIV 15 and 22 ($p<0.001$).

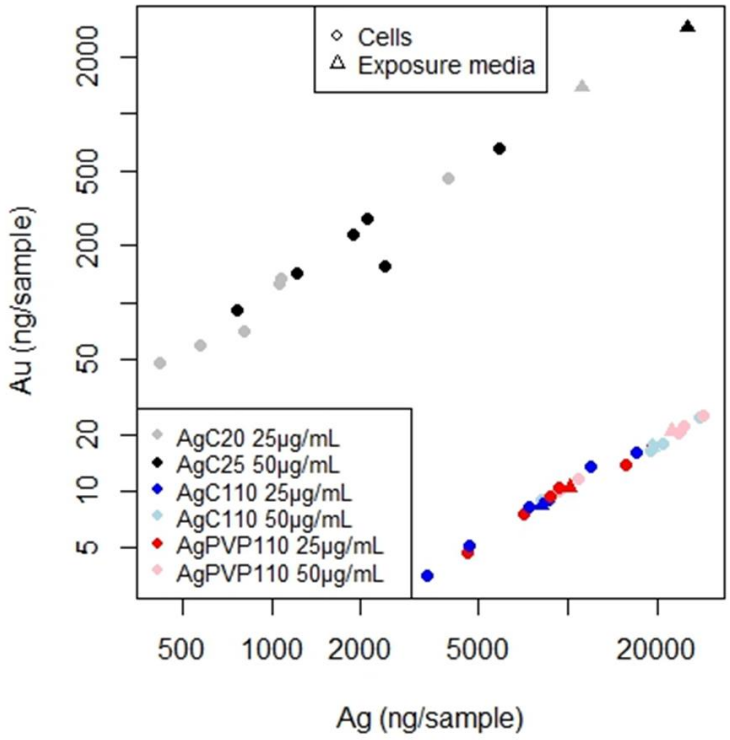

Figure 5. Ag and Au in cell fraction following 24 hour AgNP exposure (circles) and exposure media prior to exposure (triangles). Relative amounts of Ag and Au and observed for each particle size. A smaller ratio of Ag to Au is observed in 20 nm particles (gray and black).

Chapter 3 References

Abeliovich, A. and R. Hammond (2007). "Midbrain dopamine neuron differentiation: factors and fates." Dev Biol **304**(2): 447-454.

Barone, S., Jr., N. Haykal-Coates, et al. (1998). "Gestational exposure to methylmercury alters the developmental pattern of trk-like immunoreactivity in the rat brain and results in cortical dysmorphology." Brain Res Dev Brain Res **109**(1): 13-31.

Braakhuis, H. M., F. R. Cassee, et al. (2016). "Identification of the appropriate dose metric for pulmonary inflammation of silver nanoparticles in an inhalation toxicity study." Nanotoxicology **10**(1): 63-73.

Brown, S., Bechter , Flint , Freeman , Jelinek, Koch, Nau, Newall, Palmer, Renault, Repetto, Vogel, Wiger (1995). "Screening Chemicals for Reproductive Toxicity: the Current Alternatives." ATLA **23**: 868-882.

Bull, R. J., P. T. McCauley, et al. (1983). "The effects of lead on the developing central nervous system of the rat." Neurotoxicology **4**(1): 1-17.

Bury, N. R. and C. M. Wood (1999). "Mechanism of branchial apical silver uptake by rainbow trout is via the proton-coupled Na(+) channel." Am J Physiol **277**(5 Pt 2): R1385-1391.

Churchill, G. A., D. C. Airey, et al. (2004). "The Collaborative Cross, a community resource for the genetic analysis of complex traits." Nat Genet **36**(11): 1133-1137.

Deng, W., R. D. McKinnon, et al. (2001). "Lead exposure delays the differentiation of oligodendroglial progenitors *in vitro*." Toxicol Appl Pharmacol **174**(3): 235-244.

Duran, N., C. P. Silveira, et al. (2015). "Silver nanoparticle protein corona and toxicity: a mini-review." J Nanobiotechnology **13**: 55.

ECVAM (2001). Statement on the Scientific Validity of the Micromass Test - an *In vitro* Test for Embryotoxicity. European Centre for the Validation of Alternative Methods Scientific Advisory Committee. Ispra, Italy.

EPA (2007). "Method 3051- A Microwave Assisted Acid Digestion Of Sediments, Sludges, Soils, and Oils."

Fennell, T. R., N. P. Mortensen, et al. (2016). "Disposition of intravenously or orally administered silver nanoparticles in pregnant rats and the effect on the biochemical profile in urine." J Appl Toxicol.

Flint, O. P. (1983). "A micromass culture method for rat embryonic neural cells." J Cell Sci **61**: 247-262.

Grandjean, P. and P. J. Landrigan (2006). "Developmental neurotoxicity of industrial chemicals." Lancet **368**(9553): 2167-2178.

Hernandez, R. B., M. Farina, et al. (2011). "Mechanisms of manganese-induced neurotoxicity in primary neuronal cultures: the role of manganese speciation and cell type." Toxicol Sci **124**(2): 414-423.

Lammer, E. J., D. T. Chen, et al. (1985). "Retinoic acid embryopathy." N Engl J Med **313**(14): 837-841.

Leo, B. F., S. Chen, et al. (2013). "The stability of silver nanoparticles in a model of pulmonary surfactant." Environ Sci Technol **47**(19): 11232-11240.

Levard, C., E. M. Hotze, et al. (2012). "Environmental transformations of silver nanoparticles: impact on stability and toxicity." Environ Sci Technol **46**(13): 6900-6914.

Loeschner, K., N. Hadrup, et al. (2011). "Distribution of silver in rats following 28 days of repeated oral exposure to silver nanoparticles or silver acetate." Part Fibre Toxicol **8**: 18.

Ma, R., C. Levard, et al. (2012). "Size-controlled dissolution of organic-coated silver nanoparticles." Environ Sci Technol **46**(2): 752-759.

Maden, M. (2007). "Retinoic acid in the development, regeneration and maintenance of the nervous system." Nat Rev Neurosci **8**(10): 755-765.

Maxwell, S. L. and M. Li (2005). "Midbrain dopaminergic development *in vivo* and *in vitro* from embryonic stem cells." J Anat **207**(3): 209-218.

Morishita, Y., Y. Yoshioka, et al. (2016). "Distribution of Silver Nanoparticles to Breast Milk and Their Biological Effects on Breast-Fed Offspring Mice." ACS Nano **10**(9): 8180-8191.
Munusamy, P., C. Wang, et al. (2015). "Comparison of 20 nm silver nanoparticles synthesized with and without a gold core: Structure, dissolution in cell culture media, and biological impact on macrophages." Biointerphases **10**(3): 031003.
Oberdorster, G., E. Oberdorster, et al. (2005). "Nanotoxicology: an emerging discipline evolving from studies of ultrafine particles." Environ Health Perspect **113**(7): 823-839.
Park JY, W. B., Hong SW, Faustman EM (2017). "Characterization of neurodevelopmental markers in C57BL/6 mouse embryonic midbrain micromass cultures." ALTEX **In submission**.
Patchin, E. S., D. S. Anderson, et al. (2016). "Size-Dependent Deposition, Translocation, and Microglial Activation of Inhaled Silver Nanoparticles in the Rodent Nose and Brain." Environ Health Perspect.
Reidy , H., Luch , Dawson , Lynch (2013). "Mechanisms of Silver Nanoparticle Release, Transformation and Toxicity: A Critical Review of Current Knowledge and Recommendations for Future Studies and Applications; Review." Materials **6**(6): 2295-2350.
Rice, D. and S. Barone, Jr. (2000). "Critical periods of vulnerability for the developing nervous system: evidence from humans and animal models." Environ Health Perspect **108 Suppl 3**: 511-533.
Robison, G., B. Sullivan, et al. (2015). "Identification of dopaminergic neurons of the substantia nigra pars compacta as a target of manganese accumulation." Metallomics **7**(5): 748-755.
Shannahan, J. H., X. Lai, et al. (2013). "Silver nanoparticle protein corona composition in cell culture media." PLoS One **8**(9): e74001.
Sidhu, J. S., R. A. Ponce, et al. (2006). "Cell cycle inhibition by sodium arsenite in primary embryonic rat midbrain neuroepithelial cells." Toxicol Sci **89**(2): 475-484.
Silbergeld, E. K. (1992). "Mechanisms of lead neurotoxicity, or looking beyond the lamppost." FASEB J **6**(13): 3201-3206.
Stebounova, L. V., A. Adamcakova-Dodd, et al. (2011). "Nanosilver induces minimal lung toxicity or inflammation in a subacute murine inhalation model." Part Fibre Toxicol **8**(1): 5.
Tang, J., L. Xiong, et al. (2009). "Distribution, translocation and accumulation of silver nanoparticles in rats." Journal of nanoscience and nanotechnology **9**(8): 4924-4932.
Tang, J., L. Xiong, et al. (2010). "Silver nanoparticles crossing through and distribution in the blood-brain barrier *in vitro*." Journal of nanoscience and nanotechnology **10**(10): 6313-6317.
Utembe, W., K. Potgieter, et al. (2015). "Dissolution and biodurability: Important parameters needed for risk assessment of nanomaterials." Part Fibre Toxicol **12**: 11.
Wang, X., Z. Ji, et al. (2014). "Use of coated silver nanoparticles to understand the relationship of particle dissolution and bioavailability to cell and lung toxicological potential." Small **10**(2): 385-398.
Whittaker, S. G. and E. M. Faustman (1991). "Effects of albendazole and albendazole sulfoxide on cultures of differentiating rodent embryonic cells." Toxicol Appl Pharmacol **109**(1): 73-84.
Whittaker, S. G., J. T. Wroble, et al. (1993). "Characterization of cytoskeletal and neuronal markers in micromass cultures of rat embryonic midbrain cells." Cell Biol Toxicol **9**(4): 359-375.
Wildt, B. E., A. Celedon, et al. (2016). "Intracellular accumulation and dissolution of silver nanoparticles in L-929 fibroblast cells using live cell time-lapse microscopy." Nanotoxicology **10**(6): 710-719.
Woodrow Wilson International Center for Scholars, W. (2016). "The project on emerging nanotechnologies." from http://www.nanotechproject.org/inventories/.
Yang, Z., Z. W. Liu, et al. (2010). "A review of nanoparticle functionality and toxicity on the central nervous system." Journal of the Royal Society, Interface / the Royal Society **7 Suppl 4**: S411-422.

Chapter 4

In vitro Benchmark Dose Analysis to Inform Risk Assessment of Inorganic Engineered Nanomaterials

Brittany A. Weldon[1,2], William C. Griffith[1,2], Tomomi Workman[1,2], David K. Scoville[2], Terrance J. Kavanagh[2], and Elaine M. Faustman[1,2]

[1]Institute for Risk Analysis and Risk Communication, University of Washington, Seattle, WA

[2]Department of Environmental and Occupational Health Sciences, University of Washington, Seattle, WA

BACKGROUND: Engineered nanomaterials are a new class of toxicants currently under review for potential toxicity; however, their use in consumer and commercial products has continued to outpace risk assessments for these materials. *In vitro* methods have been utilized as tools to improve the efficiency of risk assessments through replacement, reduction, and refinement of classic *in vivo* hazard characterization for chemicals. The present study proposes a framework to compare relationships between *in vitro* findings and *in vivo* results for selected engineered nanomaterials using benchmark dose and dosimetric assessment methods. These methods may be used to better utilize *in vitro* findings and improve the quality and efficiency of *in vivo* studies and risk assessment.

OBJECTIVES:

We aimed to evaluate the utility of benchmark dose modeling as a tool to compare the relative relationships of *in vitro* studies and evaluate *in vivo* relevance using cadmium-selenium containing quantum dots (Qdots) as a case study.

METHODS:

Previously published findings of Qdot toxicity *in vitro* and *in vivo* were made available through the NIEHS Centers for Nanotechnology Health Implications Research (NCNHIR) Consortium. *In vitro* studies assessed effects of Qdots in three pulmonary cell types in two inbred mouse strains. Significant dose-response effects including proinflammatory responses were modeled and a standardized method of benchmark dose analysis was performed as a function of both exposure dose and dosimetric dose. *In vivo* studies assessed pulmonary effects of Qdots in eight collaborative cross strains. Dose response data from studies were modeled and benchmark doses were calculated and used as a basis of relative comparison between *in vitro* studies.

RESULTS:

Our analysis found consistent responses in common endpoints between *in vitro* and *in vivo* studies. Strain sensitivity was consistent between *in vitro* and *in vivo* analyses, showing the A/J strain was more sensitive to Qdots compared to other strains. Alveolar macrophages (AM), bone marrow derived macrophages (BMDM), and mouse tracheal epithelial cells (MTEC) were found to differentially take up Qdots. However, dosimetric adjustments identified similar sensitivity among these various cell types.

CONCLUSIONS:

Benchmark dose analysis can be used as an effective tool to compare the sensitivity of different strains, cell types, and assays to Qdots and other inorganic nanomaterials *in vitro* and *in vivo*. Dosimetry plays a critical role in these comparisons. *In vitro* assays can be used to inform *in vivo* studies of sensitive strains, cell types, and assays that can be predictive of critical *in vivo* responses that are predictive of pathogenicity. These findings provide insight for utilizing *in vitro* findings to improve risk assessment.

Introduction

Recent technological developments have employed the use of a wide array of nano-scaled materials (<100 nm), referred to generally as Engineered Nanomaterials (ENMs), for their attractive qualities including small size, large surface area, charge, and lightness of weight. ENMs are being used increasingly in medicine, manufacturing, and industry (Dabbousi BO, 1997; Azzazy et al., 2007). Applications of ENMs continue to accelerate, however the ability to fully characterize the risks associated with human exposures to nanomaterials has been somewhat limited.

Risk assessments of environmental health hazards have long been dependent on *in vivo* toxicity testing to determine acceptable levels of exposure to toxicants. This approach can require extensive testing in animals at high cost and time requirements. *In vitro* methods can mediate some of these time and financial burdens by providing more rapid, high throughput assessments that can inform *in vivo* effects. The National Research Council (NRC) has outlined a vision of improved toxicity testing for efficiency and pathway-specific assessments (NRC, 2007). These methods rely heavily on linking toxicity assessments across biological contexts including linking *in vitro* to *in vivo* animal studies, and *in vivo* animal studies to humans effects.

Recent efforts have been made by the United States Environmental Protection Agency (EPA) and the European Chemicals Agency (ECHA) to promote the use of *in vitro* toxicity testing of chemicals and other toxicants to improve the efficiency of toxicological assessments. EPA and the National Institute of Health's (NIH) Toxicology in the 21st Century (Tox21) goals for increasing high throughput testing promotes the use of *in vitro* models for predictive toxicity testing. In addition, recent efforts by EPA to reform the Toxic Substances Control Act (TSCA) through the Frank R. Lautenberg Chemical Safety for the 21st Century Act promotes the use of non-animal testing and other *in vitro* and *in silico* techniques (EPA,

2016). The ECHA has employed these same principles in their REACH legislation that supports the use of alternative testing methods for improved efficiency and reduced animal testing (EU, 2006). In order to better utilize *in vitro* studies in risk assessment, tools are needed to translate *in vitro* findings to predict *in vivo* results for the reduction and refinement of *in vivo* studies.

Likewise, the rapid pace of development in nanotechnology creates an urgent need for improved efficiency in risk assessment. While some *in vitro* studies have been shown to be predictive of *in vivo* effects for some chemicals (Browne et al., 2015), the unique properties of ENMs may affect *in vitro* behavior (Teeguarden et al., 2007). As such, there has been some question as to the utility of the sole use of *in vitro* screening for toxicity of nanoparticles (Donaldson et al., 2009). An EPA Nanotechnology Workgroup identified the need to determine whether current testing methods for chemical hazards, such as the use of *in vitro* studies, are appropriate for evaluation of hazard of nanomaterials for risk assessment (EPA Science Policy Council, 2007).

To begin to address this question, the goal of our study was to investigate the relative relationships between *in vitro* and *in vivo* findings using poly(maleic anhydride-alt-1-tetradecene), tri-n-octylphosphine oxide (PMAT-TOPO) co-polymer coated CdSe core/ZnS shell composite quantum dots (Qdots), a commonly used inorganic ENM, as a case study. We developed a benchmark dose (BMD)-based model for assessing sensitivity of multiple cell types, strains and assays to Qdot exposure by common endpoints between test systems. We hypothesized that BMD analysis may serve as a tool to characterize relative sensitivity of *in vitro* endpoints, cell types, and strains. We propose that this method can serve as an effective tool to translate *in vitro* sensitivity to better inform *in vivo* studies for the hazard identification and risk characterization of ENMs in risk assessments.

Materials and methods

To investigate the relationships between *in vitro* and *in vivo* findings, we accessed previously published data made available through the NIEHS Chemical Effects in Biological Systems (CEBS) database repository from NCNHIR Centers. *In vitro* investigations of PMAT-TOPO coated CdSe/ZnS quantum dots (Qdots) were reported by Lee et al. (2015) and *in vivo* studies of Qdot effects in mice are reported in Scoville et al. (2015).

In vitro study methods

Briefly, Lee et al. investigated TOPO-PMAT-coated Qdots in three murine cell types including bone marrow derived macrophages (BMDM), alveolar macrophages (AM) obtained from *in vivo* bronchoalveolar lavage, and mouse tracheal epithelial cells (MTECs) cultured *in vitro*. Effects in these cell types were investigated in two mouse strains, C57BL/6J and A/J. MTECs were grown in organotypic cell cultures at an air-liquid interface. BMDMs were cultured in growth factor-containing medium for 7 days, while AMs were obtained via bronchoalveolar lavage from sacrificed mice.. Cells were exposed to 0, 10, 40, 80, or 100 nM Qdots for 24 hours. Uptake of Cd, cytotoxicity, and proinflammatory cytokine expression by relative quantification (RQ) of their mRNAs were assessed. Results showed dose-dependent increases in Cd uptake into all cell types in both strains when analyzed by inductively coupled plasma- mass spectrometry (ICP-MS). BMDMs and AMs were observed to take up greater amounts of Cd compared to MTECs. No significant dose-response was observed in cytotoxicity assessments. Qdots were observed to induce a dose-dependent increase in levels of CXCL1 (CXC Motif Chemokine Ligand 1, previously called KC) and IL-6 (Interleukin 6) neutrophil recruiting cytokines in A/J BMDM and AM cultures. MTECs showed a significant Qdot dose response for expression of CXCL1.

In vivo study methods

Scoville et al. (2015) performed an *in vivo* investigation of TOPO-PMAT-coated Qdot effects on the eight genetically diverse founder mouse strains of the Collaborative Cross (Churchill et al., 2004). Animals were exposed to 0 or 6 μg Cd equivalents/kg body weight of 10 nM Qdots by oropharyngeal aspiration and sacrificed 8 hours after exposure. Bronchoalveolar lavage (BAL) was performed at the time of sacrifice and BAL fluid (BALF) was assessed for neutrophil infiltration and proinflammatory cytokine protein levels. Tissue cadmium dosimetry was assessed via ICP-MS and total glutathione in lung tissue was determined. Qdots were found to induce variable inflammatory responses among the mouse strains. Significant neutrophil infiltration was found in CAST and NZO strains, while the A/J strain was found to have significant increases in cytokines assessed in BALF including KC (also known as CXCL1), MIP1α, MIP1γ, and G-CSF.

Benchmark dose modeling methods

Dose Response modeling

In order to compare toxicity responses observed in these datasets, we first established fitness criteria for dose response and benchmark dose modeling. Fitness criteria were based on a modified version of EPA's framework for BMD modeling and technical guidance (USEPA, 2012). From these criteria, studies were limited to those showing a significant dose-response effects and were amenable to model fits and estimates for BMDs. We modeled dose response curves for *in vitro* and *in vivo* endpoints in Lee et al. (2015) and Scoville et al. (2015) that fit these conditions. *In vitro* assessments included mRNA expression

of proinflammatory markers IL-6 and CXCL1 in cells from A/J and C57BL/6J mice. *In vivo* assessments included proinflammatory marker KC (also known as CXCL-1) and neutrophil infiltration in BALF across eight mouse strains.

Data sets that did not pass fitness criteria (e.g. lack of significant dose-response) were excluded from analysis. For *in vitro* assessments that showed very steep responses, we utilized the initial cytokine response that defined the curve (first dose). Only the initial cytokine response was used for in vitro studies as higher doses showed a decreasing trend with dose which was not amenable to model fits and calculations of BMDs. Overall, linear dose response models were fit to both the *in vitro* data and the *in vivo* data, which relied on a single dose.

From the dose response models, we calculated benchmark doses using EPA's Benchmark Dose Software following a modified version of EPA's framework for BMD modeling (USEPA, 2012). When calculating a BMD, a standardized benchmark response level (BMR) was used to calculate the dose at which a significant response will occur (Kavlock et al., 1995; Wignall et al., 2014). A BMR of 1 standard deviation change in response relative to controls was used for *in vitro* endpoints and *in vivo* cytokine endpoints (Davis et al., 2011; Meyer et al., 2012). A BMR of 1 standard deviation change in response relative to the mean of the control is equivalent to a approximately a 10% change in response relative to the control mean (Crump, 1995).

All BMDs were calculated and compared by nominal exposure dose and by dosimetric dose of Cd (from Qdots) in cells. Exposure dose was defined as the concentration of Qdots in exposure media at the time of treatment (nM Qdots), while dosimetric dose is defined as the amount of Cd measured in or associated with cells at the time of toxicity assessment (ng Cd/100,000 cells).

Relative comparisons between in vitro and in vivo

In vitro benchmark doses were used as a basis for comparison of sensitivity of *in vitro* and *in vivo* systems to Qdot exposure by both nominal (exposure) dose as well as by dosimetric dose. BMDs with common dose units, nM Qdots or ng Cd/100,000 cells, allowed for the direct comparison between endpoints, cell types, and strains. Sensitivity was compared across test assay, cell type, and strain, where sensitivity was defined as having a lower BMD.

We used R statistical software to visualize BMD relationships among varying test conditions (RCoreTeam, 2015). Sensitive assays and strains identified in *in vitro* comparisons were compared with *in vivo* findings for consistency in results. *In vitro* assays were considered predictive if sensitivity was identified among common endpoints consistently between *in vitro* and *in vivo* studies.

Significance tests between BMDs

Statistical significance between benchmark doses was determined by calculating standard error and p-values based on asymptotic normality and confidence intervals at BMDs (Supplemental information, equations 1 and 2).

Results

Data collection and suitability for benchmark dose modeling

We accessed previously published data from *in vitro* investigations of Qdot toxicity from Lee et al. (2013) and *in vivo* studies of effects in mice from Scoville et al. (2015). Endpoints assessed following *in vitro* Qdot exposure included cytotoxicity and pro-inflammatory responses in three cell types. Of these

endpoints, pro-inflammatory responses CXCL1 and IL6 in all cell types passed the established fitness criteria, while no significant dose-response was observed for other endpoints in the study such at cytotoxicity. Of the responses assessed *in vivo*, pro-inflammatory responses KC (CXCL1) and neutrophils in BALF passed fitness criteria and were modeled for comparison with corresponding *in vitro* assessments. Because of the limited number of doses utilized, all endpoints were fit to a linear model.

Comparison of BMDs in in vitro assessments

We modeled dose response curves and calculated benchmark doses (BMDs) by exposure dose and dosimetric dose for two *in vitro* pro-inflammatory marker (IL6 and CXCL1) endpoints and compared BMDs between cell types, strains, and endpoints. Sensitivity of each factor was determined as showing a statistically significantly lower BMD.

Exposure dose comparison

Table 1 shows BMDs and BMDLs (BMD of the 95% confidence interval) for each *in vitro* endpoint by exposure dose (second column from right). MTECs were significantly less sensitive to Qdots than AMs and BMDMs for both endpoints in both strains ($p<0.05$). AMs and BMDMs showed similar BMDs within each endpoint in the C57BL/6J strain ($p>0.05$), while there were significant differences in sensitivity between these cell types in the A/J strain ($p<0.05$). Overall, the A/J strain was significantly more sensitive to Qdots in the CXCL1 endpoint for all cell types ($p<0.05$), and slightly more sensitive in the IL6 assessment for BMDMs ($p=0.058$). AMs and BMDMs were similar in sensitivity between IL6 and CXCL1 assays in both strains ($p>0.05$).

Dosimetric dose comparison

When comparing BMDs by dosimetric dose (Table 1, rightmost column), MTECs were generally observed to be equally as sensitive as AMs and BMDMs in both strains and both endpoints ($p>0.05$, $p>0.05$, respectively). The A/J strain was observed to be more sensitive by all cell types compared to the C57BL6 strain in the CXCL1 endpoint ($p<0.05$). The CXCL1 assay was a more sensitive endpoint in MTECs in both strains compared to the IL6 assay. IL6 and CXCL1 assays were similarly sensitive for both AMs and BMDMs across both strains ($p>0.05$).

Exposure dose and dosimetric dose BMD comparisons

BMD and BMDL relationships by exposure dose and dosimetric dose were compared among cell type, strain, and proinflammatory cytokine expression in *in vitro* assays (Figure 1). BMD analysis of CXCL1 and IL6 expression by exposure dose (exposure concentration, Figure 1A) shows BMDs and BMDLs for MTECs to be higher than those for BMDMs ($p<0.05$) and AMs ($p<0.05$) by both endpoints, with no overlap in confidence limits of the BMD (BMDL, or the BMD of the 95% confidence limit). This suggests that MTECs may be less sensitive to Qdots by one to two orders of magnitude across both strains and endpoints. AMs and BMDMs were similarly sensitive to Qdots in the C57BL/6J strain ($p>0.05$). BMDs for AMs and BMDMs were significantly different in the A/J strain ($p<0.05$) however, BMDs and BMDLs were generally within one order of magnitude in both endpoints.

In contrast, when assessing the same responses as a function of dosimetric dose (Figure 1B), we observed that the MTECs were generally equally sensitive as BMDMs ($p>0.05$) and AMs ($p>0.05$) overall, as indicated by similar BMD values and a high degree of overlap of confidence limits (BMDLs). AMs and BMDMs were similarly sensitive to each other within each endpoint and strain in both exposure dose and dosimetric assessments. The relative relationships between AMs and BMDMs remained consistent

between the two assessments, while the MTEC shows a higher degree of sensitivity when assessing BMDs by dosimetry.

In vivo results

Scoville et al. quantified the protein expression of KC (also known as CXCL1) in BALF of eight mouse strains after *in vivo* exposure to Qdots (Figure 2). KC (CXCL1) expression was significant in the A/J, NOD, and NZO strains, with A/J ranking as the most sensitive. A significant amount of genetic variability in KC (CXCL1) expression response was observed among strains. For example, A/J mice showed about two times more KC (CXCL1) after exposure to Qdots compared to strain-specific controls than C57BL/6J mice. In addition, there was a large amount of genetic variability in control response where controls in the AJ strain showed about twice as much KC in BALF as controls of the C57BL/6 strain. Significant responses were not observed in C57BL/6J, 129S1, PWK, WSB, or CAST strains compared to strain specific control values.

Dose responses were modeled for significant *in vivo* endpoints in Scoville et al. (2015) including KC (CXCL1) protein expression and percent neutrophil infiltration in BALF. BMDs were calculated by exposure dose (μg Cd equivalents/ kg body weight) and by dosimetric dose (ng Cd/kg tissue) and are shown in Table 2. The 129S1, C57BL/6J, CAST, PWK, and WSB strains did not show significant dose responses by either of these endpoints, and thus BMDs were not calculated. A/J was the most sensitive strain by the KC (CXCL1) endpoint by both the exposure dose and dosimetric dose. Both endpoints were similarly sensitive indicators of response.

Exposure dose and dosimetric dose comparison

Comparison of responses across strains *in vivo* shows the A/J strain has the lowest BMDs by both exposure dose and by dosimetric dose (Table 2), indicating the A/J strain is the most sensitive strain by this endpoint. When corrected for dosimetry, the A/J strain was statistically significantly lower than both the NOD and NZO strains ($p<0.05$). The NOD and NZO strains were not significantly different from each other by either endpoint, both by exposure dose and dosimetric dose assessments ($p>0.05$). Significant dose response effects were not observed in several of the strains including C57BL/6J, 129S1, PWK, WSB, and CAST strains.

Comparison across model systems (in vitro and in vivo)

We found the A/J strain was the more sensitive to Qdot exposure than the C57BL/6J both *in vitro* and *in vivo*. The A/J strain was more sensitive in both the IL6 and CXCL1 assays *in vitro* as well as in the KC (CXCL1) and neutrophil assays *in vivo*.

Discussion

The risk assessment framework utilizes *in vitro* studies as part of hazard identification to identify possible mechanisms of toxicity and inform potential endpoints of toxicity *in vivo*. Risk characterization however, depends heavily on the use of *in vivo* studies that can be time and resource intensive. The state of the field of toxicology in the 21st century and beyond requires risk assessment methods that are efficient and lean processes (EU, 2006; NRC, 2007). *In vitro* research has been proposed as an inexpensive and more efficient alternative to replace, reduce, and refine *in vivo* toxicity assessments (Zurlo et al., 1996; Nel et al., 2006).

In this study, we hypothesized that *in vitro* toxicity assessments of engineered nanomaterials can be useful in better informing and refining *in vivo* studies for risk assessment. We used standardized BMD analysis as a tool to identify *in vitro* endpoints and test systems that are most sensitive to Qdots. Similarly, Wignall et al. (2014) used a standardized BMD approach (BMD_{1SD} and BMD_{10}) to compare across many environmental chemicals for investigation of effects across various studies and chemicals. We found that the A/J mouse strain was more sensitive to Qdot exposure than the C57BL/6J strain consistently in both *in vitro* and *in vivo* using common endpoints. This effect was observed when assessing by both nominal and dosimetry dose metrics. Strain sensitivity is a critical consideration for *in vivo* assessments for hazard identification of Qdots and other inorganic ENMs. The C57BL/6J mouse strain is one of the most frequently used inbred strains in toxicological assessments of nanoparticles and other chemicals (Zurita et al., 2011; JacksonLaboratory, 2016). Our findings suggest that studies investigating effects of nanoparticles in solely the C57BL/6J strain may overlook effect levels in other genetic backgrounds. The genetic differences among the eight founder strains represents approximately 90% of murine genetic variability and captures a similar distribution of allele frequencies as humans (Churchill et al., 2004; Roberts et al., 2007). As such, capturing this variability can better inform risk assessments of potential effect levels in sensitive populations.

While BMD analysis by exposure dose showed MTECs were less sensitive to Qdots than AMs and BMDMs, analysis by dosimetry showed that MTECs were generally equally as sensitive to Qdot exposure, in general. MTECs were observed to take up less Cd (Qdots) per nominal exposure than AMs and BMDMs, however their proinflammatory cytokine response is equally as pronounced per amount of Cd, indicating that dosimetry is critical in the consideration of ENM toxicity *in vitro* for comparison of cell types. This observation of difference in uptake between cell type may be due to the differing biological functions of cell types as AMs and BMDMs are phagocytic cell types and have been shown to take up

greater amounts of ENMs including Qdots (Zhang et al., 2013). In contrast, MTECs are epithelial cells whose primary biological functions do not necessarily include phagocytizing particles or other foreign materials. Similar findings in sensitivity among cell types may be used to inform future *in vitro* work and promote studies in cell types that are faster and less resource intensive to yield similar results.

Measuring dosimetry allows for the assessment of toxicity of particles based on delivery of material to the cell culture following an exposure. This approach is based on the assumption and basic tenet of toxicology that effects observed are caused by the material delivered to, and thus able to interact with the receptor (cell or tissue, etc.). Assessing *in vitro* effects as a function of dosimetric dose creates a common denominator by which different ENMs, assays, cell types, strains, and culture conditions can be compared (Teeguarden et al., 2007). Because dosimetry can also be measured *in vivo*, *in vitro* findings as a function of dosimetry can be translated to effects in similar cell types *in vivo*. This is especially relevant for organotypic cell culture models where cultures more closely represent tissue structure and function, and delivery of particles to culture systems more closely represents *in vivo* exposure kinetics (Weber et al., 2016).

Unlike many chemicals, *in vitro* investigation of ENMs pose unique challenges relating to physicochemical properties of the materials. Particles in culture media have a propensity to aggregate or agglomerate, significantly affecting the delivery rate and contact of particles to the cells in culture (Teeguarden et al., 2007). Dissolution, or the dissolving of ions from soluble or semi-soluble particles in solution, is influenced by particle physicochemical characteristics as well as local culture conditions (Shannahan et al., 2013; Utembe et al., 2015). Slight differences in particle physicochemical properties (e.g., size or stabilizing coating) and culture conditions (e.g., pH or presence of protein in media) may

result in differing extent of effects on cells in culture. Measuring the dosimetry of materials in cells after exposure allows for the direct comparison between culture systems.

We observed consistency in response by common endpoints in both *in vitro* and *in vivo* studies. Assessments of the BMDs by the proinflammatory marker CXCL1 (referred to as KC in Scoville et al.) were found to be sensitive endpoints in both test systems. The CXCL1 endpoint also showed the A/J strain was more sensitive than the C57BL/6J strain both *in vitro* and *in vivo*. CXCL1 plays a critical role in neutrophil recruitment to sites of injury and inflammation, and was found to be highly correlated with neutrophil presence in the airway following exposure in Scoville et al. Acute lung injury has been shown to initiate proinflammatory cytokines such as CXCL1 and quickly progress into fibrotic responses (Wynn, 2011). Both macrophage and airway epithelial cell types used in these studies have been associated with the development of pathologies such as pulmonary fibrosis. Several mechanistic hypotheses describe how environmental insults such as exposure to ENMs can activate neutrophils and other cell types to contribute proinflammatory factors that can go on to activate fibroblasts and eventually lead to fibrosis (Bringardner et al., 2008). Airway epithelial cells have been described to contribute to this process by proliferating and transitioning into microfibroblasts or fibroblasts (Kim et al., 2006).

Our analysis showed dosimetry was critical to identify cell type sensitivity and strain sensitivity in both *in vitro* and *in vivo* systems. Because dosimetry of inorganic nanomaterials can be easily quantified *in vitro* and *in vivo* using ICP-MS and other metals quantification methods, this framework for the assessment of *in vitro* ENM studies to inform *in vivo* studies and risk assessment may be applied to other inorganic nanomaterials, such as silver nanoparticles (AgNPs). AgNPs are increasingly being used in consumer and commercial products for their antimicrobial activity and have been actively studied for potential health effects using both *in vitro* and *in vivo* studies.

While this framework of utilizing BMD analysis and dosimetry-based *in vitro* studies can provide insights useful in informing *in vivo* studies and ENM risk assessment, several limitations of this work are noted. First, the database available provided data that was fairly limited. Given the experimental nature of ENM assessment, our BMD analysis focused on the area of the dose response curve where significant change was observed. As such, our dose-response analyses were constrained to a single dose both *in vivo* and *in vitro*. The addition of further lower doses that would show an increasing response across multiple doses could better represent the dose-response effect and BMD. In addition, interpretation of *in vivo* data was limited as the dosimetric Cd measures were taken 8 hours after exposure. As such, the Cd measured may not represent the original dose to the tissue, rather represents the residual Cd after exposure. Differences in toxicokinetics and clearance among the strains may have affected this residual Cd level. Next, a standardized benchmark response (BMR) of 1 standard deviation change relative to controls was used across all BMD analyses. This approach allowed for a consistent benchmark to compare across endpoints and has been utilized by other groups to make comparisons across endpoints (Wignall et al., 2014). However, this effect level may not necessarily represent a biologically significant effect for all endpoints. Therefore, the BMDs calculated within this framework may not necessarily be used as a point of departure for risk assessment purposes. Findings within this framework are best geared toward informing directions of *in vivo* research non-quantitatively. Finally, while A/J strain sensitivity relative to the C57BL/6J was identified both *in vitro* and *in vivo*, the *in vitro* dataset was limited to just these two strains. Further *in vitro* studies investigating sensitivity of effects in other strains may further substantiate the relationships.

In summary, we found that a standardized BMD and dosimetric analysis allows for the comparison of sensitivity of assay, cell type, and animal strains to inorganic ENMs. We observed that when assessed by

dosimetry, exposure dose findings of differential toxicity and inflammation by cell type are not significant. We observed significant mouse strain dependent heterogeneity in response to Qdots. While C57BL/6J mice are commonly used in toxicology studies, they tend to be relatively resistant to inorganic ENM-induced pulmonary inflammation compared to the A/J strain. This suggests that assessment of the relative hazards of ENMs should include exposure modeling, toxicokinetic and toxicodynamic modeling, as well as gene/environment interactions. We found that when put into context, *in vitro* assays provide valuable insight on critical factors for ENM risk assessment approaches.

Table 1. Summary of BMDs and BMDLs calculated from Lee et al. (2015) *in vitro* exposures to CdSe/ZnS Qdots. BMDs and BMDLs are calculated by exposure concentration (0 or 10 nM Qdots) and by dosimetric dose (ng Cd/100,000 cells) for significant endpoints of response (IL6 and CXCL1) for A/J and C57BL/6J mice in three cell types. n=4 per dose group.

Endpoint	Strain, Species	Cell type	Dosimetric Dose (ng Cd/100,000 cells)	Exposure Conc. BMD (BMDL) (nM Qdots)	Dosimetric Dose BMD (BMDL) (ng Cd/100,000 cells)
IL6	A/J mouse	AM	0.3, 25.55	0.58 (0.40)	1.45 (1.01)
		BMDM	0.3, 36.9	0.24 (0.17)	0.87 (0.60)
		MTEC	0.12, 1.02	27.54 (6.51)	2.48 (0.59)
IL6	C57BL/6J mouse	AM	0.3, 29.15	0.43 (0.30)	1.25 (0.87)
		BMDM	0.3, 36.0	0.40 (0.28)	1.42 (0.99)
		MTEC	0.12, 2.54	31.49 (6.72)	7.62 (1.63)
CXCL1	A/J mouse	AM	0.3, 25.55	0.10 (0.07)	0.26 (0.18)
		BMDM	0.3, 36.9	0.37 (0.26)	1.35 (0.94)
		MTEC	0.12, 1.02	2.84 (1.84)	0.26 (0.17)
CXCL1	C57BL/6J mouse	AM	0.3, 29.15	0.76 (0.53)	2.2 (1.52)
		BMDM	0.3, 36.0	0.89 (0.62)	3.17 (2.19)
		MTEC	0.12, 2.54	9.69 (4.40)	2.35 (1.07)

Table 2. Summary of BMDs and BMDLs calculated from Scoville et al. (2015) *in vivo* exposures to CdSe/ZnS Qdots. BMDs and BMDLs are calculated by exposure concentration (μg Cd equivalents/ kg body weight) and by dosimetric dose (ng Cd/mg tissue) for significant endpoints of response. n=6 per exposure group.

Exposure Concentration (μg Cd equivalents/ kg body weight)	Endpoint	Strain	Dosimetric Dose (ng Cd/mg tissue)	Exposure Conc. BMD (BMDL) (μg Cd equivalents/ kg body weight)	Dosimetric Dose BMD (BMDL) (ng Cd/mg tissue)
0, 6	KC (CXCL1)	A/J	0.002, 0.165	2.87 (1.84)	0.08 (0.05)
		NOD	0.0, 0.252	4.34 (2.29)	0.18 (0.10)
		NZO	0.0, 0.335	3.61 (2.10)	0.20 (0.12)
		129S1	Not significant	Not significant	Not significant
		C57BL/6J	Not significant	Not significant	Not significant
		CAST	Not significant	Not significant	Not significant
		PWK	Not significant	Not significant	Not significant
		WSB	Not significant	Not significant	Not significant
0, 6	% Neutrophils in BALF	A/J	0.002, 0.165	5.45 (2.76)	0.15 (0.08)
		NOD	0.0, 0.252	2.50 (1.61)	0.11 (0.07)
		NZO	0.0, 0.335	3.33 (2.01)	0.19 (0.11)
		129S1	Not significant	Not significant	Not significant
		C57BL/6J	Not significant	Not significant	Not significant
		CAST	Not significant	Not significant	Not significant
		PWK	Not significant	Not significant	Not significant
		WSB	Not significant	Not significant	Not significant

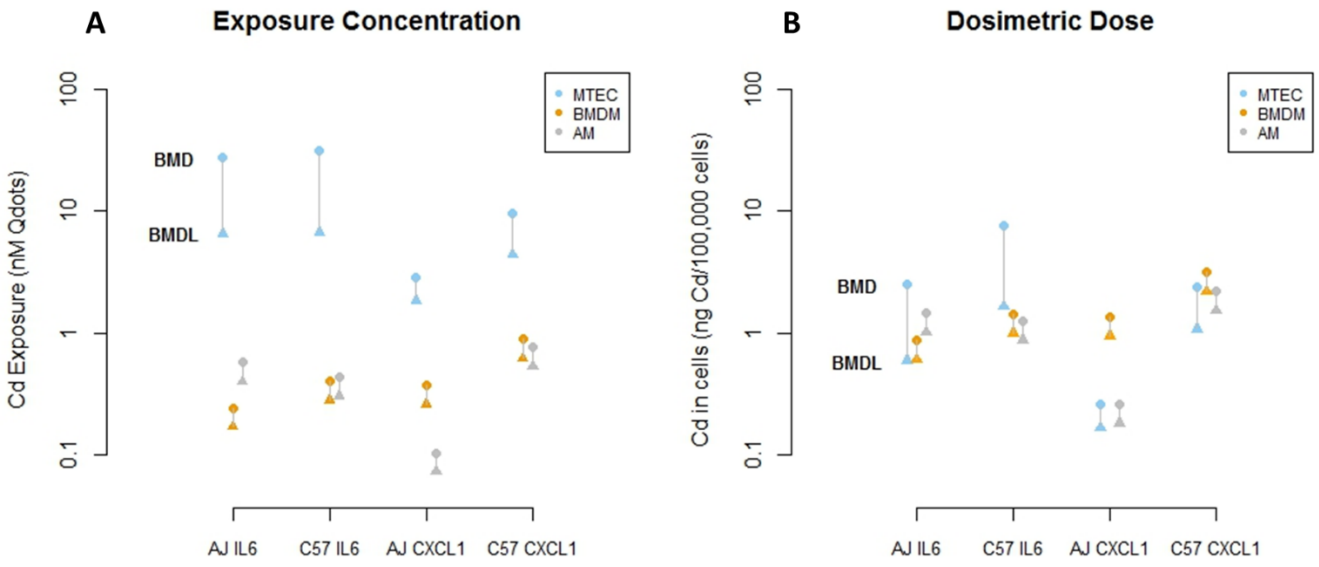

Figure 1. BMD and BMDL values for IL-6 and CXCL-1 responses following *in vitro* Cd Qdot exposure by exposure dose (A) and dosimetric dose (B). BMDs are shown for multiple cell types, two different rodent strains (vertical panels). AMs and BMDMs are similarly sensitive across all endpoints and dose metrics. MTECs were significantly less sensitive than AMs and BMDMs by exposure dose assessment (A), but equally sensitive when adjusted for dosimetry (B).

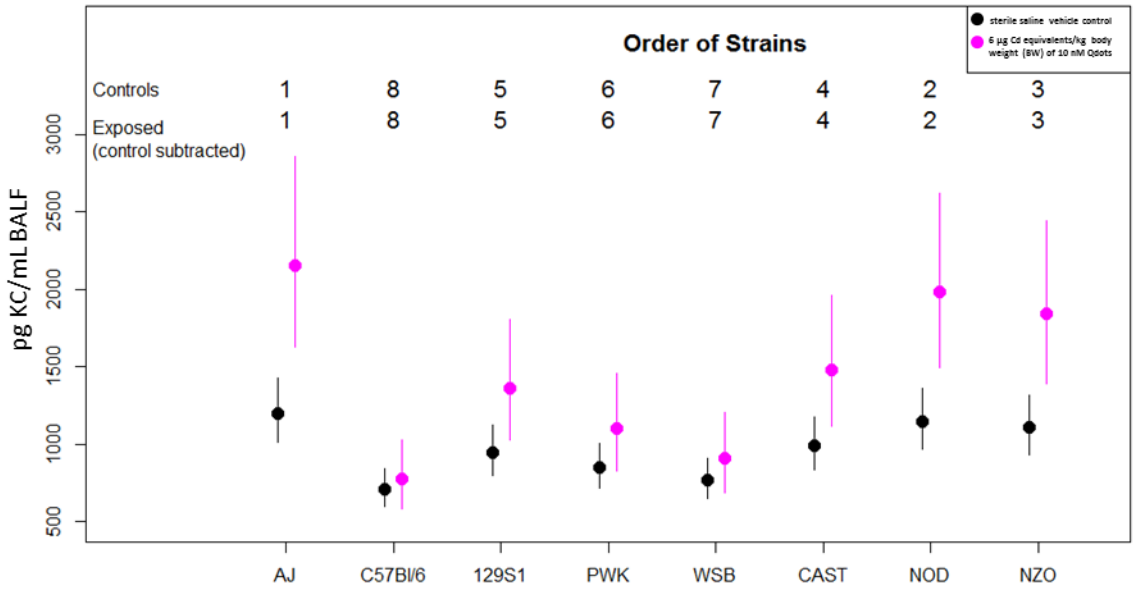

Figure 2. KC (CXCL-1) protein expression in BALF after oropharyngeal aspiration exposure to Qdots across eight mouse strains from Scoville et al. (2015). Significant increases in KC expression was observed in the A/J, NOD, and NZO strains. The A/J strain showed the greatest increase in KC relative to controls while the C57BL/6J strain ranked last in sensitivity by this endpoint. A large amount of genetic variability was observed across strains in both treated and control animals.

Chapter 4 References

Azzazy, H. M., M. M. Mansour, et al. (2007). "From diagnostics to therapy: prospects of quantum dots." Clin Biochem **40**(13-14): 917-927.

Bringardner, B. D., C. P. Baran, et al. (2008). "The role of inflammation in the pathogenesis of idiopathic pulmonary fibrosis." Antioxidants & redox signaling **10**(2): 287-301.

Browne, P., R. S. Judson, et al. (2015). "Screening Chemicals for Estrogen Receptor Bioactivity Using a Computational Model." Environmental science & technology **49**(14): 8804-8814.

Churchill, G. A., D. C. Airey, et al. (2004). "The Collaborative Cross, a community resource for the genetic analysis of complex traits." Nat Genet **36**(11): 1133-1137.

Crump, K. S. (1995). "Calculation of Benchmark Doses from Continuous Data." Risk Analysis **15**(1): 79-89.

Dabbousi BO, R.-V. J., Mikulec FV, Heine JR, Mattoussi H, Ober R, Jensen KF, Bawendi MG (1997). "(CdSe)ZnS core–shell quantum dots: synthesis and characterization of a size series of highly luminescent nanocrystallites." J. Phys. Chem(101): 9463-9475.

Davis, J. A., J. S. Gift, et al. (2011). "Introduction to benchmark dose methods and U.S. EPA's benchmark dose software (BMDS) version 2.1.1." Toxicol Appl Pharmacol **254**(2): 181-191.

Donaldson, K., P. J. Borm, et al. (2009). "The limits of testing particle-mediated oxidative stress *in vitro* in predicting diverse pathologies; relevance for testing of nanoparticles." Particle and fibre toxicology **6**: 13.

EPA Science Policy Council (2007). Nanotechnology White Paper. U. S. E. P. Agency. Washington, D.C.

EPA, U. (2016). H.R. 2576 — 114th Congress: Frank R. Lautenberg Chemical Safety for the 21st Century Act. U. S. Congress.

EU (2006). Regulation (EC) No 1907/2006 concerning the Registration, Evaluation, Authorisation and Restriction of Chemicals (REACH), establishing a European Chemicals Agency, Official Journal of the European Union. **396:** 1-849.

JacksonLaboratory. (2016). "C57BL/6J Mouse Strain Data Sheet." from https://www.jax.org/strain/000664.

Kavlock, R. J., B. C. Allen, et al. (1995). "Dose-response assessments for developmental toxicity. IV. Benchmark doses for fetal weight changes." Fundam Appl Toxicol **26**(2): 211-222.

Kim, K. K., M. C. Kugler, et al. (2006). "Alveolar epithelial cell mesenchymal transition develops *in vivo* during pulmonary fibrosis and is regulated by the extracellular matrix." Proceedings of the National Academy of Sciences of the United States of America **103**(35): 13180-13185.

Lee, V., R. S. McMahan, et al. (2015). "Amphiphilic polymer-coated CdSe/ZnS quantum dots induce pro-inflammatory cytokine expression in mouse lung epithelial cells and macrophages." Nanotoxicology **9**(3): 336-343.

Meyer, K. C., G. Raghu, et al. (2012). "An official American Thoracic Society clinical practice guideline: the clinical utility of bronchoalveolar lavage cellular analysis in interstitial lung disease." Am J Respir Crit Care Med **185**(9): 1004-1014.

Nel, A., T. Xia, et al. (2006). "Toxic potential of materials at the nanolevel." Science **311**(5761): 622-627.

NRC (2007). Toxicity Testing in the 21st Century: A Vision and a Strategy.

RCoreTeam (2015). R: A language and environment for statistical computing. Vienna, Austria, R Foundation for Statistical Computing.

Roberts, A., F. Pardo-Manuel de Villena, et al. (2007). "The polymorphism architecture of mouse genetic resources elucidated using genome-wide resequencing data: implications for QTL discovery and systems genetics." Mamm Genome **18**(6-7): 473-481.

Scoville, D. K., C. C. White, et al. (2015). "Susceptibility to quantum dot induced lung inflammation differs widely among the Collaborative Cross founder mouse strains." Toxicol Appl Pharmacol **289**(2): 240-250.

Shannahan, J. H., X. Lai, et al. (2013). "Silver nanoparticle protein corona composition in cell culture media." PLoS One **8**(9): e74001.
Teeguarden, J. G., P. M. Hinderliter, et al. (2007). "Particokinetics *in vitro*: dosimetry considerations for *in vitro* nanoparticle toxicity assessments." Toxicol Sci **95**(2): 300-312.
USEPA (2012). Benchmark Dose Technical Guidance. U. S. E. P. Agency. Washington, DC.
Utembe, W., K. Potgieter, et al. (2015). "Dissolution and biodurability: Important parameters needed for risk assessment of nanomaterials." Part Fibre Toxicol **12**: 11.
Weber, E. J., A. Chapron, et al. (2016). "Development of a microphysiological model of human kidney proximal tubule function." Kidney Int **90**(3): 627-637.
Wignall, J. A., A. J. Shapiro, et al. (2014). "Standardizing benchmark dose calculations to improve science-based decisions in human health assessments." Environ Health Perspect **122**(5): 499-505.
Wynn, T. A. (2011). "Integrating mechanisms of pulmonary fibrosis." J Exp Med **208**(7): 1339-1350.
Zhang, Y., H. Pan, et al. (2013). "Functionalized quantum dots induce proinflammatory responses *in vitro*: the role of terminal functional group-associated endocytic pathways." Nanoscale **5**(13): 5919-5929.
Zurita, E., M. Chagoyen, et al. (2011). "Genetic polymorphisms among C57BL/6 mouse inbred strains." Transgenic Res **20**(3): 481-489.
Zurlo, J., D. Rudacille, et al. (1996). "The three Rs: the way forward." Environ Health Perspect **104**(8): 878-880.

Supplemental Information

Equation 1. Confidence intervals at BMD:

$$CI = \text{BMD} \pm \left[\frac{|\text{BMD} - \text{BMDL}|}{1.645}\right] x\ 1.96$$

Equation 2. P-value for significant differences between BMDs from was calculated from Z score based on a normal distribution:

$$Z\ score = \frac{|BMD_1 - BMD_2|}{\sqrt{(BMD_1)^2 + (BMD_2)^2}}$$

Supplemental Table 1. In vitro BMD confidence intervals

Dose	Endpoint	Strain, Species	Cell type	BMD	BMD Lower CI	BMD Upper CI	BMDL
Exposure	IL6	A/J mouse	AM	0.58	0.37	0.79	0.4
			BMDM	0.24	0.16	0.32	0.17
			MTEC	27.54	2.48	52.60	6.51
	IL6	C57BL/6J mouse	AM	0.43	0.28	0.58	0.3
			BMDM	0.4	0.26	0.54	0.28
			MTEC	31.49	1.98	61.00	6.72
	CXCL1	A/J mouse	AM	0.1	0.06	0.14	0.07
			BMDM	0.37	0.24	0.50	0.26
			MTEC	2.84	1.65	4.03	1.84
	CXCL1	C57BL/6J mouse	AM	0.76	0.49	1.03	0.53
			BMDM	0.89	0.57	1.21	0.62
			MTEC	9.69	3.39	15.99	4.4
Dosimetric	IL6	A/J mouse	AM	1.45	0.93	1.97	1.01
			BMDM	0.87	0.55	1.19	0.6
			MTEC	2.48	0.23	4.73	0.59
	IL6	C57BL/6J mouse	AM	1.25	0.80	1.70	0.87
			BMDM	1.42	0.91	1.93	0.99
			MTEC	7.62	0.48	14.76	1.63
	CXCL1	A/J mouse	AM	0.26	0.16	0.36	0.18
			BMDM	1.35	0.86	1.84	0.94
			MTEC	0.26	0.15	0.37	0.17
	CXCL1	C57BL/6J mouse	AM	2.2	1.39	3.01	1.52
			BMDM	3.17	2.00	4.34	2.19
			MTEC	2.35	0.82	3.88	1.07

Supplemental Table 2. In vivo BMD confidence intervals

Dose	Endpoint	Strain, Species	BMD	Lower CI	Upper CI	BMDL
Exposure	KC	A/J mouse	2.87	1.64	4.10	1.84
		NOD mouse	4.34	1.90	6.78	2.29
		NZO mouse	3.61	1.81	5.41	2.1
	% Neutrophils	A/J mouse	5.45	2.24	8.66	2.76
		NOD mouse	2.5	1.44	3.56	1.61
		NZO mouse	3.33	1.76	4.90	2.01
Dosimetric	KC	A/J mouse	0.08	0.04	0.12	0.05
		NOD mouse	0.18	0.08	0.28	0.1
		NZO mouse	0.2	0.10	0.30	0.12
	% Neutrophils	A/J mouse	0.15	0.07	0.23	0.08
		NOD mouse	0.11	0.06	0.16	0.07
		NZO mouse	0.19	0.09	0.29	0.11

Supplemental Figure 1. Benchmark dose modeling decision criteria

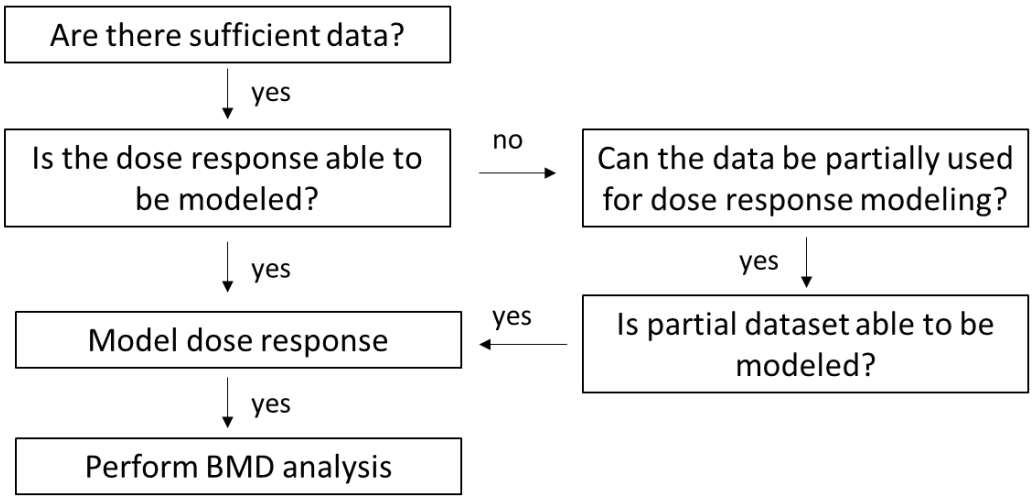

Chapter 5

Conclusions and Future Directions

Brittany A. Weldon

Technological advancements in the ability to synthesize nano-sized particles have led to an increase in production and use of engineered nanomaterials. Silver nanoparticles (AgNPs) are a form of engineered nanomaterials that have been applied to many consumer and medical products for their antimicrobial properties. The potential health risks from human exposures to AgNPs are yet to be thoroughly characterized. Like other heavy metals, silver is known to have potential adverse health effects in humans. In addition, the unique physicochemical properties of nano-sized materials create unique exposure scenarios where humans may be affected differently by nanomaterials than larger sized particles of the same composition. The Precautionary Principle states that in the face of uncertainty and gaps in evidence, society should take precautionary measures to avert risks where the potential to harm human or environmental health is possible (Wingspread Consensus Statement on the Precautionary Principle, 1998). This paradigm has been embraced by the European Chemicals Agency through their REACH legislation and the United States Environmental Protection Agency in recent advancements in the Toxic Substances Control Act; however, AgNP application and use in products has continued to accelerate despite lacking critical risk assessments. The work presented in this dissertation aimed to assess human health risks from exposure to AgNPs in an occupational scenario and support and inform future risk assessments in other contexts.

The increased application of AgNPs and integration into various consumer products can be expected to impact the exposure of workers to AgNPs during manufacturing, handling, and disposal of AgNP-containing products. Silver dusts, consisting of micro-sized particles and soluble silver compounds have

established occupational exposure limits (OELs), silver nanoparticles exhibit different physicochemical properties from bulk materials. Currently, no OEL has yet been suggested specifically for AgNPs. Chapter 2 discussed work we have done to assess potential risks to workers that may be exposed to AgNPs in occupational settings. We determined inhalation of airborne AgNPs to be the exposure route of highest exposure and potential risk and we suggest an OEL of 0.19μg/m^3 for aerosolized AgNPs in the workplace. The proposed OEL of 0.19 μg/m3, derived from dosimetric measurements of silver in lung and liver, as well as recovery studies, is expected to prevent liver and lung damage and argyria from AgNPs exposure in workers. Though there is a lack of long-term toxicity data, exposure data, and human health effect information, the proposed OEL will protect workers' health from exposure based on best available data in the literature. Exposure mitigation technologies, including isolation and encapsulation, industrial ventilation, and administrative control to limit access to the high exposure area should be implemented to lower workplace exposure levels below the proposed OEL. Future work may involve more extensive characterization of exposures in the workplace and effectiveness of mitigation technologies and personal protective equipment.

The use of AgNPs in consumer products and medical equipment for children and maternal usage creates the potential for AgNP exposure to the developing brain. Like other heavy metals, silver has been shown to interact with the developing nervous system. Silver has been found in fetal brain and other tissue following maternal exposure to AgNPs during pregnancy and lactation, there is a potential for exposure during this critical period of development. There is a need to determine the risks of AgNP exposure to the developing nervous system. As such, in *Chapter 3* we described the use of a 3-dimensional *in vitro* neurodevelopment model to characterize toxicity of AgNPs of differing sizes and shapes on developing neural cultures. We found that developing neural cultures are susceptible to toxic effects from exposure to AgNPs. Cultures were more sensitive to AgNP exposures at differentiation stages of development,

with greater uptake of particles occurring at later time points. Cultures were more sensitive to smaller sized AgNPs, despite less overall uptake of Ag compared to larger particles. We found dissolution of AgNPs in media may not contribute to the cytotoxic effects observed. Future work can be done to investigate the contributions of cell type in differentiating cultures to investigate the mechanisms by which cultures show increased sensitivity to AgNPs at these time points. For example, the presence of microglia and other glial cell types or differential uptake between cell types may inform mechanisms of uptake and cytotoxicity. Specialized neuronal cell types, such as dopaminergic neurons may also be targeted by silver and AgNPs. Assays that identify cell-type specific endpoints will allow for identification of these mechanisms and targets.

Because of the rapid rate of development and use of engineered nanomaterials including AgNPs, there is a need to accelerate the pace of risk assessment of these materials. While *in vitro* studies have long been used to suggest mechanisms and possible endpoints of toxicity for risk assessments, there is a potential to better use *in vitro* studies to inform *in vivo* studies and risk assessments for ENMs. Because of the unique physicochemical characteristics of nanoparticles, there has been some question as to the utility of *in vitro* studies of ENMs. The study discussed in *Chapter 4* showed how benchmark dose analysis can be used to determine whether *in vitro* findings of ENM toxicity could have predicted *in vivo* findings using previously published literature. As such, this method can be applied to other *in vitro* assessments of ENMs and used to better inform *in vivo* research and ENM risk assessments. We found benchmark dose and dosimetric analysis allows for the comparison of sensitivity of *in vitro* assay, cell type, and animal strains to inorganic ENMs. We observed Qdots induce differential toxicity and inflammation, depending on the cell type and significant mouse strain dependent heterogeneity in response to Qdots. Interestingly, we found C57BL/6 mouse strains, the most commonly used in toxicology studies, were relatively resistant to inorganic ENM-induced inflammation. As such, risk

assessments should provide more weight to other strains found to be more sensitive to ENMs. *In vitro* assays provide valuable insight on these critical factors in ENM risk assessment approaches. Future work may use data available through the NIEHS NCNHIR consortium and the broader literature to determine the utility of this framework for other inorganic nanomaterials, such as silver nanoparticles. Data sets assessing a wide variety of endpoints in various cell types and organ systems across different test systems and including dosimetry measurements may be best suited for this approach. Our methods found *in vitro* studies to be predictive of *in vivo* sensitives, despite a very limited dataset. More robust datasets may provide further insights into consistency in responses across systems and applications of this work.

In this dissertation we have presented critical works that add to the body of knowledge that's supports risk assessment and risk management decisions for AgNPs. We found that health risks from exposure to aerosolized AgNPs in the workplace are greater than those for larger sized silver dust and fumes and require a lower exposure limit for worker protection. We found that AgNP exposure during critical windows of development can potentially affect developing neural systems. In addition, we developed a method by which *in vitro* studies can be applied to risk assessment and better inform *in vivo* AgNP studies to improve efficiency and capture population variability and sensitivity. Overall, this research demonstrates that significant risks to humans from exposures to AgNPs may exist, and that precautions should be taken to reduce exposures while risk assessment methods can be efficiently applied to better characterize risks.

Appendix I.

Urinary microRNAs as Potential Biomarkers of Pesticide Exposure

Brittany A. Weldon[1,2], Sara Pacheco Shubin[1,2], Marissa N. Smith[1,2], Tomomi Workman[1,2], Alexander Artemenko[1,2], William C. Griffith[1,2], Beti Thompson[3], and Elaine M. Faustman[1,2]

[1]Institute for Risk Analysis and Risk Communication, University of Washington, Seattle, WA

[2]Department of Environmental and Occupational Health Sciences, University of Washington, Seattle, WA

[3]Fred Hutchinson Cancer Research Center, Seattle, WA

Published in Toxicology and Applied Pharmacology. Published online 2016 Jan 27.

Correspondence to:
Elaine M. Faustman
Department of Environmental Health
University of Washington
4225 Roosevelt Way NE Suite 100
Seattle, WA 98105
Phone: 206-685-2269
E-mail: faustman@uw.edu

Keywords: microRNA, organophosphate, pesticides, exposure biomarkers

Abstract

MicroRNAs (miRNAs) are post-transcriptional regulators that silence messenger RNAs. Because miRNAs are stable at room temperature and long-lived, they have been proposed as molecular biomarkers to monitor disease and exposure status. While urinary miRNAs have been used clinically as potential diagnostic markers for kidney and bladder cancers and other diseases, their utility in non-clinical settings has yet to be fully developed. Our goal was to investigate the potential of urinary miRNAs to act as biomarkers of pesticide exposure and early biological response by identifying the miRNAs present in urine from 27 parent/child, farmworker/non-farmworker pairs (16FW/11NFW) collected during two agricultural seasons (thinning and post-harvest) and characterizing the between- and within-individual variability of these miRNA epigenetic regulators. MiRNAs were isolated from archived urine samples and identified using PCR arrays. Comparisons were made between age, households, season, and occupation. Of 384 miRNAs investigated, 297 (77%) were detectable in at least one sample. Seven miRNAs were detected in at least 50% of the samples, and one miRNA was present in 96% of the samples. Principal components and hierarchical clustering analyses indicate significant differences in miRNA profiles between farmworker and non-farmworker adults as well as between seasons. Six miRNAs were observed to be positively associated with farmworkers status during the post-harvest season. Expression of five of these miRNA trended towards a positive dose response relationship with organophosphate pesticide metabolites in farmworkers. These results suggest that miRNAs may be novel biomarkers of pesticide exposure and early biological response.

Introduction

MicroRNAs (miRNAs) are short, single-stranded non-coding RNAs that are ~22 nucleotides in length that act as post transcriptional regulators that silence messenger RNAs. This function allows them to influence RNA translation to protein through partial complementary binding. MiRNAs have also been observed to cause functional changes by up-regulating target mRNA translation (Vasudevan et al., 2007).

MiRNAs are found ubiquitously throughout human tissues, existing in a wide variety of bodily fluids including urine and saliva (Weber et al., 2010). Unlike other types of RNA, miRNAs are stable at room temperature and do not rapidly degrade. These characteristics give miRNAs the potential to persist in non-ideal conditions for extended periods of time making them ideal candidates for use as molecular biomarkers to monitor disease and exposure status. While some miRNAs may be produced in a tissue-specific or cell-specific manner (Wang et al., 2009), miRNAs identified in human urine have the potential to serve as biomarkers of systemic conditions (Weber et al., 2010). Urinary miRNAs have previously been used clinically as potential diagnostic markers of prostate, bladder, and kidney diseases (Hanke et al., 2010; Catto et al., 2011). A recent review indicated several studies have attempted to utilize miRNAs as biomarkers of environmental exposures including cigarette smoke, air pollution, endocrine disruptors, and other environmental toxicants (Vrijens et al., 2015). These characteristics and previous applications suggest that miRNAs may also be novel biomarkers of pesticide exposure and early response.

Organophosphate (OP) pesticides are heavily used in agriculture, leading to occupational and community exposures (Thompson et al. 2014). Chronic OP exposure has been implicated in several adverse health outcomes including respiratory and neurological effects (Eskenazi et al., 1999; Gray and Lawler 2011). Azinphos-methyl (AZM) is a dimethyl OP pesticide that was frequently used in agricultural production of pome fruits (e.g. apples and pears) until the United States Environmental Protection

Agency (USEPA) mandated a phase-out process that began in 2012 (USEPA 2009). However, assessing pesticide exposure can be complex, as seasonal use rates and subsequent exposures vary substantially. For example, AZM is the primary pesticide used on pome fruit trees during the thinning season (mid-June to mid-August). Following application of AZM, farmworkers actively trim pome fruit tree branches, potentially resulting in high AZM exposures in farmworkers (Thompson et al., 2014). During the harvest season (early September to late-October) AZM and other OP use are reduced. However, farmworkers may continue to be exposed as they actively harvest tree fruits and may apply other pesticides as needed. While direct pesticide application is reduced in post-harvest season (mid-November to mid-December), pesticide exposure is likely to persist through this season through house-dust and other take-home pathways of exposure. Peak amounts of AZM and other OPs, Phosmet and Diazinon, have been previously observed in house dust in the harvest season compared to thinning season. House dust has been shown to be a critical exposure pathway as it allows for continued exposure to pesticides. The high amounts of OPs found in the home during and immediately following the harvest season may result in pesticide exposures in the home, especially as more time is spent indoors during the post-harvest season (Thompson et al., 2014). Additionally, there may be cumulative effects from the preceding thinning and harvest seasons of exposures. This dynamic exposure pattern requires multiple measurements to fully assess.

One approach to assess pesticide exposure is through measurement of pesticides, metabolites and other biomarkers in urine. Because providing urine samples is relatively non-invasive, it can be collected at multiple seasons throughout the year. Urinary metabolites and biomarkers can provide insight into systemic and tissue-specific conditions, allowing for the identification of both markers of exposure and effect. One group of urinary biomarkers that are hypothesized to indicate both exposure and early biological response are miRNAs. Because extracellular miRNAs are known to be representative of cell and tissue-specific conditions (Lee et al., 2012), miRNAs in the urine may indicate biochemical

changes in response to exposures and a potential early epigenetic response. A recent study by (Mall et al., 2013) found that urinary miRNAs remain stable throughout a variety of storage conditions, further supporting their potential for urine to provide reliable biomarkers in both clinical and archived samples.

The goal of our study was to determine if miRNAs can be extracted from archived, home-collected urine samples from farmworker and non-farmworker adults and children and be used to characterize between- and within-individual variability of these miRNAs, to evaluate biomarker potential, and to gain molecular insight into systems affected by associated OP pesticide exposure. We hypothesized that urinary miRNAs profiles can be used to predict occupational status and OP pesticide exposure in a cohort of farmworker and non-farmworker households. To determine how exposure to OP pesticides may impact miRNA profiles, we utilized global miRNA profiling techniques.

Methods

Study Population

The University of Washington Center for Child Environmental Health Risks Research (CHC) Cohort is situated in one of Washington State's primary agricultural regions, the lower Yakima Valley. Study participants were recruited from the larger CHC cohort to participate in this nested study of environmental influences on urinary miRNA. The CHC cohort has been described in two recent studies, Thompson et al., 2014 and Smith et al., 2015. Briefly, in 2011, 27 women of childbearing age (18-49 years) and one child from each household were recruited from the larger CHC cohort to participate in this study. All participants self-reported "fair" to "excellent" health in a single item perceived health status questionnaire administered at the time of sample collection. None of the participants reported "poor" health. Participants were asked about their smoking status as well as smokers in their households and all reported themselves as non-smokers with no smokers in their households. Children

were between the ages of 6 and 10 years. Roughly half of the women recruited are pome fruit (e.g., apple or pear) farmworkers (FWs, n=16) and half are non-farmworkers (NFWs, n=11) employed in other sectors including factories, schools, and stores in the same region. Nearly all speak Spanish as a primary language. A detailed description of the nested study participants can be found in Smith et al. 2015.

Sampling Design and Collection

Urine samples were collected in the thinning (June- August) and post-harvest (November-December) agricultural seasons of 2011. In each season, first morning void urine samples were collected from adults and children on four separate days over a 7 day period (days 1, 3, 5, and 7). Participants stored samples in their home refrigerator until the samples were collected by study personnel. Urine samples were then secured in plastic bags and transported to the University of Washington in a cooler with frozen ice packs. Once at the University, samples were inverted to ensure homogenous mixing, divided into 10mL aliquots and stored at -20°C until analysis. All sample collection procedures were reviewed and approved by the Fred Hutchinson Cancer Research Center's Institutional Review Board (File IR 5946).

Pesticide Metabolite Analysis:

All urine samples from adults and children were analyzed for three dimethyl organophosphate pesticide metabolites: dimethyl-phosphate (DMP), dimethyl-thiophosphate (DMTP), and dimethyl-dithiophosphate (DMDTP) and three diethyl (DE) metabolites: diethyl-phosphate (DEP), diethyl-thiophosphate (DETP), and diethyl-dithiophosphate (DEDTP). Samples were analyzed using methods described previously in Thompson et al., 2014 and Odetokun et al., 2010. Metabolite concentrations are reported without creatinine, as done in Barr et al., 2004 and Thompson et al., 2014. Briefly, samples were prepared for analysis by HPLC-MS/MS as described in Thompson et al., 2014. Each HPLC-MS/MS

run contained a full 8-point calibration plot, 3 quality-control materials spiked at concentrations spanning the entire calibration range, 2 blank samples, and 36 unknown urine samples. Isotope dilution calibration was used to quantify the analytes and to provide concentrations in ng/ml units. Quality control parameters, described in Westgard's multirules were used to determine whether the data were valid.

Samples with metabolites below the limit of detection:

Concentrations of metabolites below the limit of detection (LOD) were estimated using a multivariate normal distribution model. Correlations between the metabolites and the probability distribution of metabolites above the LOD were used to inform the censored values below the LOD (Griffith et al., 2011). Therefore, in this analysis, values below the limit of detection are treated as censored values, with a distribution that was constrained to be below the limit of detection and dependent on the observed values of the other metabolites in the same sample. These methods have been well utilized in several studies to inform values below the limit of detection (Lyles et al., 2001; Thiebaut and Jacqmin-Gadda 2004; Egeghy et al., 2005). The components of variance model can be expressed as:

$$\log(X_{jkl}) \sim MVN_3(\theta_k + \alpha_l + \mu_j , \Sigma w)$$

$$\text{for } j=1,\ldots,n_j,\ k= 1,2,3,\ l=1,\ldots,n_l$$

$$\text{and } \mu_j \sim MVN_3(0, \Sigma b)$$

where MVN_3 is a three-dimensional multivariate normal distribution of either the dimethyl OP metabolites DMP, DMTP, DMDTP, or diethyl OP metabolites DEP, DETP, DEDTP, X_{jkl} is the vector of the measured OP metabolite concentrations of the *j*th household on the *l*th collection day, μ_j is the vector of the random effects for the means of the three metabolites for the *j*th household, α_l is the mean for the

lth day, θ_k is the vector of the means of the three metabolites, Σw is the within-household variance–covariance matrix (3x3), Σb is the between-household variance–covariance matrix (3x3). The number of households is n_j , the number of collection days is n_l , and k indexes the 3 metabolites. Separate multivariate Normal distributions, MVN_3 , were estimated for each season, FWs and NFWs, adult and child, and dimethyl and diethyl metabolites. Because of the large number of samples below the LOD, distributions of the model parameters were estimated using a Bayesian Markov chain Monte Carlo method known as Gibbs sampling. The model was run using the WinBUGS 1.4.3 software program available at www.mrc-bsu.cam.ac.uk/bugs (Lunn et al., 2000). The model output was used in the subsequent analyses. Metabolites are reported as the cumulative amounts of all dimethyl and diethyl metabolites, total dialkyl phosphate metabolites (DAPs).

***RNA Isolation from Urine*:**

One 10mL archived urine sample per participant from sampling day 1 was thawed on ice and then stabilized with 1mL EDTA. Samples were inverted five times to mix well and centrifuged (3,000 x G for 30 min at 4°C). Urinary supernatant was removed and set aside while the remaining pellet was washed with 1mL PBS and centrifuged (12,000 x G for 10 minutes at 4°C). After the spin, the 1mL PBS supernatant was discarded and Ambion mirVana PARIS miRNA (Ambion, Austin, TX) kit-sourced *denaturing buffer* was mixed thoroughly with the retained pellet. 1mL of the urinary supernatant was added back to the denatured pellet and RNA isolation proceeded according to the Ambion mirVana PARIS miRNA kit manufacturer's protocol. Potential DNA contamination was removed using Ambion's DNA-free DNA Removal kit (Ambion, Austin, TX) per the manufacturer's protocol. Finally, RNA samples were cleaned and concentrated using Qiagen's RNeasy MinElute Cleanup Kit (Qiagen, Ltd) following the manufacturer's protocol.

Total RNA concentrations were determined on a NanoDrop spectrophotometer [NanoDrop Technologies, Wilmington, DE]. Urinary miRNA samples were profiled using TaqMan Array Human miRNA Panel A (4398977) [LifeTechnologies Carlsbad, CA] covering 384 human miRNAs following manufacturer instructions. The top three most frequently expressed miRNAs were validated by RT-PCR.

Statistical Analysis

MiRNA levels were normalized to an embedded internal control gene, MammU6, and relative miRNA levels were determined using the ΔCt method where ΔCt= Ct (miRNA of interest) - Ct (internal control). ΔΔCt was calculated as =ΔCt (FWs) – ΔCt (NFWs) and fold change was calculated as $2^{-\Delta\Delta Ct}$. Fold changes greater than 2 were considered significant (Livak and Schmittgen 2001).

The top 10 most frequently expressed miRNAs among all groups were identified and Principal Components Analysis (PCA) and Hierarchical Clustering Analysis (HCA) of these top expressed miRNAs for groups (n=27adults, n=27 children) were performed using JMP (SAS Institute Inc., Cary, NC) to identify differential expression of urinary miRNAs between groups and seasons. Analyses were performed using normalized (–ΔCt) values, where greater expression of miRNA is represented by larger –ΔCt values. Eigenvectors and loading values were extracted for the primary principal component. PCAs generated were used to visualize relationships among the variables (miRNAs) and eigenvectors were used to identify underlying indicators of variability in the data. Hierarchical clustering was used to visualize upregulated and downregulated genes and identify expression-based grouping of the variables. Linear regression was used to determine dose-response relationships between total urinary DAPs and miRNAs expression.

Results

Of the 384 mircroRNAs probed, 297 (77%) were detected in at least one sample (Supplemental Table 1). Seven miRNAs were detected in at least 50% of the samples, and one miRNA (miR-223) was present in 96% of samples. Comparison of groups showed households (parent and child combined) expressed a greater number of miRNAs in their urine during post-harvest than during thinning seasons (mean=31 [range, 3-169] vs. 57 [6-197]). This seasonal difference was more drastic in adults (mean=25 [range, 3-130] vs. 74 [6-169]) than children (mean=38 [6-169] vs. 40 [9-173]) when analyzed separately. The top 10 most frequently expressed miRNAs in all groups are indicated in Table 1.

microRNA profile analysis

Principal Components Analyses (PCAs) were performed to visualize relationships among the top 10 most expressed miRNAs. PCAs of miRNA profiles were generated for adult farmworkers (FWs) and non-farmworkers (NFWs) during thinning and post-harvest seasons. During the post-harvest, miRNA expression illustrated clear clustering by occupation (Figure 1A). Between the two components, over 65% of the variability in miRNA expression was explained. Principal Component 1 (PC1) explained 54.3% of the variability between miRNA profiles. PC1 was predominately characterized by the presence (reflected by positive loadings) of miRNAs -223, -518d-3p, -597, -517b, -133b, & -28-5p and the relative absence (reflected by negatively loadings) of miRNAs -320a, -203a, -24-1, & -30c-1 (Figure 1B). There was a clear division by FW status along PC1, with FWs having positive scores and NFWs having negative scores. The positive scores in PC1 for the FWs are consistent with the presence (positive loadings) of miRNAs -223, -518d-3p, -597, -517b, -133b, & -28-5p and a relative absence of miRNAs -320a, -203a, -24-1, & -30c-1. Negative scores in PC1 for the NFWs are consistent with the presence of miRNAs 2-320a, -203a, -24-1, & -30c-1 and the relative absence of miRNAs -223, -518d-3p, -597, -517b, -133b, & -28-5p.

There was no separation between FW and NFWs observed in the thinning season (Supplemental Figure 1).

Hierarchical Cluster Analysis (HCA) and dendrograms (Figure 2) allowed for two-way visualization of grouping of miRNA expression where relatively higher expression of miRNA is indicated with brighter shades of red and lower levels of expression are indicated by brighter shades of green. The cluster showed two main branches, grouping the FWs and NFWs. FWs generally cluster in the bottom branch (B) while NFWs generally cluster in the top branch (A). MiRNAs are observed to cluster into two main branches (C and D), where six miRNAs (miR -223, -518d-3p, -597, -517b, -133b, & -28-5p, branch C) appear to be upregulated in FWs (generally showing red) compared to NFWs (generally showing green). Analyses indicate that higher levels of miR-223, -518d-3p, -597, -517b, -133b, & -28-5p may be associated with FW status. These findings are consistent with our PCA results.

Fold changes in the top 10 miRNAs were plotted to illustrate the differences in expression of the six identified upregulated miRNAs in FWs compared to NFWs (Figure 3). FWs are observed to express 58 times as much miR-223, 50 times as much miR-518d-3p, 15 times as much miR517b, 4 times as much miR-597, 8 times as much miR-133b, and 4 times as much miR-28-5p as NFWs in the post-harvest season. During the thinning season FWs were observed to express 2 times as much miR-223, 3 times as much miR-320a, 6 times as much miR-203a, and 2 times as much miR-133b as NFWs.

Total urinary concentration of DAPs, major metabolites of OP pesticides in humans, in the 16 FW and 11 NFW adults were regressed with –ΔCt of each of the top 10 miRNAs to determine the dose-response relationship between pesticide metabolites and miRNAs. A statistically significant occupational difference between FWs and NFWs was observed in miR-223 ($p<0.05$). Of the six miRNAs observed to be positively associated with FWs in the PCA and HCA during post-harvest season, five (miR-223, -518d-3p, -597, -517b, & 133b) were observed to show a positive dose-response trend with total DAPs (Figure 4). However, we were not able to observe significant correlations ($p>0.1$) between total DAPs and the six miRNAs.

Analyses showed no differences in miRNA profile expression in children between FW and NFW groups or between seasons (Supplemental Figures 2, 3).

Discussion

Our analyses showed six miRNAs (miR-223, -518d-3p, -597, -517b, -133b, & -28-5p) have relatively higher expression in FWs compared to NFWs in the post-harvest season. MiRNA databases including miRBase.org and miRo (miR-Ontology Database) that utilize three motif recognition software, TargetScan, miRanda, and PicTar, have identified several potential miRNA target sites, cellular processes and functions associated with these miRNAs (Enright et al., 2003; Krek et al., 2005; Grimson et al., 2007; Lagana et al., 2009). MiR-517b, -133b, and -597 have been identified as associated with target genes involved in neurological functions including neurotransmitter activity and receptor binding, among many other associated functions. Interestingly, miR-28-5p has been identified as associated with acetylcholine binding, acetylcholinesterase activity, and cholinesterase activity, hallmark pathways affected by organophosphate pesticide exposure. Many studies have identified neurobehavioral impacts of OP pesticides at levels that do not cause the hallmark inhibition of the acetylcholinesterase enzyme (Eaton

et al., 2008). A recent review by (Dluzen and Lazarus 2015) highlighted several miRNAs with functional effects on the expression or activity of several metabolic enzymes. MiR-223, which was observed to be upregulated in FWs in our study, has been shown to modulate activities of CYP 3A4 and CYP2E1 (Takahashi et al., 2014). Another upregulated miRNA in FWs, miR-133b has been observed to impair the expression of Glutathione-S-Transferase (GSTP1) in HeLa cells (Patron et al., 2012). These effects are of particular interest as these enzymes are highly involved in metabolism or OPs and other pesticides and may further suggest early biological effect from exposure.

In this study, we found changes in miRNA profiles at relatively low metabolite concentrations, potentially implicating epigenetic mechanisms in the low-dose effects of OP pesticides. These results suggest that the six miRNAs upregulated in FWs during the post-harvest season may serve to predict occupational status and as potential biomarkers of both pesticide exposure and early biological effects. Further investigation into the pathways involved with the miRNAs altered in FWs may be used to interpret the biological processes, functions, and pathways involved in pesticide exposures. Further characterization of pesticide use and exposure during the post-harvest and thinning seasons may prove to better identify dose-response relationships for other pesticides used in addition to OPs.

Urinary biomarkers offer a potential non-invasive method for identification of environmental pesticide exposure. However, existing urinary pesticide exposure biomonitoring involves costly analysis of specific pesticide metabolites. We have demonstrated that six specific urinary miRNAs are predictive of occupational status and may serve as effective biomarkers for pesticide exposures. Further, we identified elevated expression of these six miRNAs in the post-harvest season, but not in the thinning season, suggesting that presence of differential miRNA profiles may be short-lived. In this way, our observations suggest our methods are able to detect miRNA changes following several months of pesticide exposure but may not detect immediate changes from exposures. Additionally, because we were able to detect differences in FWs between the two seasons, we hypothesize that the effects

occurring in the post-harvest season may not persist into the following seasons. These findings are consistent with those observed in an *in vivo* study investigating effects of formaldehyde exposure on miRNA profile expression in rats (Rager et al., 2014). Short-term changes in plasma miRNA expression profiles have also been observed in smokers after quitting smoking (Takahashi et al., 2013). Previously, long-term effects in miRNA expression from environmental exposures have not been studied and our findings offer insight on the transitory nature of miRNAs (Vrijens et al., 2015). To our knowledge, our study reports the first observation of transient characteristics of miRNAs in extra-bodily fluids in humans in a longitudinal study. Future studies investigating additional time points in the time period immediately following cessation of exposure may show how long the miRNA levels remain altered and further explain the temporality and seasonality we observed in our study.

Previous work with miRNA has often focused on specific tissue samples or assessed systemic expression through blood samples. While urine is beginning to be more widely used (Yang et al., 2012; Kanki et al., 2014; Yang et al., 2015), field-collected samples are still rarely measured. In this study, we were able to successfully isolate and quantify miRNA expression in field collected urine samples that had be archived in our biorepository. Not only does this demonstrate the robustness of our methods, but it also contributes to the applicability of miRNA in environmental exposure assessment. Additionally, urinary miRNA analysis may provide the benefit of molecular insight on multiple endpoints and concurrent monitoring for co-exposures. MiRNAs have the potential to act as more sensitive biomarkers of effect than overt clinical or other indications of damage and disease (Heinloth et al., 2004).

While AZM is the primary pesticide in use during the thinning season, FWs are exposed to a variety of other agricultural pesticides and potentially other chemicals during the season tested. In our study, FWs showed a positive trend in OP metabolite concentrations and five of the miRNA expression changes. While our small sample size (FW n=16, NFW n=11) was able to detect statistically significant occupational differences in associations of one of these five miRNAs with OP metabolites, these analyses

performed on a larger sample size may show further statistical significance of the observed dose-response trends.

While we did not detect the strongest signal of occupational differences during the season with greatest OP use, the large combination of various pesticide exposures occurring in these settings throughout these agricultural seasons may contribute to the observed occupational differences immediately following the exposures in the post-harvest season. Further analysis of additional pesticide metabolites is underway to better characterize these exposures in each season studied. Other factors such as differing lifestyle habits or non-chemical stressors may also be contributing to observed differences between groups and seasons. Because samples were not obtained clinically, quality and quantity of miRNA extracted from urine samples were not ideal compared to blood, plasma, or other tissues. However by concentrating samples we were able to identify critical miRNAs associated with FW adults. In doing so, we utilized a combination of multiple manufacturer-sourced kits in our methods, which can potentially become costly should a similar study be done with a larger cohort. While miRNAs were observed to persist in our frozen archived samples, it is still possible that "fresh" urine samples, collected as such in clinical environments and processed rapidly may provide stronger signals or identify other critical miRNAs involved.

We did not observe any differences in miRNA profiles between FW and NFW children in either season. The quantity of miRNA measured in child urine samples in our study was generally much lower than in adult samples, which may suggest that our methods may not be sensitive enough to detect differences in miRNA profiles in children. Future improvements on our method sensitivity to detect miRNA changes in children are critical as miRNAs are highly involved in development (Alvarez-Garcia and Miska 2005; Wienholds and Plasterk 2005) and exposure to environmental toxicants during development that result in short-term changes in miRNA expression have the potential to lead to

significant developmental issues (Marsit et al., 2006). This may provide further insight into mechanisms of characteristic developmental neurotoxic effects of pesticides (Gray and Lawler 2011).

Conclusion

Our study implements a novel method to identify biomarkers of exposure and early biological response in archived, field-collected urine samples. We have identified six miRNA associated with occupational farm work, thereby demonstrating the utility of urinary miRNAs and their potential to act as biomarkers of environmental pesticide exposure and early biological response. We have shown that miRNAs can be extracted from archived urinary samples and the ability to detect 273 different miRNAs. We observed differences in miRNA expression in adult FWs compared to NFWs. We observed a seasonal difference in relative miRNA expression in FWs suggestive of transient characteristics of miRNAs in extra-bodily fluids. These differences between groups were not observed in children, suggesting potential limitations of the sensitivity of our methods. Additional work is underway to investigate miRNA profiles associated with pesticide exposure and the roles of these miRNAs in adverse outcome pathways.

This work was made possible through funding from the Eunice Kennedy Shriver National Institute of Child Health and Human Development, National Institutes of Health, Department of Health and Human Services (Contract Nos.HHSN275200800015C and HHSN2672007023C), the National Institutes of Environmental Health Sciences (Grants 5P01 ES009601 and 5 P30 ES007033) and from the United States Environmental Protection Agency (EPA) (Grants RD-83451401, RD-83170901, and RD-83273301).

Appendix I. References

Alvarez-Garcia, I. and E. A. Miska (2005). "MicroRNA functions in animal development and human disease." Development **132**(21): 4653-4662.

Barr, D. B., R. Bravo, G. Weerasekera, L. M. Caltabiano, R. D. Whitehead, Jr., A. O. Olsson, S. P. Caudill, S. E. Schober, J. L. Pirkle, E. J. Sampson, R. J. Jackson and L. L. Needham (2004). "Concentrations of dialkyl phosphate metabolites of organophosphorus pesticides in the U.S. population." Environ Health Perspect **112**(2): 186-200.

Catto, J. W., A. Alcaraz, A. S. Bjartell, R. De Vere White, C. P. Evans, S. Fussel, F. C. Hamdy, O. Kallioniemi, L. Mengual, T. Schlomm and T. Visakorpi (2011). "MicroRNA in prostate, bladder, and kidney cancer: a systematic review." Eur Urol **59**(5): 671-681.

Dluzen, D. F. and P. Lazarus (2015). "MicroRNA regulation of the major drug-metabolizing enzymes and related transcription factors." Drug Metab Rev: 1-15.

Eaton, D. L., R. B. Daroff, H. Autrup, J. Bridges, P. Buffler, L. G. Costa, J. Coyle, G. McKhann, W. C. Mobley, L. Nadel, D. Neubert, R. Schulte-Hermann and P. S. Spencer (2008). "Review of the toxicology of chlorpyrifos with an emphasis on human exposure and neurodevelopment." Crit Rev Toxicol **38 Suppl 2**: 1-125.

Egeghy, P. P., J. J. Quackenboss, S. Catlin and P. B. Ryan (2005). "Determinants of temporal variability in NHEXAS-Maryland environmental concentrations, exposures, and biomarkers." J Expo Anal Environ Epidemiol **15**(5): 388-397.

Enright, A. J., B. John, U. Gaul, T. Tuschl, C. Sander and D. S. Marks (2003). "MicroRNA targets in Drosophila." Genome Biol **5**(1): R1.

Eskenazi, B., A. Bradman and R. Castorina (1999). "Exposures of children to organophosphate pesticides and their potential adverse health effects." Environ Health Perspect **107 Suppl 3**: 409-419.

Gray, K. and C. P. Lawler (2011). "Strength in Numbers: Three Separate Studies Link in Utero Organophosphate Pesticide Exposure and Cognitive Development." Environmental Health Perspectives **119**(8): A 328-A 329.

Griffith, W., C. L. Curl, R. A. Fenske, C. A. Lu, E. M. Vigoren and E. M. Faustman (2011). "Organophosphate pesticide metabolite levels in pre-school children in an agricultural community: within- and between-child variability in a longitudinal study." Environ Res **111**(6): 751-756.

Grimson, A., K. K. Farh, W. K. Johnston, P. Garrett-Engele, L. P. Lim and D. P. Bartel (2007). "MicroRNA targeting specificity in mammals: determinants beyond seed pairing." Mol Cell **27**(1): 91-105.

Hanke, M., K. Hoefig, H. Merz, A. C. Feller, I. Kausch, D. Jocham, J. M. Warnecke and G. Sczakiel (2010). "A robust methodology to study urine microRNA as tumor marker: microRNA-126 and microRNA-182 are related to urinary bladder cancer." Urol Oncol **28**(6): 655-661.

Heinloth, A. N., R. D. Irwin, G. A. Boorman, P. Nettesheim, R. D. Fannin, S. O. Sieber, M. L. Snell, C. J. Tucker, L. Li, G. S. Travlos, G. Vansant, P. E. Blackshear, R. W. Tennant, M. L. Cunningham and R. S. Paules (2004). "Gene expression profiling of rat livers reveals indicators of potential adverse effects." Toxicol Sci **80**(1): 193-202.

Kanki, M., A. Moriguchi, D. Sasaki, H. Mitori, A. Yamada, A. Unami and Y. Miyamae (2014). "Identification of urinary miRNA biomarkers for detecting cisplatin-induced proximal tubular injury in rats." Toxicology **324**: 158-168.

Krek, A., D. Grun, M. N. Poy, R. Wolf, L. Rosenberg, E. J. Epstein, P. MacMenamin, I. da Piedade, K. C. Gunsalus, M. Stoffel and N. Rajewsky (2005). "Combinatorial microRNA target predictions." Nat Genet **37**(5): 495-500.

Lagana, A., S. Forte, A. Giudice, M. R. Arena, P. L. Puglisi, R. Giugno, A. Pulvirenti, D. Shasha and A. Ferro (2009). "miRo: a miRNA knowledge base." Database (Oxford) **2009**: bap008.

Lee, Y., S. El Andaloussi and M. J. Wood (2012). "Exosomes and microvesicles: extracellular vesicles for genetic information transfer and gene therapy." Hum Mol Genet **21**(R1): R125-134.

Livak, K. J. and T. D. Schmittgen (2001). "Analysis of relative gene expression data using real-time quantitative PCR and the 2(-Delta Delta C(T)) Method." Methods **25**(4): 402-408.

Lunn, D. J., A. Thomas, N. Best and D. Spiegelhalter (2000). "WinBUGS—a Bayesian modelling framework: concepts, structure, and extensibility." Stat. Comput. **10**(2000): 325-337.

Lyles, R. H., D. Fan and R. Chuachoowong (2001). "Correlation coefficient estimation involving a left censored laboratory assay variable." Stat Med **20**(19): 2921-2933.

Mall, C., D. M. Rocke, B. Durbin-Johnson and R. H. Weiss (2013). "Stability of miRNA in human urine supports its biomarker potential." Biomark Med **7**(4): 623-631.

Marsit, C. J., K. Eddy and K. T. Kelsey (2006). "MicroRNA responses to cellular stress." Cancer Res **66**(22): 10843-10848.

Odetokun, M. S., M. A. Montesano, G. Weerasekera, R. D. Whitehead, Jr., L. L. Needham and D. B. Barr (2010). "Quantification of dialkylphosphate metabolites of organophosphorus insecticides in human urine using 96-well plate sample preparation and high-performance liquid chromatography-electrospray ionization-tandem mass spectrometry." J Chromatogr B Analyt Technol Biomed Life Sci **878**(27): 2567-2574.

Patron, J. P., A. Fendler, M. Bild, U. Jung, H. Muller, M. O. Arntzen, C. Piso, C. Stephan, B. Thiede, H. J. Mollenkopf, K. Jung, S. H. Kaufmann and J. Schreiber (2012). "MiR-133b targets antiapoptotic genes and enhances death receptor-induced apoptosis." PLoS One **7**(4): e35345.

Rager, J. E., B. C. Moeller, S. K. Miller, D. Kracko, M. Doyle-Eisele, J. A. Swenberg and R. C. Fry (2014). "Formaldehyde-associated changes in microRNAs: tissue and temporal specificity in the rat nose, white blood cells, and bone marrow." Toxicol Sci **138**(1): 36-46.

Smith, M. N., C. S. Wilder, W. C. Griffith, T. Workman, B. Thompson, R. Dills, G. Onstad, M. Vredevoogd, E. M. Vigoren and E. M. Faustman (2015). "Seasonal variation in cortisol biomarkers in Hispanic mothers living in an agricultural region." Biomarkers **20**(5): 299-305.

Takahashi, K., Y. Oda, Y. Toyoda, T. Fukami, T. Yokoi and M. Nakajima (2014). "Regulation of cytochrome b5 expression by miR-223 in human liver: effects on cytochrome P450 activities." Pharm Res **31**(3): 780-794.

Takahashi, K., S. Yokota, N. Tatsumi, T. Fukami, T. Yokoi and M. Nakajima (2013). "Cigarette smoking substantially alters plasma microRNA profiles in healthy subjects." Toxicol Appl Pharmacol **272**(1): 154-160.

Thiebaut, R. and H. Jacqmin-Gadda (2004). "Mixed models for longitudinal left-censored repeated measures." Comput Methods Programs Biomed **74**(3): 255-260.

Thompson, B., W. C. Griffith, D. B. Barr, G. D. Coronado, E. M. Vigoren and E. M. Faustman (2014). "Variability in the take-home pathway: farmworkers and non-farmworkers and their children." J Expo Sci Environ Epidemiol **24**(5): 522-531.

USEPA. (2009). "Azinphos-methyl Phase Out." from http://www.regulations.gov/#!docketDetail;D=EPA-HQ-OPP-2005-0061.

Vasudevan, S., Y. Tong and J. A. Steitz (2007). "Switching from repression to activation: microRNAs can up-regulate translation." Science **318**(5858): 1931-1934.

Vrijens, K., V. Bollati and T. S. Nawrot (2015). "MicroRNAs as potential signatures of environmental exposure or effect: a systematic review." Environ Health Perspect **123**(5): 399-411.

Wang, K., S. Zhang, B. Marzolf, P. Troisch, A. Brightman, Z. Hu, L. E. Hood and D. J. Galas (2009). "Circulating microRNAs, potential biomarkers for drug-induced liver injury." Proc Natl Acad Sci U S A **106**(11): 4402-4407.

Weber, J. A., D. H. Baxter, S. Zhang, D. Y. Huang, K. H. Huang, M. J. Lee, D. J. Galas and K. Wang (2010). "The microRNA spectrum in 12 body fluids." Clin Chem **56**(11): 1733-1741.

Wienholds, E. and R. H. Plasterk (2005). "MicroRNA function in animal development." FEBS Lett **579**(26): 5911-5922.

Yang, X., J. Greenhaw, Q. Shi, Z. Su, F. Qian, K. Davis, D. L. Mendrick and W. F. Salminen (2012). "Identification of urinary microRNA profiles in rats that may diagnose hepatotoxicity." Toxicol Sci **125**(2): 335-344.

Yang, X., W. F. Salminen, Q. Shi, J. Greenhaw, P. S. Gill, S. Bhattacharyya, R. D. Beger, D. L. Mendrick, W. B. Mattes and L. P. James (2015). "Potential of extracellular microRNAs as biomarkers of acetaminophen toxicity in children." Toxicol Appl Pharmacol **284**(2): 180-187.

Table 1. Top 10 detected microRNAs and frequency of detection in adults and children by occupation (farmworker-FW, non-farmworker- NFW).

microRNA	Counts All Groups All Seasons¥ (n=107)	Frequency All Groups All Seasons¥ (n=107)	Frequency Adult FW All Seasons¥ (n=32)	Frequency Adult NFW All Seasons¥ (n=22)	Frequency Child FW All Seasons¥* (n=31)	Frequency Child NFW All Seasons¥ (n=22)
miR-223	103	96%	100%	95%	91%	95%
miR-518d-3p	88	82%	72%	64%	91%	100%
miR-320a	68	64%	56%	86%	50%	68%
miR-203a	61	57%	53%	55%	47%	77%
miR-517b	61	57%	63%	50%	47%	68%
miR-597	55	51%	47%	45%	53%	59%
miR-24-1	54	50%	41%	55%	50%	59%
miR-133b	50	47%	44%	41%	44%	59%
miR-28-5p	50	47%	38%	50%	50%	50%
miR-30c-1	49	46%	44%	59%	31%	59%

¥ One sample collected per season for two seasons for each individual adult and child participant. Adult FW n=16, Adult NFW n=11, Child FW n=16, Child NFW n=11.

**Missing sample, Child FW during thinning season*

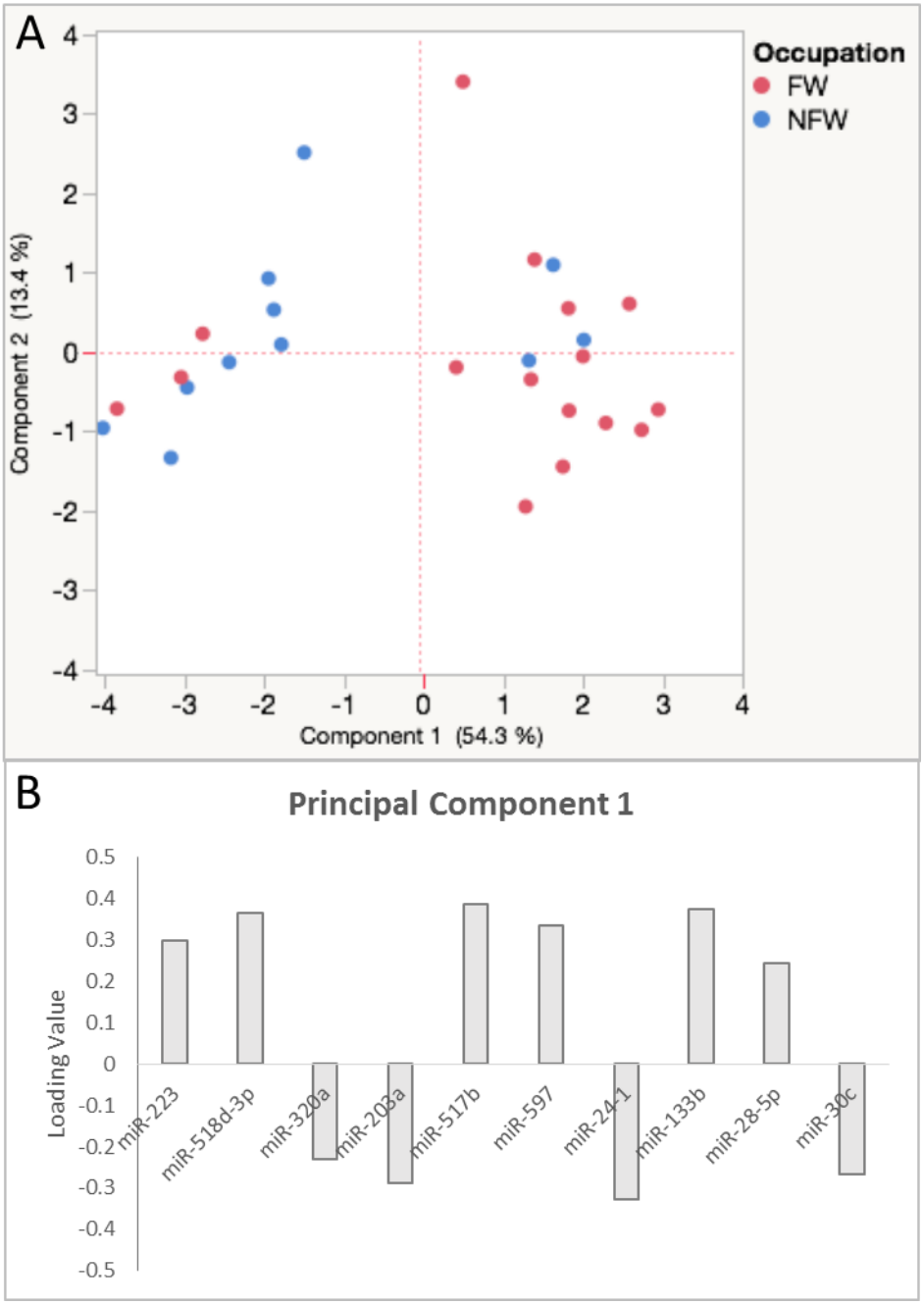

Figure 1. (**A)** PCA of the top 10 miRNAs expressed in 16 FW (red) and 11 NFW (blue) adults during post-harvest season. The abundance of each miRNA relative to the internal control (-ΔCt) was expressed as a fraction of the total miRNA abundance. Component 1 described 54.3% of the variance and Component 2 explains 13.4% of the variance. Between the two components, 67.7% of the variability is explained. **(B)** Eigenvector analysis of the top 10 expressed miRNAs shows principal component 1 is positive for miRNA -223, -518d-3p, -597, -517b, -133b, & -28-5p and negative for miRNAs -320a, -203a, -24-1, & -30c-1.

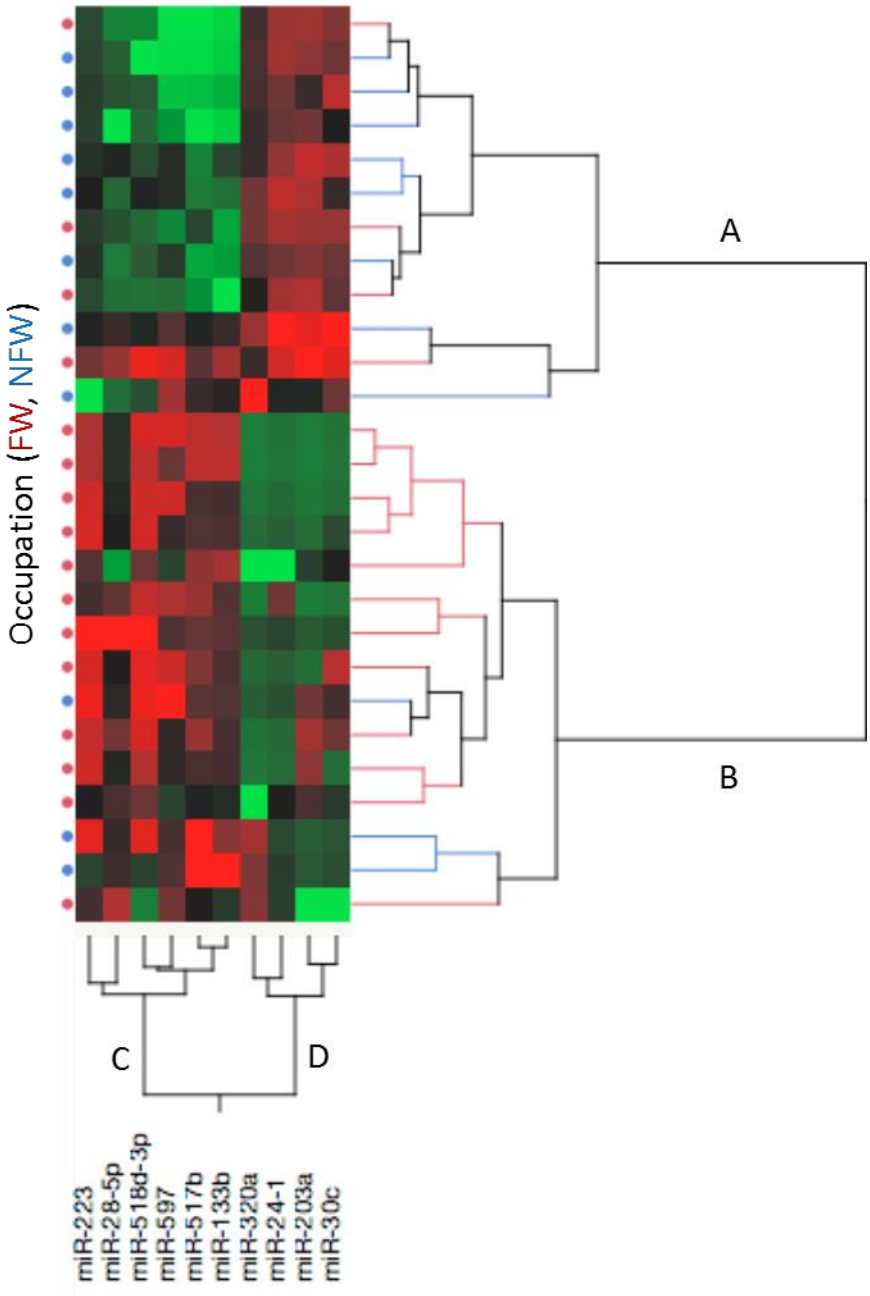

Figure 2. Hierarchical clustering analysis of the top 10 miRNAs expressed was performed using normalized Ct values (-ΔCt) in adults during post-harvest season using Ward's algorithm. The color scale indicates relative expression of miRNA with brighter shades of red indicating higher miRNA expression and green indicating lower levels of expression. Participants are indicated on the left panel as farmworker (FW, red circle) or non-farmworkers (NFW, blue circle). MiRNAs are listed on the bottom of the figure. The figure shows the clustering of the six miRNAs (-223, -518d-3p, -597, -517b, -133b, & -28-5p) that distinguish FWs from NFWs where FWs are generally observed to have higher expression of these six miRNAs relative to NFWs during this season.

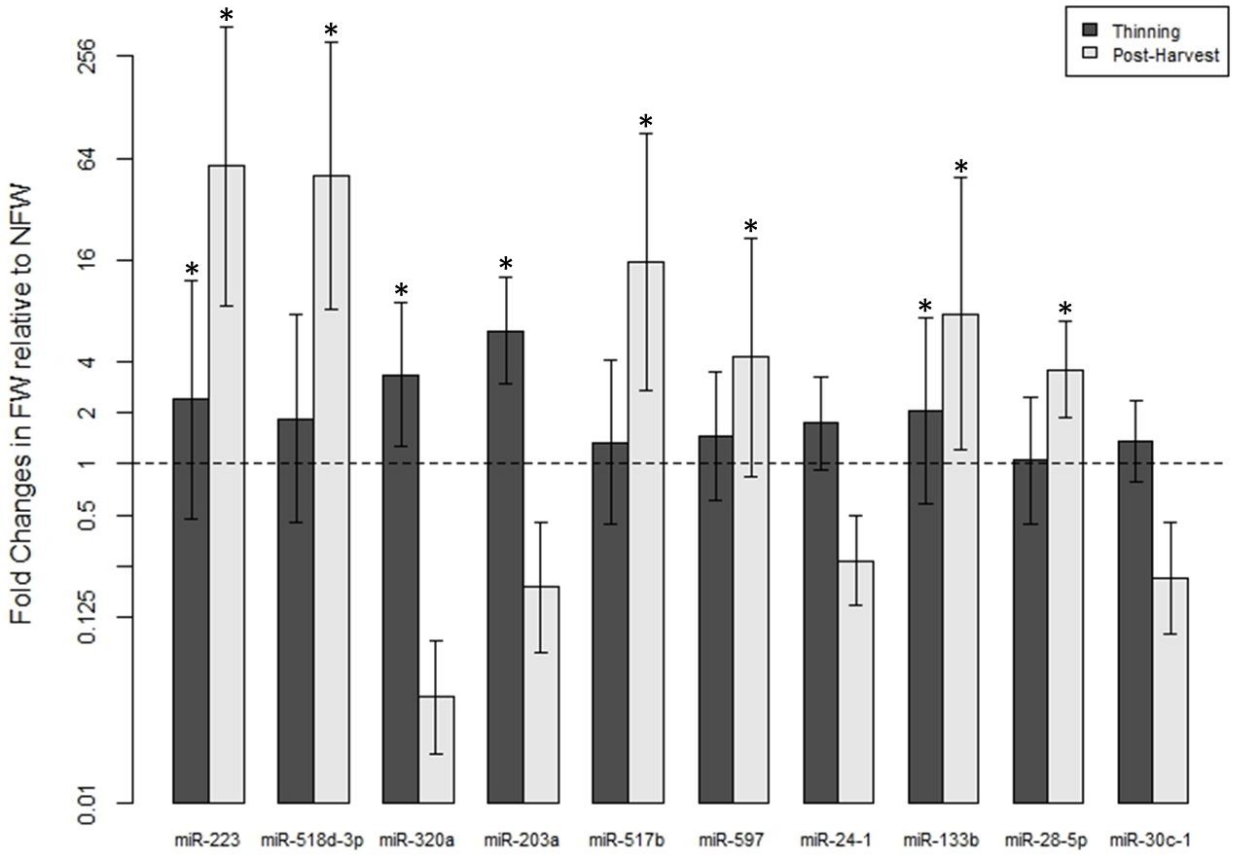

Figure 3. Fold increases in FW relative to NW in the thinning and post-harvest seasons for the top 10 most expressed miRNAs. ΔΔCt was calculated as =ΔCt (FWs) – ΔCt (NFWs) and fold change was calculated as $2^{-\Delta\Delta Ct}$. Fold changes >2 were considered significant and are indicated by *. The fold changes represent the average miRNA expression of the 16 FW samples and 11 NFW samples for each miRNA investigated.

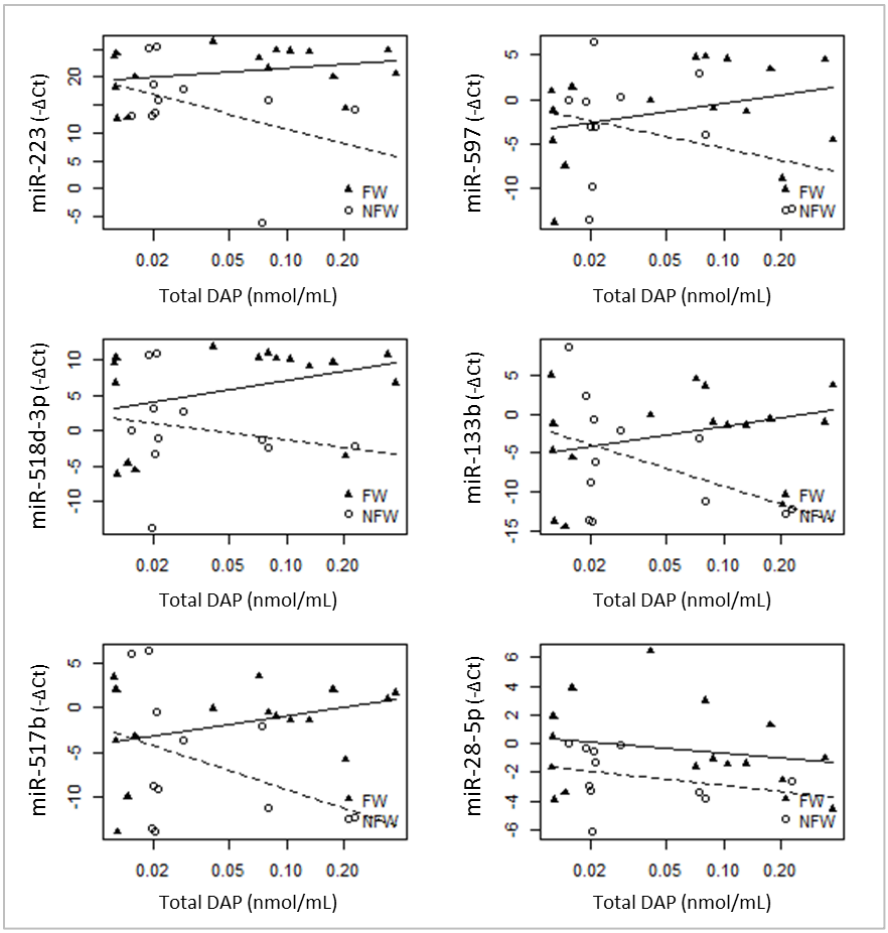

Figure 4. Regression of total DAPs and six FW-related miRNAs in FW and NFW adults in the post-harvest. FWs are indicated by triangles with solid trend lines and NFWs are indicated by open circles and hashed trend lines. Metabolites are reported as nmol total DAPs/mL urine and miRNA levels are reported as –ΔCt where greater expression of miRNA corresponds with a positive trend. A significant occupational effect was observed in miR-223 ($p<0.05$). A positive-trending dose-response for FW adults is observed in five of the six miRNAs (-223, -518d-3p, -517b, -597, & -133b) and negative trending dose-response for NFW adults is observed in all six miRNAs ($p>0.05$).

Supplementary Information

Supplementary Table 1. Frequencies of all mircoRNAs investigated

Detector	Count All groups All seasons n=107	Frequency %
hsa-miR-223-4395406	103	96%
hsa-miR-518d-3p-4373248	88	82%
hsa-miR-320-4395388	68	64%
hsa-miR-203-4373095	61	57%
hsa-miR-517b-4373244	61	57%
hsa-miR-597-4380960	55	51%
hsa-miR-24-4373072	54	50%
hsa-miR-133b-4395358	50	47%
hsa-miR-28-5p-4373067	50	47%
hsa-miR-30c-4373060	50	47%
hsa-miR-222-4395387	49	46%
hsa-miR-193b-4395478	46	43%
hsa-miR-484-4381032	45	42%
hsa-miR-191-4395410	44	41%
hsa-miR-106b-4373155	41	38%
hsa-miR-636-4395199	41	38%
hsa-miR-345-4395297	40	37%
hsa-miR-19b-4373098	39	36%
hsa-miR-30b-4373290	39	36%
hsa-miR-483-5p-4395449	39	36%
hsa-miR-886-3p-4395305	39	36%
RNU48-4373383	39	36%
hsa-miR-218-4373081	38	36%
has-miR-155-4395459	36	34%
hsa-miR-375-4373027	36	34%
hsa-miR-886-5p-4395304	36	34%
hsa-miR-200c-4395411	35	33%
hsa-miR-204-4373094	34	32%
hsa-miR-548a-3p-4380948	34	32%
hsa-miR-574-3p-4395460	34	32%
hsa-miR-328-4373049	33	31%
hsa-miR-133a-4395357	32	30%
hsa-miR-186-4395396	32	30%
hsa-miR-26a-4395166	32	30%
hsa-miR-29a-4395223	32	30%
hsa-miR-618-4380996	32	30%

hsa-miR-125b-4373148	31	29%
hsa-miR-184-4373113	31	29%
hsa-miR-192-4373108	31	29%
hsa-miR-212-4373087	31	29%
hsa-miR-520e-4373255	31	29%
hsa-miR-532-3p-4395466	31	29%
hsa-miR-150-4373127	30	28%
hsa-miR-21-4373090	30	28%
hsa-miR-374a-4373028	30	28%
hsa-miR-92a-4395169	30	28%
hsa-miR-99b-4373007	30	28%
hsa-miR-146a-4373132	29	27%
hsa-miR-16-4373121	29	27%
hsa-miR-29c-4395171	29	27%
hsa-miR-885-5p-4395407	29	27%
hsa-let-7e-4395517	28	26%
hsa-miR-193a-3p-4395361	28	26%
hsa-miR-27a-4373287	28	26%
hsa-miR-17-4395419	27	25%
hsa-miR-202-4395474	27	25%
hsa-miR-20a-4373286	27	25%
hsa-miR-331-3p-4373046	27	25%
hsa-miR-548c-3p-4380993	27	25%
hsa-miR-193a-5p-4395392	26	24%
hsa-miR-205-4373093	26	24%
hsa-let-7d-4395394	25	23%
hsa-miR-10a-4373153	25	23%
hsa-miR-142-3p-4373136	25	23%
hsa-miR-28-3p-4395557	25	23%
hsa-miR-324-3p-4395272	25	23%
hsa-miR-422a-4395408	25	23%
hsa-miR-708-4395452	25	23%
hsa-miR-106a-4395280	24	22%
hsa-miR-125a-5p-4395309	24	22%
hsa-miR-146b-5p-4373178	24	22%
hsa-miR-194-4373106	24	22%
hsa-miR-25-4373071	24	22%
hsa-miR-489-4395469	24	22%
hsa-miR-503-4373228	24	22%
hsa-miR-141-4373137	23	21%
hsa-miR-19a-4373099	23	21%
hsa-miR-31-4395390	23	21%
hsa-let-7c-4373167	22	21%

hsa-miR-100-4373160	22	21%
hsa-miR-152-4395170	22	21%
hsa-miR-26b-4395167	22	21%
hsa-miR-429-4373203	22	21%
hsa-miR-888-4395323	22	21%
hsa-miR-200b-4395362	21	20%
hsa-miR-27b-4373068	21	20%
hsa-miR-342-3p-4395371	21	20%
hsa-miR-362-5p-4378092	21	20%
hsa-miR-95-4373011	21	20%
hsa-miR-99a-4373008	21	20%
hsa-let-7b-4395446	20	19%
hsa-miR-126-4395339	20	19%
hsa-miR-138-4395395	20	19%
hsa-miR-145-4395389	20	19%
hsa-miR-302b-4378071	20	19%
hsa-miR-374b-4381045	20	19%
hsa-miR-576-3p-4395462	20	19%
hsa-miR-660-4380925	20	19%
hsa-miR-136-4373173	19	18%
hsa-miR-140-5p-4373374	19	18%
hsa-miR-181a-4373117	19	18%
hsa-miR-195-4373105	19	18%
hsa-miR-20b-4373263	19	18%
hsa-miR-339-3p-4395295	19	18%
hsa-miR-365-4373194	19	18%
hsa-miR-744-4395435	19	18%
hsa-miR-10b-4395329	18	17%
hsa-miR-124-4373295	18	17%
hsa-miR-324-5p-4373052	18	17%
hsa-miR-335-4373045	18	17%
hsa-miR-34a-4395168	18	17%
hsa-miR-455-5p-4378098	18	17%
hsa-miR-491-5p-4381053	18	17%
hsa-miR-518f-4395499	18	17%
hsa-miR-523-4395497	18	17%
hsa-miR-642-4380995	18	17%
hsa-miR-93-4373302	18	17%
hsa-let-7g-4395393	17	16%
hsa-miR-103-4373158	17	16%
hsa-miR-132-4373143	17	16%
hsa-miR-135b-4395372	17	16%
hsa-miR-140-3p-4395345	17	16%

hsa-miR-221-4373077	17	16%
hsa-miR-224-4395210	17	16%
hsa-miR-454-4395434	17	16%
hsa-miR-494-4395476	17	16%
hsa-miR-500-4395539	17	16%
hsa-miR-532-5p-4380928	17	16%
hsa-miR-652-4395463	17	16%
hsa-miR-210-4373089	16	15%
hsa-miR-376a-4373026	16	15%
hsa-miR-502-3p-4395194	16	15%
hsa-miR-598-4395179	16	15%
hsa-miR-101-4395364	15	14%
hsa-miR-135a-4373140	15	14%
hsa-miR-423-5p-4395451	15	14%
hsa-miR-452-4395440	15	14%
hsa-miR-590-5p-4395176	15	14%
hsa-miR-125a-3p-4395310	14	13%
hsa-miR-149-4395366	14	13%
hsa-miR-200a-4378069	14	13%
hsa-miR-301a-4373064	14	13%
hsa-miR-361-5p-4373035	14	13%
hsa-miR-451-4373360	14	13%
hsa-miR-485-3p-4378095	14	13%
hsa-miR-520b-4373252	14	13%
hsa-miR-9-4373285	14	13%
hsa-miR-128-4395327	13	12%
hsa-miR-130a-4373145	13	12%
hsa-miR-148a-4373130	13	12%
hsa-miR-520f-4373256	13	12%
hsa-miR-548c-5p-4395540	13	12%
hsa-miR-548d-5p-4395348	13	12%
hsa-miR-758-4395180	13	12%
hsa-miR-330-3p-4373047	12	11%
hsa-miR-363-4378090	12	11%
hsa-miR-628-5p-4395544	12	11%
hsa-miR-671-3p-4395433	12	11%
hsa-miR-127-3p-4373147	11	10%
hsa-miR-143-4395360	11	10%
hsa-miR-29b-4373288	11	10%
hsa-miR-340-4395369	11	10%
hsa-miR-548b-5p-4395519	11	10%
hsa-miR-130b-4373144	10	9%
hsa-miR-142-5p-4395359	10	9%

hsa-miR-147b-4395373	10	9%
hsa-miR-185-4395382	10	9%
hsa-miR-23b-4373073	10	9%
hsa-miR-323-3p-4395338	10	9%
hsa-miR-424-4373201	10	9%
RNU44-4373384	10	9%
hsa-miR-15b-4373122	9	8%
hsa-miR-197-4373102	9	8%
hsa-miR-486-5p-4378096	9	8%
hsa-miR-492-4373217	9	8%
hsa-miR-520d-5p-4395504	9	8%
hsa-miR-146b-3p-4395472	8	7%
hsa-miR-148b-4373129	8	7%
hsa-miR-372-4373029	8	7%
hsa-miR-373-4378073	8	7%
hsa-miR-521-4373259	8	7%
hsa-miR-196b-4395326	7	7%
hsa-miR-362-3p-4395228	7	7%
hsa-miR-410-4378093	7	7%
hsa-miR-449a-4373207	7	7%
hsa-miR-517c-4373264	7	7%
hsa-miR-539-4378103	7	7%
hsa-miR-545-4395378	7	7%
hsa-miR-629-4395547	7	7%
hsa-miR-891a-4395302	7	7%
hsa-let-7a-4373169	6	6%
hsa-miR-147-4373131	6	6%
hsa-miR-296-5p-4373066	6	6%
hsa-miR-302a-4378070	6	6%
hsa-miR-616-4395525	6	6%
hsa-miR-625-4395542	6	6%
hsa-miR-874-4395379	6	6%
hsa-miR-107-4373154	5	5%
hsa-miR-183-4395380	5	5%
hsa-miR-367-4373034	5	5%
hsa-miR-381-4373020	5	5%
hsa-miR-425-4380926	5	5%
hsa-miR-450a-4395414	5	5%
hsa-miR-455-3p-4395355	5	5%
hsa-miR-508-3p-4373233	5	5%
hsa-miR-515-3p-4395480	5	5%
hsa-miR-1-4395333	4	4%
hsa-miR-187-4373307	4	4%

hsa-miR-190-4373110	4	4%
hsa-miR-199a-3p-4395415	4	4%
hsa-miR-338-3p-4395363	4	4%
hsa-miR-34c-5p-4373036	4	4%
hsa-miR-487b-4378102	4	4%
hsa-miR-518b-4373246	4	4%
hsa-miR-542-5p-4395351	4	4%
hsa-miR-551b-4380945	4	4%
hsa-miR-589-4395520	4	4%
hsa-miR-627-4380967	4	4%
hsa-miR-181c-4373115	3	3%
hsa-miR-214-4395417	3	3%
hsa-miR-299-3p-4373189	3	3%
hsa-miR-302c-4378072	3	3%
hsa-miR-330-5p-4395341	3	3%
hsa-miR-346-4373038	3	3%
hsa-miR-376c-4395233	3	3%
hsa-miR-449b-4381011	3	3%
hsa-miR-501-5p-4373226	3	3%
hsa-miR-519e-4395481	3	3%
hsa-miR-522-4395524	3	3%
hsa-miR-579-4395509	3	3%
hsa-miR-182-4395445	2	2%
hsa-miR-18b-4395328	2	2%
hsa-miR-208-4373091	2	2%
hsa-miR-215-4373084	2	2%
hsa-miR-22-4373079	2	2%
hsa-miR-220-4373078	2	2%
hsa-miR-220b-4395317	2	2%
hsa-miR-337-5p-4395267	2	2%
hsa-miR-383-4373018	2	2%
hsa-miR-486-3p-4395204	2	2%
hsa-miR-487a-4378097	2	2%
hsa-miR-509-5p-4395346	2	2%
hsa-miR-516b-4395172	2	2%
hsa-miR-517a-4395513	2	2%
hsa-miR-519a-4395526	2	2%
hsa-miR-520g-4373257	2	2%
hsa-miR-542-3p-4378101	2	2%
hsa-miR-582-3p-4395510	2	2%
hsa-miR-655-4381015	2	2%
hsa-miR-672-4395438	2	2%
hsa-miR-871-4395465	2	2%

hsa-miR-872-4395375	2	2%
hsa-miR-105-4395278	1	1%
hsa-miR-134-4373299	1	1%
hsa-miR-15a-4373123	1	1%
hsa-miR-18a-4395533	1	1%
hsa-miR-198-4395384	1	1%
hsa-miR-199a-5p-4373272	1	1%
hsa-miR-208b-4395401	1	1%
hsa-miR-211-4373088	1	1%
hsa-miR-216b-4395437	1	1%
hsa-miR-219-2-3p-4395501	1	1%
hsa-miR-220c-4395322	1	1%
hsa-miR-23a-4373074	1	1%
hsa-miR-296-3p-4395212	1	1%
hsa-miR-301b-4395503	1	1%
hsa-miR-325-4373051	1	1%
hsa-miR-329-4373191	1	1%
hsa-miR-331-5p-4395344	1	1%
hsa-miR-33b-4395196	1	1%
hsa-miR-369-3p-4373032	1	1%
hsa-miR-379-4373349	1	1%
hsa-miR-380-4373022	1	1%
hsa-miR-382-4373019	1	1%
hsa-miR-384-4373017	1	1%
hsa-miR-411-4381013	1	1%
hsa-miR-433-4373205	1	1%
hsa-miR-450b-5p-4395318	1	1%
hsa-miR-493-4395475	1	1%
hsa-miR-499-5p-4381047	1	1%
hsa-miR-502-5p-4373227	1	1%
hsa-miR-505-4395200	1	1%
hsa-miR-507-4373232	1	1%
hsa-miR-509-3-5p-4395266	1	1%
hsa-miR-511-4373236	1	1%
hsa-miR-512-3p-4381034	1	1%
hsa-miR-518a-3p-4395508	1	1%
hsa-miR-518d-5p-4395500	1	1%
hsa-miR-519c-3p-4373251	1	1%
hsa-miR-519d-4395514	1	1%
hsa-miR-524-5p-4395174	1	1%
hsa-miR-548d-3p-4381008	1	1%
hsa-miR-556-5p-4395455	1	1%
hsa-miR-570-4395458	1	1%

hsa-miR-876-5p-4395316	1	1%
hsa-miR-890-4395320	1	1%
hsa-miR-892a-4395306	1	1%
ath-miR159a-4373390	0	0%
hsa-let-7f-4373164	0	0%
hsa-miR-122-4395356	0	0%
hsa-miR-127-5p-4395340	0	0%
hsa-miR-129-3p-4373297	0	0%
hsa-miR-129-5p-4373171	0	0%
hsa-miR-137-4373301	0	0%
hsa-miR-139-3p-4395424	0	0%
hsa-miR-139-5p-4395400	0	0%
hsa-miR-153-4373305	0	0%
hsa-miR-154-4373270	0	0%
hsa-miR-188-3p-4395217	0	0%
hsa-miR-199b-5p-4373100	0	0%
hsa-miR-216a-4395331	0	0%
hsa-miR-217-4395448	0	0%
hsa-miR-219-1-3p-4395206	0	0%
hsa-miR-219-5p-4373080	0	0%
hsa-miR-298-4395301	0	0%
hsa-miR-299-5p-4373188	0	0%
hsa-miR-32-4395220	0	0%
hsa-miR-326-4373050	0	0%
hsa-miR-339-5p-4395368	0	0%
hsa-miR-342-5p-4395258	0	0%
hsa-miR-369-5p-4373195	0	0%
hsa-miR-370-4395386	0	0%
hsa-miR-371-3p-4395235	0	0%
hsa-miR-376b-4373196	0	0%
hsa-miR-377-4373025	0	0%
hsa-miR-409-5p-4395442	0	0%
hsa-miR-412-4373199	0	0%
hsa-miR-431-4395173	0	0%
hsa-miR-448-4373206	0	0%
hsa-miR-450b-3p-4395319	0	0%
hsa-miR-453-4395429	0	0%
hsa-miR-485-5p-4373212	0	0%
hsa-miR-488-4395468	0	0%
hsa-miR-490-3p-4373215	0	0%
hsa-miR-491-3p-4395471	0	0%
hsa-miR-495-4381078	0	0%
hsa-miR-496-4386771	0	0%

hsa-miR-499-3p-4395538	0	0%
hsa-miR-501-3p-4395546	0	0%
hsa-miR-504-4395195	0	0%
hsa-miR-506-4373231	0	0%
hsa-miR-508-5p-4395203	0	0%
hsa-miR-510-4395352	0	0%
hsa-miR-512-5p-4373238	0	0%
hsa-miR-513-5p-4395201	0	0%
hsa-miR-515-5p-4373242	0	0%
hsa-miR-516a-5p-4395527	0	0%
hsa-miR-518a-5p-4395507	0	0%
hsa-miR-518c-4395512	0	0%
hsa-miR-518e-4395506	0	0%
hsa-miR-520a-3p-4373268	0	0%
hsa-miR-520a-5p-4378085	0	0%
hsa-miR-525-3p-4395496	0	0%
hsa-miR-525-5p-4378088	0	0%
hsa-miR-526b-4395493	0	0%
hsa-miR-541-4395312	0	0%
hsa-miR-544-4395376	0	0%
hsa-miR-548a-5p-4395523	0	0%
hsa-miR-548b-3p-4380951	0	0%
hsa-miR-556-3p-4395456	0	0%
hsa-miR-561-4380938	0	0%
hsa-miR-576-5p-4395461	0	0%
hsa-miR-582-5p-4395175	0	0%
hsa-miR-615-3p-4386777	0	0%
hsa-miR-615-5p-4395464	0	0%
hsa-miR-624-4395541	0	0%
hsa-miR-651-4381007	0	0%
hsa-miR-653-4395403	0	0%
hsa-miR-654-3p-4395350	0	0%
hsa-miR-654-5p-4381014	0	0%
hsa-miR-674-4395193	0	0%
hsa-miR-873-4395467	0	0%
hsa-miR-875-3p-4395315	0	0%
hsa-miR-876-3p-4395336	0	0%
hsa-miR-885-3p-4395483	0	0%
hsa-miR-887-4395485	0	0%
hsa-miR-889-4395313	0	0%
hsa-miR-891b-4395321	0	0%
hsa-miR-96-4373372	0	0%
hsa-miR-98-4373009	0	0%

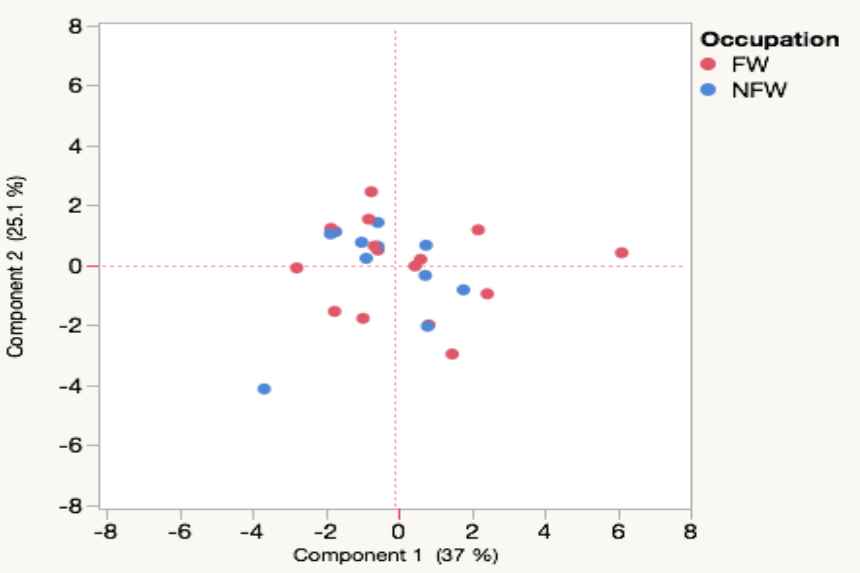

Supplementary Figure 1. PCA analyses of the top 10 miRNAs expressed in farmworkers (red) and non-farmworker (blue) adults during thinning season. The abundance of each miRNA relative to the internal control (-ΔCt) was expressed as a fraction of the total miRNA abundance. The figure indicates little separation between FW and NFW groups.

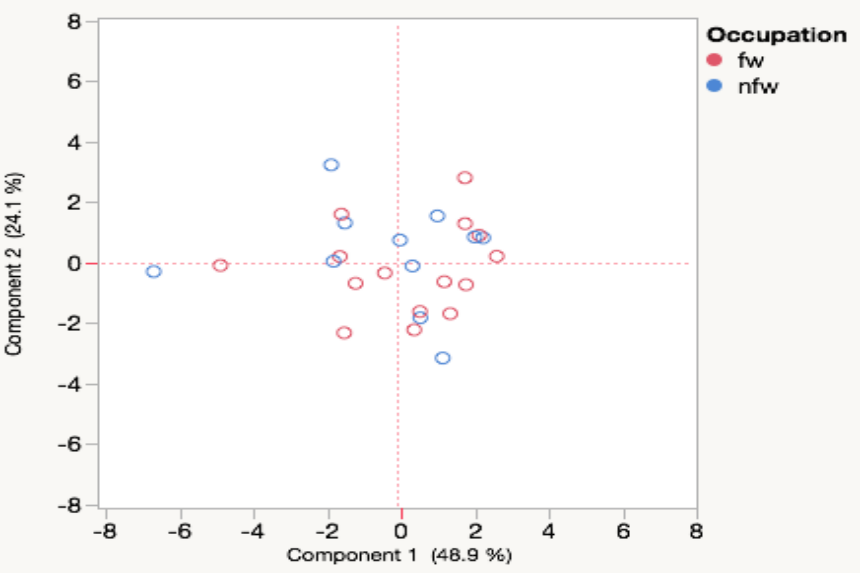

Supplementary Figure 2. PCA analyses of the top 10 miRNAs expressed in FWs (red) and NFW (blue) children during post-harvest season. The abundance of each miRNA relative to the internal control (-ΔCt) was expressed as a fraction of the total miRNA abundance. The figure indicates little separation between children in FW and NFW households.

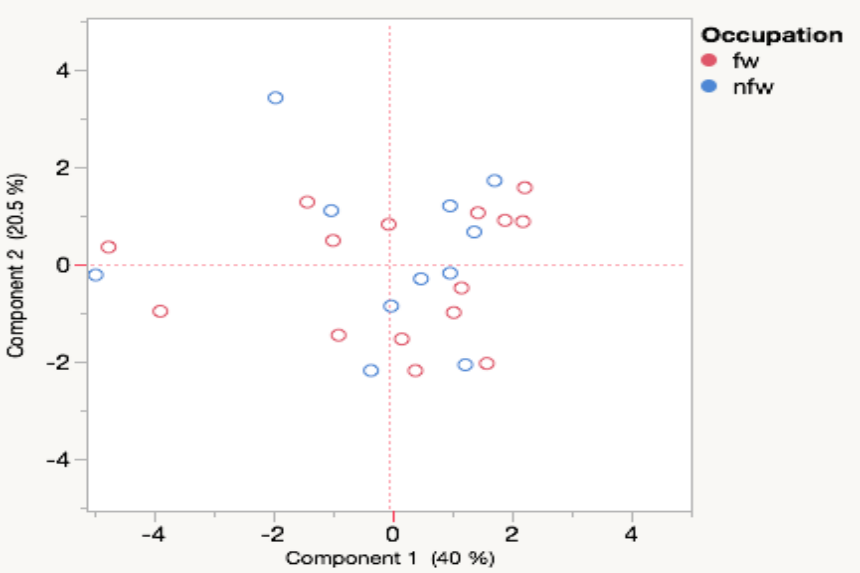

Supplementary Figure 3. PCA analyses of the top 10 miRNAs expressed in FWs (red) and NFW (blue) children during thinning season. The abundance of each miRNA relative to the internal control (-ΔCt) was expressed as a fraction of the total miRNA abundance. The figure indicates little separation between children in FW and NFW households.